DAVIDE PILASTRO

INNOVATIVE CONTROL TECHNIQUES AND STRATEGIES FOR ROBOTICS REHABILITATION

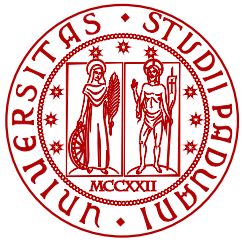

UNIVERSITÀ
DEGLI STUDI
DI PADOVA

Sede amministrativa: Università degli studi di Padova

Dipartimento di Tecnica e Gestione dei Sistemi Industriali

SCUOLA DI DOTTORATO IN INGEGNERIA MECCATRONICA
E DELL'INNOVAZIONE MECCANICA DEL PRODOTTO

CICLO XXVIII

INNOVATIVE CONTROL TECHNIQUES AND STRATEGIES FOR ROBOTICS REHABILITATION

Direttore della scuola: Ch.mo Prof. Alessandro Persona

Supervisore: Ch.mo Prof. Roberto Oboe

Dottorando: Davide Pilastro

Davide Pilastro: *Innovative control techniques and strategies for robotics rehabilitation,* January 28, 2016

Dedicated to the loving memory of
my grandfather Aldo.

SOMMARIO

Il tema principale del progetto di dottorato descritto in questa tesi è la robotica riabilitativa, che è, oggigiorno, un campo di ricerca molto attiva, dato che stiamo assistendo ad una crescente richiesta di terapie riabilitative. L'obiettivo principale del progetto è lo sviluppo di innovative soluzioni e strumenti nell'ambito dei sistemi di controllo, che permettono e promuovono l'uso di dispositivi robotici low-cost per la riabilitazione. Così facendo, è possibile far fronte a una delle principali problematiche legate alla fornitura di terapie robotiche, cioè renderle accessibili al maggior numero di persone di cui ne hanno bisogno, ed in particolare poterle eseguire direttamente nelle case dei pazienti.
Focalizzandosi sulla questi obiettivi, il progetto è stato suddiviso in due macro attività: lo sviluppo di nuove soluzioni per aumentare la backdrivibility dei dispositivi aptici e robotici e lo sviluppo di un sistema di controllo ad assistenza adattativa stand-alone. Entrambi gli studi hanno dedicato particolare attenzione nel contenimento dei costi di realizzazione e della complessità del dispositivo.
In particolare, il primo studio consiste nello sviluppo di un algoritmo di sensor fusion, che fonde insieme tradizionali misure di posizione fornite da encoder e segnali di accelerazione ottenute da accelerometri MEMS a basso costo, ed una procedura di identificazione non lineare, basato su un algoritmo RLS, per la stima dei principali parametri meccanici del dispositivo. Le più accurate informazioni di velocità e le più precise stime dei parametri del dispositivo, ottenute grazie alla soluzioni sviluppate, porta ad un miglioramento delle prestazioni (cioè aumento delle bande passanti dei filtri passa-basso e la riduzione del rumore sovrapposto) di due strumenti, DOB e RTOB/RFOB che, senza senza utilizzo di sensori di forza, permettono di ottenere un controllo di forza preciso e una migliore stima della forza di interazione uomo-robot, anche in dispositivi robotici a basso costo.
Il secondo studio consiste nello sviluppo di un controllo ad assistenza adattativa per scopi riabilitativi. Tale algoritmo di controllo è basato su un controllore PD adattativo non lineare, in cui l'adattamento dei parametri del controllo è guidato dal grado di disabilità (valutato attraverso la capacità del paziente stesso di seguire un target in movimento visualizzato a schermo).
Efficacia e benefici degli approcci proposti sono stati valutati mediante la realizzazione di specifici esperimenti con dispositivi robotici a basso costo reali ed eseguendo dei test clinici riabilitativi con dei veri pazienti.

ABSTRACT

The main topics of the Ph.D. project described in this thesis is the rehabilitation robotics, which is, nowadays, a very active field of research, as we are witnessing an increasing demand for rehabilitation therapies. The leading aim of the project is the development of novel control system solutions and tools, which allow and support the use of low-cost rehabilitation robot devices. So doing, it is possible to address main issues related to the provision of robotic therapies, i.e. to make them accessible to a grater number of users and to perform them directly in patients homes.
Focused on these goals, the project has been divided in two macro activities: the development of novel solutions to increase backdrivibility in robotic and hapitc devices and the development of a stand-alone adaptive assistance control system. Both studies have paid special attention in containing device implementation's costs and complexity.
In particular, the first study consists in the development of a sensor fusion algorithm, merging together position encoder measurements and acceleration signals from a low-cost MEMS accelerometer, together with a non-linear identification procedure, based on a RLS algorithm. The more accurate velocity information and more precise device parameter estimations, obtained thanks to the developed solutions, lead to the performance improvement (i.e. higher low-pass filter bandwidths and reduction of added noise) of two force-sensoreless tools DOB and RTOB/RFOB, useful to obtain accurate force control and better estimation of the human-robot interaction force, even in low-cost robotic devices.
The second study deals with the development of an adaptive assistance control for rehabilitation purposes. Such control algorithm is based on an adaptive non-linear compliance controller, in which the adaptation of PD control parameters is driven by the patient's degree of impairments (assessed by the ability of patients to follow a moving target displayed in a screen).
Effectiveness and benefits of proposed approaches have been evaluated performing significative experiments with real low-cost robotic device and actually performing some rehabilitation trials with patients.

PUBLICATIONS

- D. Pilastro, R. Oboe, T. Shimono, "A nonlinear adaptive compliance controller for rehabilitation", *IEEJ Journal of Industry Applications* (Accepted)
- R. Oboe , R. Antonello, D. Pilastro, K. Ito, "Use of MEMS inertial sensors for performance improvement of low-cost motion control systems", *IEEJ Journal of Industry Applications* (Accepted)
- M. Agostini, A. D'Andrea, O. A. Daud, R. Oboe, D. Pilastro, M. Reggiani, A. Turolla, "A PhysX-based framework to develop rehabilitation systems using haptics and virtual reality" in Hu, Fei, Jiang Lu, and Ting Zhang. "*Virtual Reality Enhanced Robotic Systems for Disability Rehabilitation*" IGI Global, 2016. 1-323. Web. 15 Dec. 2015. doi:10.4018/978-1-4666-9740-9
- R. Oboe, D. Pilastro. "Use of Load-side MEMS Accelerometers in Servo Positioning of Two-Mass-Spring Systems", *Proceedings of 41st Annual Conference of the IEEE Industrial Electronics Society*, 2015
- R. Oboe, D. Pilastro. "Stability analysis of a non-linear adaptive impedance controller for rehabilitation purposes". *Proceedings of The IEEE/IES International Conference on Mechatronics* (ICM2015), pp 454-459, 2015.
- R. Oboe, D. Pilastro. "Non-linear adaptive impedance controller for rehabilitation purposes". *Proceedings of the 13th International Workshop on Advanced Motion Control* (AMC2014), pp. 272 - 277, 2014.
- R. Antonello, R. Oboe, D. Pilastro, S. Viola, I. Kazuaki, A. Cenedese. "IMU-based image stabilization in a HSM-driven camera positioning unit". *Proceedings of the IEEE International Conference on Mechatronics* (ICM 2013), pp. 156-161, 2013.

ACKNOWLEDGMENTS

Immeasurable appreciation and deepest gratitude for the help and support are extended to the following persons who in one way or another have contributed or encouraged me in making this study possible.
First of all, I would like to thank to all my family, in particular my mother, my father and my sister, for their love and support. They always believe in me and encourage me during all my course of studies, especially when I doubted of my skills and capabilities.
Also, I can't forget all my friends, in particular Giovanni, Enrico, Filippo, Riccardo, Giulia, Martina, Rossana, Noemi, Silvia, Sebastiano, Andrea, Stefano and many others. With them, I spent lot of my time during these years and they have contributed, in their own way, to the achievement of this work.
Special thanks are due to my Supervisor Prof.Roberto Oboe for his meaningful assistance, tireless guidance and patience. His right advices at the right time, valuable comments and suggestions were fundamental in the completion and success of this study. It was a pleasure working with him and under his supervision. He has been able to convey his passion for the research job and, in particular, for his research topics. And he is a model to be aspired to, not only from the academic point of view.
I would like to express my gratitude to all other professors who, using their knowledge and their time, have taught me very interesting and useful subjects.
In addition, I would like to thank the Japanese professors, prof. Kouhei Ohnishi and prof. Tomoyuki Shimono, whom welcomed me in their own laboratories for a few months. They kindly supported my researches, providing me useful advices. Their laboratories were very exciting and challenging environments, where I had the opportunity to work with the most advance haptic technologies available.
In addition, I would like to thank colleagues and technicians working with me in the laboratory,in particular Riccardo, Fabio, Roberto and Koyo. Their supports, advice and help has been fundamental in the development of my researches.
Finally, I would like to thank Ms. Yuri Hasegawa, Prof. Shinichiro Ishii and physical therapists at the "Kazenotani project" rehabilitation center in Miura, Kanagawa, Japan, for their support and collaboration in the performing of the clinical tests. Also, a special thanks go to patients who, kindly, participated in the trials.

CONTENTS

LIST OF FIGURES

LIST OF TABLES

ACRONYMS

aaKF acceleration aided Kalman filter

ADL activities of daily living

AFO ankle-foot orthosis

ARM Assisted Rehabilitation and Measurement

ARMA autoregressive moving average

DAC digital to analog converter

DOB disturbance observer

DOF degree of freedom

EMG electromyography

ETFE empirical transfer function estimate

IMU inertial measurement unit

I/O input/output

KF Kalman filter

LMS least mean squares

LQE linear quadratic estimation

LTI linear time invariant

MAE mean absolute error

MEMS micro electro-mechanical systems

MIME Mirror Image Movement Enabler

MIT Massachusetts Institute of Techonology

PAM pneumatic artificial muscles

PD proportional-derivative

PMA pneumatic muscle actuators

RBF radial-basis function

RLS recursive least squares

RFOB reaction force observer

RTOB reaction torque observer

RTOB/RFOB reaction torque/force observer

RR rehabilitation robots

VR virtual reality

SCI spinal cord injury

SDE standard deviation error

UN United Nations

ZOH zero order hold

Part I

INTRODUCTION

1 INTRODUCTION

The rehabilitation robotics is the main topic of the Ph.D project presented in this thesis. Such novel field of research is dedicated to understanding and promoting rehabilitation through the application of robotic devices. It is becoming a common approach for treating motor disability induced by several pathologies, such as stroke, neurologic injuries and muscoloskeletal disorders. In fact, it helps patients in regaining essential skills and relearning simple movements.
In recent years, due to the increase in demand for rehabilitation therapies, many research projects and studies have started the development of specific robotic systems, focused on particular rehabilitation robotics applications. This has been further spurred by recent technology improvements and progresses, which provide fundamental software and hardware tools useful to the design of these robot devices and control systems. As a result, rehabilitation robotics is currently a very active field of research, attracting the attention and interest of many researchers.

1.1 MOTIVATIONS

According to the annual United Nations (UN) report [1], we are witnessing an increase of the worldwide elderly population, as Fig.1 shows. In the last few decades, the number of people over 65 years is constantly growing worldwide and, based on some forecasts, by 2050 it will be almost two times the present one.
Furthermore, such phenomenon occurs more intensely in industrialized countries. In Italy, for example, by 2050, the population over 65 years will be more than 35% of the overall population (see Fig.2), while worldwide elderly population will be just 16%.
One of the major issues related to increase of the elderly population is that such age group is particularly prone to cerebrovascular injuries (e.g. strokes) neurological diseases (e.g. Parkinson's disease, tremor, Guillain-Barre syndrome, multiple sclerosis) and muscoloskeletal disorders. Nevertheless, progresses in medicine have made treatments of such pathologies possible, reducing the severity of their effects and increasing the survival rate. However, such higher disability incidence leads to an increase in demand of rehabilitation therapies [2].
Indeed, such increasing trend is sustained and promoted by several scientific studies showing how the plasticity of the human nervous system can be better exploited in relearning simple movements and regaining everyday life skills, if patients perform more therapies and treatments. In particular, this is a clear evidence in stroke patients, where it is also very important the timeliness in performing such rehabilitation therapies, after the acute events. So, it is easily understandable how the amount of recovery is closely linked to the amount,

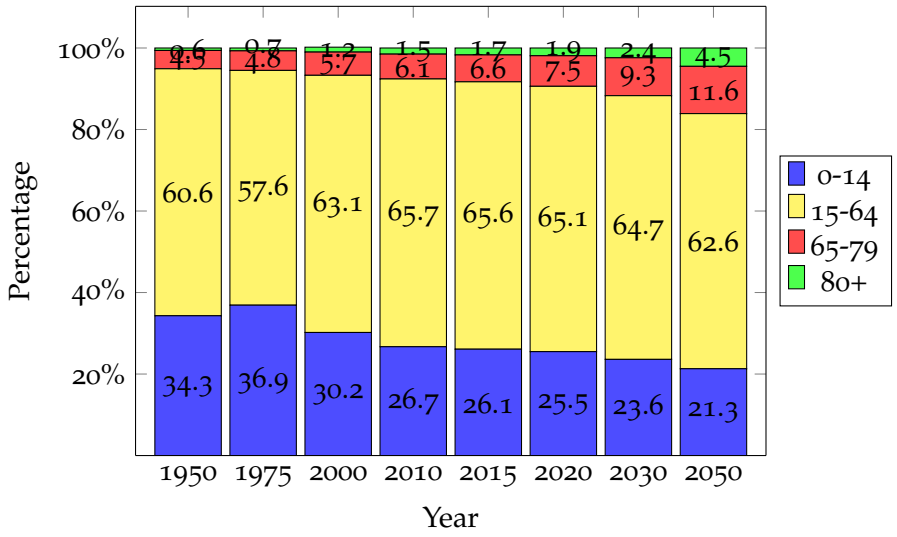

Figure 1: World population by age (rates and forecastings) [1].

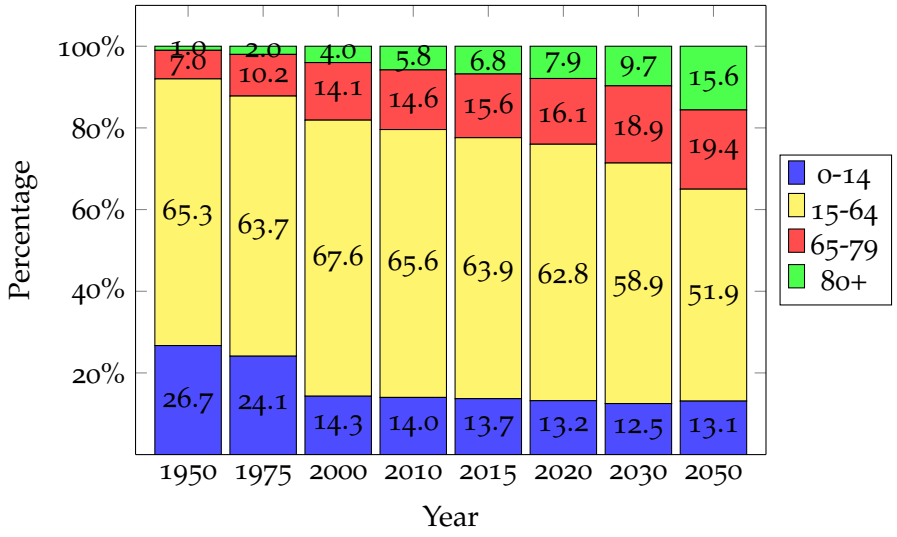

Figure 2: Italian population by age (rates and forecastings) [1].

frequency and task-orientation of trainings and practices [3–6].
In order to help to increase the amount and the intensity of treatments, a new field of research, called rehabilitation robotics, has grown in recent years. In fact, such engineering branch is dedicated to understanding and promoting rehabilitation through the application of robotic devices.
A number of research project in the field of robotics and bioengineering have been launched, with the main purpose of designing and testing robotic devices and haptic interfaces, to be use in rehabilitation. Moreover, many studies have been focused on the development of control strategies which manage how such robotic devices interact with participants. Their leading purposes consist in the development of robotic systems which can implement specific exercises to be performed by the subjects, promoting their motor plasticity and speeding motor recovery. Currently, however, there are not clear and specific scientific evidences of how such goals can be achieved in the best

but simplest way. Consequently, the designed control strategies take inspiration from concepts developed in rehabilitation, neuroscience and motor learning literature, trying to emulate physiotherapist behaviors during treatments.

1.2 BACKGROUND

1.2.1 *Strokes*

Stroke, also known as cerebrovascular accident or brain attack, occurs when poor blood flow to the brain results in cell death. There are two main types of stroke: ischemic, due to clot obstructing the blood flow to the brain, and hemorrhagic due to a blood vessel rupture, which prevents blood flow to the brain.
If a stroke occurs some brain regions cannot get blood, that carries oxygen and nutrients they need, therefore they start not to function properly. Since the brain controls several body functions, when a stroke occurs, body parts, controlled by the affected brain regions, will not work as they should. As consequence, signs and symptoms depends on the specific brain areas where stroke takes place. They may include:

- sudden weakness;
- paralysis or numbness of the face, arms, or legs, especially on one side of the body;
- problems speaking or understanding speech;
- loss of vision in one or both eyes;
- dizziness, trouble walking, loss of balance or coordination.

Focusing on the motor impairment aspects, hemiparesis/hemiplegia is the most common and severe outcome of strokes. It leads weaknesses and movement deficits in limbs on the opposite side of the brain affected by the stroke. The main characteristics observed in hemiparetic subjects are:

- abnormal muscle tone, which refers to an increase in the felt resistance to passive movement of a limb;
- impaired inter-joint coordination, which can lead in loss in control degrees of freedom and decreased smoothness of movement;
- loss of somato-sensation, which refers to a decreased ability to sense the movement of body parts;
- muscle atrophy, resulting in decreased passive range of motion of joints.

The incidence of such disease is very severe. Indeed, in 2013, stroke was the second most frequent cause of death after coronary artery

disease, accounting for 6.4 million deaths worldwide (12% of the total)[7]. Overall, two thirds of strokes occurred in those over 65 years old, showing how this age group are highly affected by such pathology [8]. In Italy, statistical data are similar (see Fig.3). In fact, stroke is the fourth leading cause of death, the first cause of disability and second one of dementia [9]. Nevertheless, progresses in medicine have made treatments of such pathologies possible. Consequently, nowadays, the number of stroke survivors is increasing.

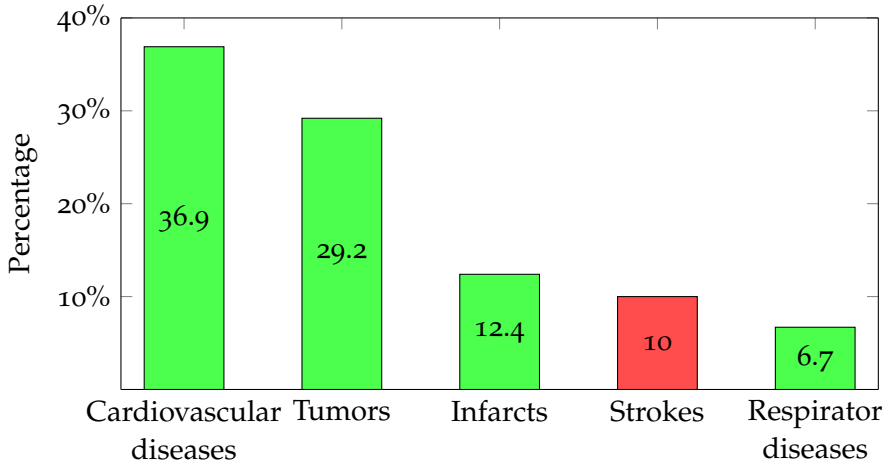

Figure 3: First five leading causes of death in Italy in 2011 [9].

1.2.2 *Manual rehabilitation therapies*

People affected by motor impairments, due to neurological diseases or injuries, such as strokes or spinal cord injury (SCI) or muscoloskeletal disorders, strongly need rehabilitation therapies to promote recovery of their lost motor functions and to improve muscular strength and movement coordination. By so doing, rehabilitation therapies aim to ensure the highest level of autonomy in performing activities of daily living (ADL) to impaired subjects and, so, the best quality of life. A secondary goal is to prevent side effects of motor inactivity, such as muscle atrophy, osteoporosis and spasticity.
Nervous system plasticity is one of the main aspects in motor recovery. In particular, in case of stroke survivors, the best recovery seems to result from reorganization in the damaged brain hemisphere. Some studies show that such neurologic and functional recovery is faster and it is possible to achieve better rehabilitation outcomes [5, 10]. In fact, higher improvements in strength, synergism, dexterity, walking ability and ADL can be observed in such period than later, in the chronic phase. Nevertheless, more and longer training sessions have positive recovery effects also in chronic phase. So, it is clear that training intensity is crucial to promote cortical reorganization after stroke, and so to obtain better rehabilitation progresses[11–14]. Similar clinical outcomes can be expected in several other diseases.
Traditional physical treatments, which aim to promote plasticity, rely in performing exercises with the supervision and support of a phys-

(a) Treadmill trainings [15] (b) Reaching object trainings [16]

Figure 4: Examples of manual rehabilitation therapies.

iotherapist, typically on a person-to-person basis. Usually, such exercises consist in repetition of task-oriented movements, e.g. treadmill trainings, reaching or contouring objects (See Fig.4). Therapist's aid is based on rehabilitation, neuroscience and motor learning theories but, also, on his/her past experiences. In fact, physiotherapists continuously tailor the exercises according to patient's impairments, challenging them to improve their skills. Patients performances and progresses are subjectively evaluated by therapist's perceptions.
At present, such physical therapies are the standard approach in treating such disabilities and impairments. Unfortunately, they are labor-intensive and very expensive. Therefore, training duration is usually limited by personnel shortage and fatigue of the therapist rather than by that of patients. As a consequence, training sessions are shorter and may not lead to desired therapeutic outcomes.
Finally, manual-assisted rehabilitation therapies lack in duration, repeatability and does not provide an objective assessments of patient state and improvements[17].

1.3 REHABILITATION ROBOTICS

The current manual medical practice does not provide suitable training intensity to subjects affected by cerebrovascular disorders, neurologic pathologies and traumatic injuries, who show partial or complete motor impairments in upper and/or lower limbs [18, 19].
Robotic rehabilitation therapies seem to be a novel and realistic approach to assist people with disabilities, providing physical trainings and assisting them in regain essential skills and relearn simple movements. In particular, robotic devices and specific virtual reality (VR) systems can help therapists, during the rehabilitation process, in two different manners: as an artificial therapist and as an evaluation tool. Firstly, they can reduce problems of high costs and limited human resources related to treatments. Indeed, rehabilitation robots (RR) are able to provide intensive rehabilitation, consistently for a longer duration. Specifically, they are more efficient in delivering repetitive and labour-intensive trainings, alleviating strain on therapists. Such robotic therapy aspect is crucial, as the recovery process is typically slow and driven by duration and intensity of the physical therapies.

In addition, such technologies allow the physiotherapist to just manage clinical decisions, before treatments (e.g. planning tasks to be performed, tailoring robot assistance according to the patient's impairments) while the robot device performs trainings autonomously. That makes possible for a single therapist to supervise more than one patient at the same time, enhancing clinician's productivity, and so leading to time and money savings.
Secondly, RR may provide a rich stream of data, thanks to several typologies of sensors that can be found on board (e.g. position sensors, force/torque sensors and electromyography (EMG) sensors). Such information may help clinicians in obtaining accurate and objective assessments of patient conditions and, also, monitoring patient strength, residual voluntary activity or motor performances. As a result, RR can be use as a tool to facilitate patient's quantitative diagnosis, patient's fatigue monitoring and customisation of the therapies and, lastly, maintenance of patient records. Moreover, patients performance histories and trends provide very useful information, that may be available to the therapists to better understand the rehabilitation process.
Finally, taking advantage of recent improvements in robotics and information technology, traditional rehabilitation practice can be enriched providing advanced and more technological tools. The latter can better enhance and quantify rehabilitation and, concurrently, productivity and, in turn, optimize the quality of care.

1.3.1 *Rehabilitation robotic devices*

In the last years, a growing number of investigations have been developed in order to design robotic system for both upper and lower limbs rehabilitation therapies. Particular interest has been focused on designing more sophisticated, many degree of freedom (DOF) robotic devices, in order to support both simple and complex limbs trainings, such as walking or multi-joint arm and hand movements. Frequently, such robot are not used in a stand-alone fashion but they integrate suitable VR tools, in order to provide a complete multi-sensory feedback (haptic[1] and visual feedback) to the user. As a result, the rehabilitative exercise may become more interactive and better motivate and coach the user. In addition, proprioceptive[2] sensation, which provides many different input to the nervous system, better encourage and promote its plasticity. A typical application consists in stand-alone rehabilitation robotic system, in which the patient interacts with a N-

1 The word haptics, which comes from the Greek words *haptós* "palpable" and *haptikós* "suitable for touch", means "related to the sense of touch". According to the psychology and neuro-science literature, haptics corresponds to the study of human touch by kinesthetic and cutaneous receptors, that are associated with perception and manipulation. In the robotics and VR literature, haptics is largely defined as real and simulated touch interactions between robots, humans, and real, remote, or simulated environments, in various combinations.

2 The word proprioception come from Latin *proprius*, meaning "one's own", "individual", and *capio*, *capere* meaning "to take or grasp". It is the sense of the relative position of neighbouring parts of the body and strength of effort being employed in movement.

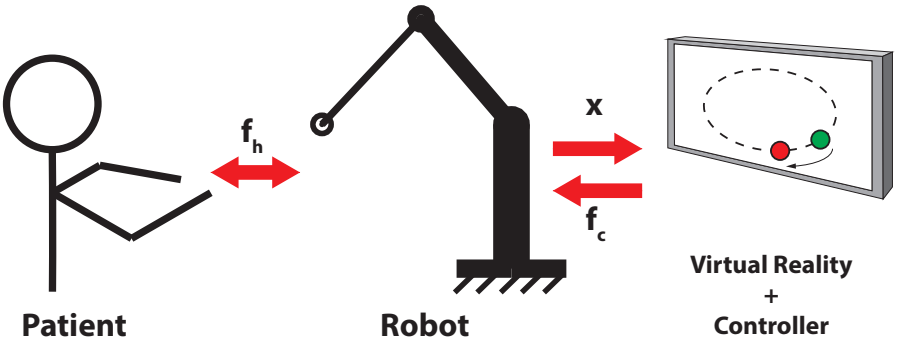

Figure 5: Schematic representation of a typical stand-alone robotic rehabilitation system and related therapy.

DOF robotic device, which is also interfaced to a VR environment. In this setting, a common rehabilitation task consists in asking the patient to follow a moving target, displayed in the VR environment, by properly moving the robot end-effector (see Fig.5). Usually, the target movement repeatedly follows a specific trajectory, defined by the therapist. More complex exercises may reproduce activities of daily living into the VR environment.
RR devices are, essentially, designed for two main applications:

- support in performing some ADLs
- provide physical therapies.

There is a increasing demand for powered devices supporting simple ADLs, such as actuated exoskeleton and orthoses, as they can actually improve quality of life and encourage independent living of users. Unfortunately, due to technical (portability, weights and energy management) and economical (multi-DOF structure, mechanical complexity, safety issues) restriction, it is possible to find only a few of them available. For these reasons such devices are not taken into account in the following discussion.
On the other hand, it is possible to see a great and persistent evolution in developing devices providing physical therapies. A great effort has been made to design suitable device which can provide functional and task-oriented trainings both for upper- and lower-limbs. Nevertheless, one of the greatest disadvantage is that a large number of these devices may be used only in specialized centers or therapeutic institutes. Additionally, their complexities and prices are often prohibitive for personal use. Furthermore, such robots usually require supervision and assistance from qualified personnel. Typically, therapists prepare the clinical setup, placing sensors (e.g. EMG sensors) and setting robot parameters and characteristics, then they teach the user to correctly interface with the robot and how to perform the exercises.
Given that patient demand for home-base therapy is expected to increase, one of the most challenging goal is developing new RR, properly designed for patient use at home. Particular aspects, that should be taken into account, are:

- simple mechanical and electrical structure;
- easy and fast set-up in order to be the most user-friendly as possible;
- adaptable behavior to tailor the exercises according to different types of patients and degree of impairments, autonomosly;
- reasonable price.

Currently, many research studies are driven by these important aspects, trying to find the best suitable solutions.

1.3.1.1 *Lower-limb robotic rehabilitation devices*

Body weight support treadmill trainings and knee and ankle trainings are widely performed with incomplete SCI and stroke patients. Their leading aims are to increase participant muscle strength, motor control and coordination ad so resulting in an overall improvement of walking capabilities. Normally, such training therapies are manually delivered. Patient's paralysed legs are physically operated by one or two physiotherapists. In order to alleviate therapists effort, in the last decades, robot-assisted therapies have become increasingly used to treat impairments affecting lower-limbs. A great number of assistive robotic systems, such as treadmill gait trainers, ankle trainers, active foot orthoses has been developed.
LOKOMAT is the best example of a driven gait orthosis, currently available in the market (see Fig.6a). It has been extensively used in many clinical researches [20–22]. It consists of three main parts: a body weight support, a treadmill and a bilateral powered leg orthosis with actuated hip and knee joints. Considerable control algorithms, such as position, impedance or adaptive controllers, have been implemented in this system in order to improve its rehabilitation performances. An other example of existing treadmill gait trainer for lower-limb rehabilitation therapy is the ReoAmbulator system (see Fig. 6b). This RR has, also, been used in many specialized centers and hospital and in many research studies [23, 24]. The system implements a powered leg orthosis with the use of robotic arms attached to the thigh and ankle of the user's legs. A stepping pattern is performed using the implemented control strategy, which provide the needed assistance to correctly complete the movements.
Furthermore, recent years have shown an increasing interest in developing pneumatic muscle-type actuators, such as McKibben artificial muscles, rubbertuators, air muscles, pneumatic artificial muscles (PAM) or pneumatic muscle actuators (PMA). Such novel actuator typologies, which are biologically inspired, have an important role in designing new assistive rehabilitation robotic systems with interesting compliant and interactive features. An example of such robot devices is a bio-inspired prototype of an ankle-foot orthosis (AFO) powered by PAMs and proposed in [26, 28, 29]. Such prototype can comfortably provide dorsiflexion and planter flexion torque during walking motion trainings. It is composed of a hinge joint, a carbon

(a) LOKOMAT [22]

(b) ReoAmbulator [25]

(c) AFO [26]

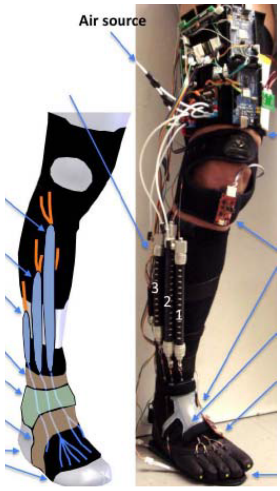

(d) Bio-inspired active soft AFO [27]

Figure 6: Lower-extremity robotic therapy devices.

fiber shell and two PAMs, as shown in Fig.6c. A proportional myoelectric control has been implemented in order to provide the assistance during patient's walking. Similar AFO rehabilitation device, for treating pathologies associated with neuromuscular disorders, has been proposed in [27]. The design of such orthosis takes inspiration from the biological musculoskeletal system, as a result the PAM actuators have been designed and placed according to muscle-tendon-ligament structure of a human leg (see Fig. 6d). Three types of sensors are used in the control system: strain sensor to measure the ankle joint angles, inertial measurement unit (IMU) for measuring orientation of the lower leg and the foot and pressure sensor to identify the foot-ground contact and gait cycle events. A feed-forward and feedback controllers are implemented providing good repeatability of the ankle joint angle control.

1.3.1.2 *Upper-limb robotic rehabilitation devices*

Subjects with upper-limb impairments have difficulties in performing many simple ADL, such as reaching to grasp objects. Such disorders specially limit the independence of the affected subject. Moreover, after a stroke attack, upper extremities are typically affected more than the lower extremities [30].
For such reasons, in the last years, a big effort has been done to develop several types of robotic devices, properly designed to deliver upper-limb rehabilitation therapies. Indeed, it has been shown that task-oriented exercises better promote recovery process, compared to functional exercises. So rehabilitation robotic systems tends to have many actuated DOFs and to interface with VR systems in order to better replicate normal daily living actions.
For example, the Assisted Rehabilitation and Measurement (ARM) Guide [31], has been designed to mimic the reaching motion. The robot consists of a single motor and chain drive which is used to move the user's hand along a linear constraints. The orientation of the guide can be manually changed to allow reaching in various directions. The ARM Guide implements an essential control technique, called "active assist therapy" which helps the users to complete a desired movement if they are not able to do by themselves. The Mirror Image Movement Enabler (MIME) therapy system [32] is a six-DOF robot device, an orthosis, supporting the user's affected arm, which is attached at robot's end-effector. Such robot device can apply forces to the limbs during both unimanual and bimanual movements in three-dimensional space. In unilateral trainings, the robot assists the impaired limb movements, which tries to follow a moving target along a pre-programmed trajectory. The bimanual mode works in a master-slave configuration, the robot assistance of the affected limb is obtained mirroring the unimpaired arm movements. The Pneu-WREX [33] is the actuated version of the previous passive device called T-WREX [34]. It is a multi-DOF robot using low-cost pneumatic actuators, which can apply a wide range of forces during normal upper extremity movements. The user, properly moving the robot, interacts with a real-time Java-based simulator, where programmable VR games, which mimic ADL (e.g. cooking, ironing, painting), can be performed. The Massachusetts Institute of Techonology (MIT)-MANUS [35] is the most famous upper-extremity RR device, and, also, the one which has received the most clinical tests. It consists of a 2-DOF robot manipulator, characterized by low inertia and friction, that assists shoulder and elbow movements by moving the user's hand in the horizontal plane. Typical trainings are performing reaching movements though interaction with a virtual environment on a computer screen.

1.3.2 *Rehabilitation robotic control strategies*

RR are becoming increasingly common both in upper and lower extremity rehabilitation therapies. Such trend is also endorsed by rele-

(a) ARM Guide [31]

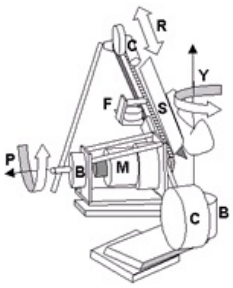

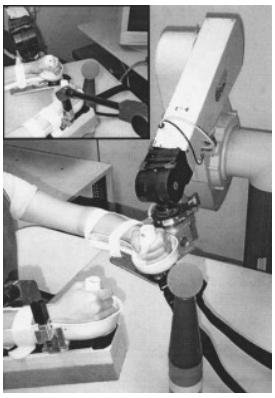

(b) MIME [32]

(c) Pneu-WREX [33]

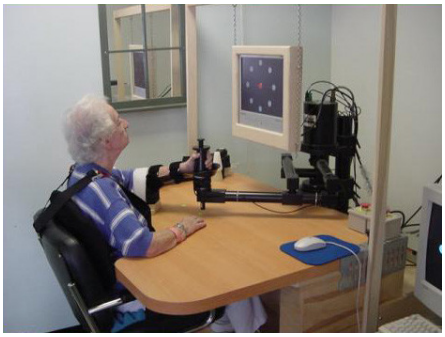

(d) MIT-MANUS [35]

Figure 7: Upper-extremity robotic therapy devices.

vant studies showing how they can contribute significantly to motor recovery [36–38]. Currently, researchers effort has focused on both design of novel and complex robot mechanisms, as shown in Sec.1.3.1, and development of control strategies which define the robot behavior and, so, how it interacts with participants.

The leading goal of rehabilitation robotic control algorithms is to control robotic devices and to provide suitable force feedbacks, during patient's execution of rehabilitation exercises. Such interaction force aims to coach and challenge participants and, at the same time, to stimoulate nervous system plasticity and, consequently, enhance motor recovery. Currently, however there are not solid scientific understanding on how such goal can be best achieved. Therefore, robotic therapy control strategies have been developed based on concepts and experiences from manual rehabilitation therapies, neuroscience and motor learning literature. Moreover, at the moment, there are not significative clinical outcomes which can address the choice of a specific control strategy typology. At most, there are some initial evidences that some control strategies are more effective and efficient in promoting rehabilitation than others.

In the following, an overview of the current control algorithms available in the literature is presented. One approach to group such control algorithms is according to the strategy they implement to stimulate plasticity [39]. As a result, four categories of controllers can be identified:

- Assistive controllers;
- Challenge-based controllers;
- Haptics control systems;
- Non-contacting coaches.

1.3.2.1 *Assistive controllers*

The most developed paradigm on rehabilitation robotic control strategy is the assistive one. Assistive controllers help participants to correctly move their weakened limbs in desired patterns, for example grasping, reaching, or walking rehabilitation trainings. It takes inspiration from traditional active assistance exercises manually performed by rehabilitation therapists.
Such active assistance exercises may provide many important benefits, such as:

- stretch muscles and connective tissues;
- move limbs in a manner that can not be performed autonomously by the patient or requires too much effort;
- reduce spasticity and increase limbs range of motion.

Furthermore, the assistive action can teach patients how to properly perform the assigned task, providing novel somatosensory stimulations that help induce brain plasticity and reestablish o create new motor output patterns [40, 41]. Physically assisting movements can also help a participant to perform more desired movements in a shorter amount of time, potentially promoting repetitive and intensive practice [32, 42].
On the other hand, there could be some drawbacks in using physical assistance during movements. In fact, it may actually decrease motor learning[42, 43]. The reason is that physically assisting a movement changes the dynamics of the task so that the learned task is not the desired one. Guiding movement also appears in some cases to reduce patient's physical effort and participation during motor training, reducing the burden on the learner's motor system to discover the necessary principles to successfully perform the task. It is clear how too much assistance may lead to poor benefits from the rehabilitation point of view. As a consequence, a more complex paradigm, called "assistance-as-needed", which means to assist the participant only as much as is needed to accomplish the task can be used in the development of assistive control strategies. More detailed discussion, regarding such controllers, will be presented in 3.1.1.

1.3.2.2 *Challenge-based controllers*

The term "challenge-base" controllers refers to controllers that behave in a opposite fashion, compared to assistive controllers, as they make movement tasks more difficult or challenging, during trainings. These controllers can provide:

- resistance to the participant's limb movements;
- require specific patterns of force generation;
- increase the size of movement errors, providing suitable force fields which push participant's limb away from desired trajectory.

Resistive exercise is a typical therapeutic strategy of providing resistance to the participant's hemiparetic limb during movements. Indeed, there is a reasonable amount of clinical evidence, in non-robotic studies, showing how such type of rehabilitation therapy can help affected persons improve their motor functions, as it requires higher effort from the impaired limb [44–46]. In the literature, several control strategy solutions can be found, in order to provide resistance forces during robotic rehabilitation therapies, such as: constant resistive forces [47–50] or viscous resistances [32] applied at the end-effector of the robots or moving against gravity in robotic systems were gravity effects can only partially compensated [51, 52].
Other researches have shown how kinematic errors, generated during movements, are a fundamental neural input that drives motor adaptation and rehabilitation process. Thus researches have addressed new robotic therapy algorithms which amplify movements errors rather decrease them, as in the assistive controller case. For example, such algorithms can amplify errors, in upper-limbs reaching trainings [53, 54] or in gait trainings [55]. Several other studies have shown that some benefits of error amplification can be achieved by distorting visual feedback from the desired task, rather than by physically altering movements [56, 57].

1.3.2.3 *Haptics control systems*

Robotic therapy devices can be also used as haptic interfaces to interact with VR systems or to design teleoperation systems.
In the first case, robots are used as tools to interact with VR simulations, where some ADLs, such as manipulating objects [58–63] or walking across a street [64, 65], are replicated (an example can be seen in Fig. 8a). Potential advantages of this rehabilitation training approach are: VR tools flexibility allows to easily change working scenarios and exercises to be performed, so a wide range of real-life situation can be simulated and exercise's difficulty can be easily set-up and adapted. Moreover, visual and haptic feedbacks can increase patient motivation e participation in trainings.
In the second case, thanks to the implementation of a bidirectional position-force control between a pair of robotic systems, it possible to achieve a bidirectional exchange of haptic sensation between patient and therapist or between affected and healthy limbs. In the first application, patients and therapists can remotely interact even though they are not in the same place, allowing to perform rehabilitation therapies directly at patient's home. The same interaction forces and movements are felt by both users, thus physical training are executed and

therapists can monitor patient's performances. The second application is particularly useful for stroke survivors, who typically present impairments in a single side of the body. Using such devices is possible to provide bimanual rehabilitation therapies where the healthy limbs can teach and assist movements of affected one, promoting also plasticity of the nervous system. Some scaling factors can be used to adapt (increase o diminish) applied forces, facilitating or challenging the patient or therapist job. An example of such device typology is the force transceiver develop by Ohnishi Laboratory in Keio University (see Fig. 8b).

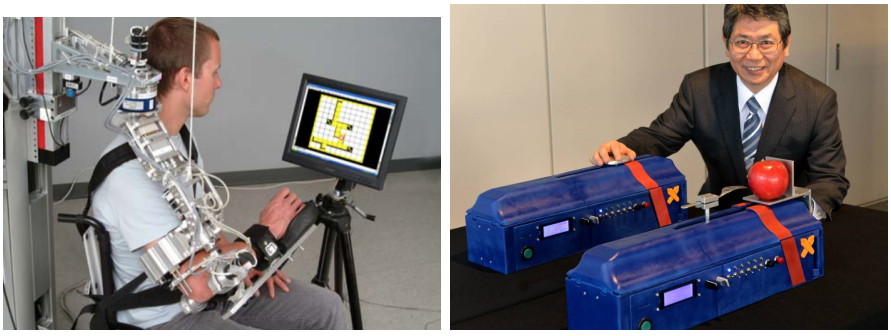

(a) ARMin [58] (b) Force transceiver [66]

Figure 8: Rehabilitation robotic haptic devices.

1.3.2.4 *Non-contacting coaches*

A recent and interesting research area in the field of rehabilitation robotics is the development of mobile robots and related control strategies which do not physically interact with participants but rather operate beside the participant, directing and encouraging therapy activities [67] (see Fig. 9). Such robots try to overcome one of the relevant lack, compared to human manual therapies, which is the therapist's psychological and motivational support. The latter may play an important role in the rehabilitation process.
Currently, a computer by itself could provide auditory and visual instructions and feedbacks, however there is evidence that people respond differently to "embodied" intelligence [68]. Therefore, physically embodying the coaching system in a robot may bring novel and relevant neuro-psychological mechanisms, which may promote recovery during movement training.

1.4 PH.D. PROJECT

From this short introduction, it is possible to understand how, nowadays, rehabilitation robotics is challenging a great number of researchers and affecting several research subjects, such as: mechanical and electrical design of new robotic devices, development of suitable control techniques, processing of patient muscular and brain signals and subsequent analysis of physical measurements (derived from assistive devices).

Figure 9: Therapist robot encouraging and monitoring stroke patient during the rehabilitation therapy [69].

Going into detail of this dissertation, studies and activities carried out during the development of this research are part of a project sponsored by the Ministry of Health, of which the University of Padua is a partner. The leading aim of such project is the development of low-cost rehabilitation robot prototypes and related control systems. So doing, it is possible to address some of the main issues related to make robotic therapies accessible to a greater number of persons who need them. More specifically, the final goal consist in the development of a robotic device suitable to perform robotic therapies directly in patients homes. Consequently, patients may autonomously perform robotic therapies increasing the number of useful trainings and promoting a faster recovery.
Research activities, described in the next chapters, are essentially dedicated to the development of novel control system solutions and tools, which allow and support the use of stand-alone and low-cost rehabilitation robot devices. Particular attention has been paid to improve fundamental device's features, such as force control and interaction force estimation capabilities. Moreover, a suitable control strategy has been developed in order to provide a stand-alone rehabilitation robotic system, which can assist participants during training sessions autonomously.
The first issue addressed is the typical low backdrivability characterising low-cost devices, due to the poor quality of inexpensive components. Their characteristics, such as mechanical friction or big inertia of the system, may lead to poor force control of the device and, consequently, inaccurate command of the interaction force. Such features are extremely important in the design of haptic and rehabilitation robot devices. Furthermore, good force control capabilities are useful for safety features of the robotic device, as it is possible to properly limit the force exerted by the robot at its end effector.
A simple solution to this problem is the use of force or torque sensors. Unfortunately, it is at odds with the development of low-cost systems, as such sensors are typically expensive and not so easy to be implemented.
In order to overcome this backdrivability issue and, at the same time,

implement a simple but effective solution, the approach described in this dissertation makes use of well known force-sensorless tools, i.e. the disturbance observer (DOB) and the reaction torque/force observer (RTOB/RFOB). In particular, some novel solutions and algorithms have been implemented to improve overall DOB and RTOB/RFOB performances. Such innovative aspects consists in the design of a sensor fusion algorithm, merging together position encoder measurements and acceleration signals from a low-cost MEMS accelerometer, and the development of a non-linear identification procedure, based on a RLS algorithm. Resulting benefits are a more accurate velocity information and a more precise identification of device parameters (in particular, the non-linear friction). Such accurate information used in the previous mentioned force-sensorless tools, leading to their performance improvement (i.e. higher low-pass filter bandwidths and reduction of added noise). Consequently, with an inexpensive and not invasive system modification, it is possible to obtain accurate force control and better estimation of the human-robot interaction force, even in low-cost robotic devices.

The goal of the second main activity, carried out in this project, deals with the development of an adaptive assistance control for rehabilitation purposes. Desired features of this controller are the capability to emulate therapist behavior, providing the least assistance needed, and the capability to estimate and evaluate participant's state and improvements. Focusing in maintaining low realization costs and a simple system's structure, this study has been carried out to obtain the best possible performances in terms of promoting rehabilitation without including additional sensors or tools except standard position sensors. Such control algorithm is based on an adaptive non-linear compliance controller, in which the adaptation of PD control parameters is driven by the patient's degree of impairments (assessed by the ability of patients to follow a moving target displayed in a screen). So doing, it is possible to obtain a very simple and flexible control system, which can be easily implemented in many different robotic device, allowing the system to autonomously assist patient in performing simple rehabilitation trainings.

The following dissertation is organised as follows. Chapter 2 presents proposed force-sensorless tools to address backdrivability issues. Both sensor fusion algorithm and non-linear identification procedure are explained, while benefits and positive results are also in shown performing significative experiments with a low cost rehabilitation robot prototype. Chapter 3 presents the novel adaptive control algorithm, its control stability proof and some preliminary clinical test with real patients. Finally, some conclusions and final remarks are reported in Chapter 4.

Part II

PH.D. PROJECT

2

HAPTICS AND BACKDRIVABILITY ISSUES

2.1 INTRODUCTION

The leading aim of this Ph.D. project is the study of innovative technologic solutions in order to support the use of low-cost rehabilitation robot devices and promote robotic therapies directly in patients homes. Focusing on the development of novel low-cost rehabilitation robot device, particular attention should be paid in the design of mechanical and electrical structure. In fact, it is very important to keep structure's complexity as simple as possible, for example by minimizing the number of sensors used. So doing, it is possible to keep devices prices reasonable, making them available to a greater number of persons.
Even with a simple structure, these low-cost device must have suitable features in order to be used in rehabilitation robotic applications, such as:

- provide sufficient forces and torques compared to the ones applied by participants;
- accurate force control, in order to design good compliant and haptic devices;
- high safety level, as there is a direct contact between robot and participants.

In order to ensure a suitable device structure and low realization costs, combination of servo motors and high-ratio gears, such as ball screws or harmonic drives, are widely used in RR [31, 58]. Unfortunately, these systems are typically characterised by high perceived inertia and friction, which lead to pure haptic performances. On the other hand, direct-drive motor solution are also suitable, as they are almost free from backlash and friction issues and can easily perform precise and safe motion. However, conventional direct-drive motor solutions are rarely used because motors are typically too big or too weak. In order to solve such limitations, ongoing researches are focused on the development of novel but more complex actuator typologies, such as helical motors described in [70].
The use of force and torque sensors (see Fig.10) can solve previously decribed force control issues. Unfortunately, they are typically very expensive, consequently, they are not convenient from a cost point of view. Moreover, they have some additional drawbacks. They are breakable, with low bandwidths and resonant structural vibrations due to the compliant structure of strain gauge. As a result, controllers relying on force measurements are often fragile in case of impact with hard environments or unintended collisions.
In order to address all the above issues, many studies have been

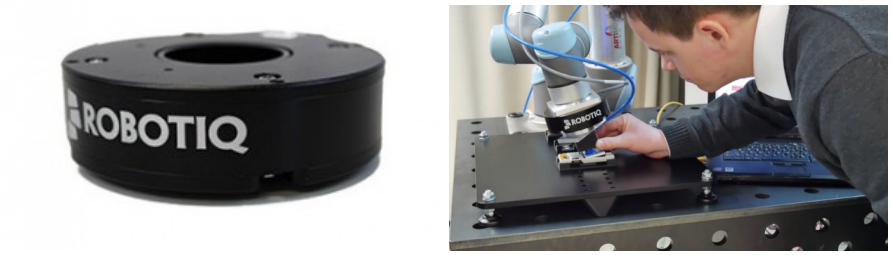

(a) (b)

Figure 10: Robotic force torque sensor from Robotiq [71].

performed on sensorless control technologies. In particular, DOB and RTOB/RFOB control tools have become a preferred approach to improve robustness of force control and accuracy in force estimation. Many applications, implementing such tools, confirmed that they can be used instead of real force sensors [72–75].

2.1.1 *Backdrivability and transparency*

Backdrivability is a fundamental feature in robotic and haptic devices. From a mechanical point of view, backdrivability ensures an equal bidirectionally force transfer between motor side (input) and load side (output), minimizing power losses (see Fig.11). In haptic application it also guarantees the robot transparency which is the ability to move the haptic device end-effector in the workspace without feeling any opposition, due to, for example, robot inertia or friction.
Without using force/torque sensors, backdrivability plays an important role in achiving good robot force control. In fact, higher backdrivability increases driver's sensitivity, allowing to correctly estimate applied forces. As a consequence, backdrivability is essential for:

- stable control of interaction forces and precise haptic sensations;
- safe robotic operations around people and in unstructured environments.

Unfortunately, this feature is affected by limitations and impediments, such as:

- Coulomb and viscous friction;
- inertia of the mechanical components.

Moreover, the introduction of reduction gears implies the amplifications of such drawbacks.
Mechanical systems and robots are typically forward-drivable. Electric current is converted to torque by a motor, that torque is transmitted through a mechanical transmission (or directly) to a driven joint, and the latter drives its associated link that supports either the next link or an end effector, which interacts with a load or an environment.

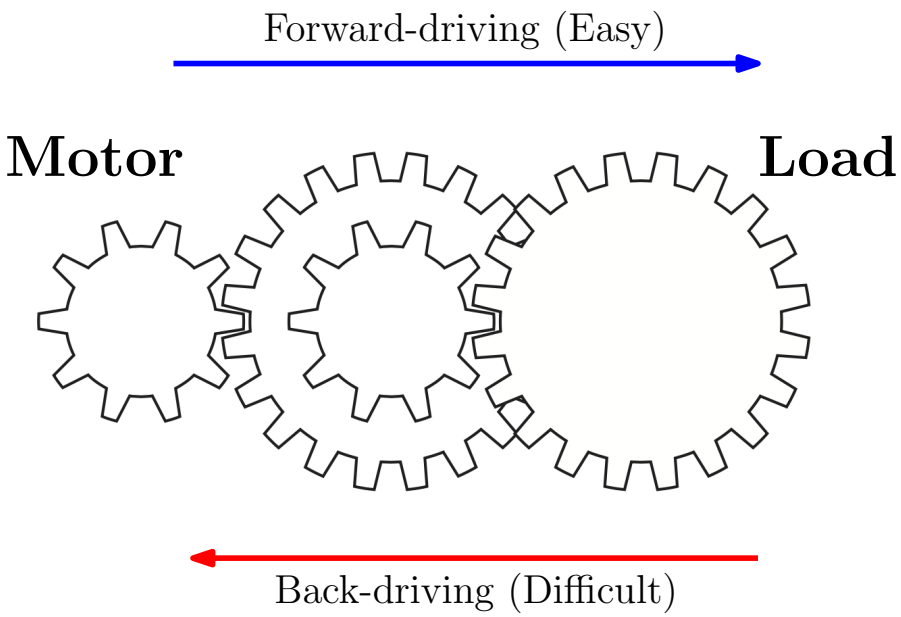

Figure 11: Schematic representation of backdrivability concept.

Some of this forward-drivable systems are simply not backdrivable regardless of the magnitude of the backdriven effort, as for example worm-drive transmissions. The remaining mechanisms are nominally backdrivable at some level of externally applied contact force.
However, functional backdrivability and, consequently, high robot transparency require very small parasitic resistive forces (i.e. inertia and friction) or the use of specific control tools to compensate such undesired effects.
Backdrivability and transparency are becoming increasingly important in applications where robots works closer to human beings and force interaction is crucial issue, such as in rehabilitation robotics. Use of low-cost mechanical components lead to poor backdrivability due to friction, inertia and reduction gears of the systems. Consequently, high force/torque must be provided to execute user-driven movements. Such drawback is critical as, for impaired patients, high friction and big inertia forces can be a barrier they may hardly exceed. On the other hand, higher backdrivability improves the patient's motivation and participation and facilitates the use of the haptic device. Moreover, higher backdrivability is fundamental to obtain correct human-robot interaction force estimation which is an important information not only for safety issues but also to monitor patients participation during therapies and perform robotic assessment of their state and progresses.

2.1.2 *DOB and RTOB/RFOB*

Focusing on robotic applications where only traditional position sensors are used (no force/torque sensors available), the approaches, that can be found in the literature, to improve device backdrivability are:

- feedforward friction and/or inertia compensations [76]

- use of disturbance observer (DOB) and reaction force observer (RFOB) control tools [73, 77].

The first solution needs a priori knowledge of robot end-effector speed and acceleration signals. Due to this fundamental aspect, such solution is not typically suitable for rehabilitation robotics usage. In fact, robot end-effectors are moved by patients and their behaviors and limbs movements are unpredictable.
The second solution doesn't need such assumptions. DOB is a simple and efficient control tool which allows to obtain robust motion control systems and it is widely used in robotics and industrial automation fields. A DOB can estimate and compensate for disturbances acting on the system, such as external disturbances (e.g. friction, load or interaction forces) and system uncertainties (e.g. inertia uncertainties from nominal value). An inner loop provides a feedforward compensation of estimated disturbances to achieve robustness. An outer-loop can be designed around the DOB-compensated system to achieve desired control goals, such as position or force controls. Interesting aspect is that outer-loop controller can be designed by considering the nominal model of the plant, since DOB and nominalizes the system.
Using a similar structure of DOB, also external interaction force can be estimated. Such control tool is called RTOB/RFOB, which has been proposed in [73]. Crucial aspect in the design of RTOB/RFOB is the correct identification of system uncertainties and friction and load forces, which should be subtracted from the inputs of a DOB in order to estimated interaction forces. RTOB/RFOB is typically used in outer-loop design to obtain a force control system. However, stability and performances of this control system are affected by identification errors of parameters used in the RTOB/RFOB design. Finally, main advantage of this approach is essentially the possibility to design robust position and sensorless force control systems.

2.1.2.1 *DOB and RTOB/RFOB implementation*

Taking into account a traditional rigid mechanical system composed by rotative motor with inertia J and torque constant Kt, DOB and RTOB can be implemented as shown in Fig.12. The system is affected by external disturbances:

$$\tau_d = \tau_f + \tau_l + \tau_{int} \tag{1}$$

Considering the nominal system, with inertia J_n and torque constant Kt_n, this is effected by external disturbances and, also, by parameters uncertainties:

$$\tau_{dis} = \tau_d + \Delta J \ddot{x}_m - \Delta Kt I_{tot} = Kt_n I_{tot} - J_n \ddot{x}_m \tag{2}$$

where $\ddot{x}_m$ is motor acceleration and parameters uncertainties are:

$$\Delta J = J - J_n \tag{3}$$

$$\Delta Kt = Kt - Kt_n \tag{4}$$

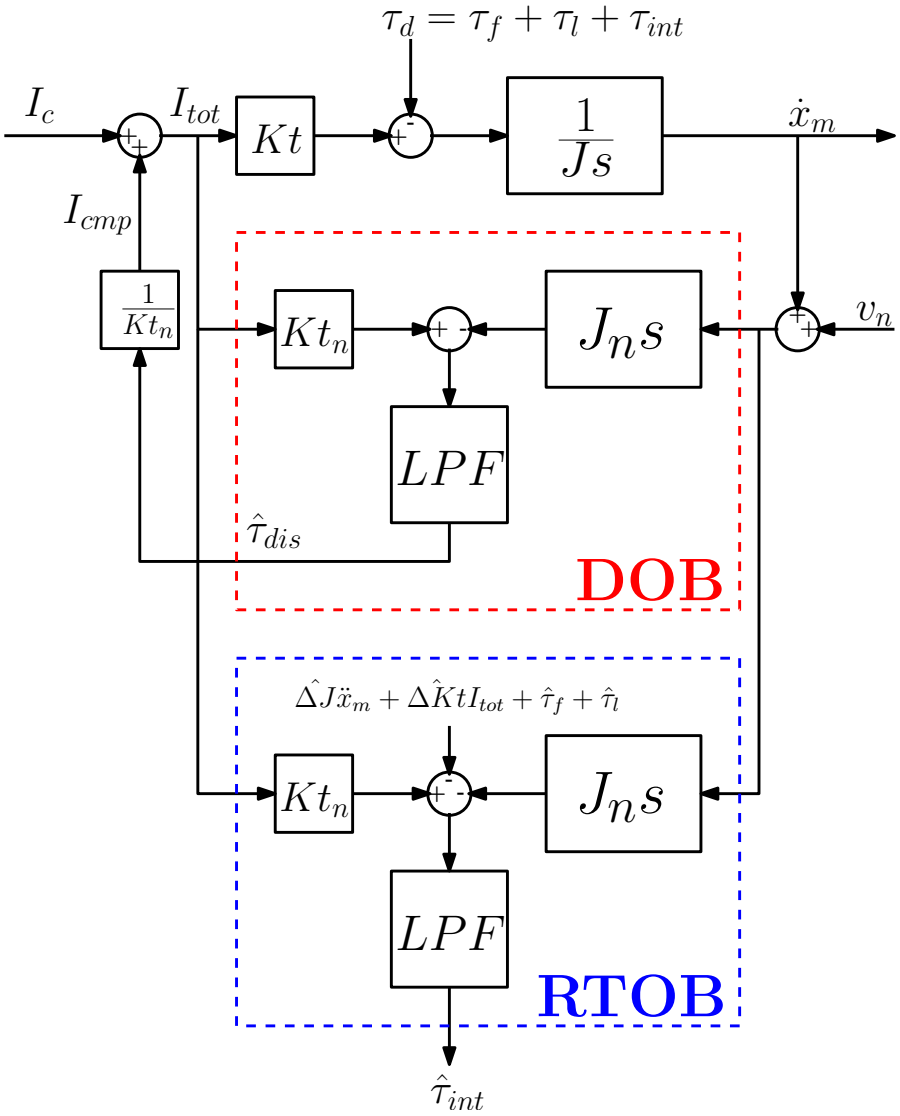

Figure 12: Block diagram of DOB and RTOB model.

and total motor current amounts to:

$$I_{tot} = I_c + I_{cmp} \tag{5}$$

where I_c and I_{cmp} are the control and compensation current, respectively.
The last equality in (2) describes how DOB works in order to estimate the equivalent disturbance τ_{dis} acting on the system. However, DOB makes use of plant acceleration, which is usually obtained by computing the time derivative of speed. The use of a low-pass filter is necessary to reduce effects due to measurement noise v_n in the speed signals. Such noise may enter in the inner-loop, leading to undesired vibrations. So, the final disturbance estimation results in:

$$\hat{\tau}_{dis} = LPF_{DOB}(s)\tau_{dis} = \frac{g_{DOB}}{s + g_{DOB}}(\tau_d + \Delta J\ddot{x}_m - \Delta KtI_{tot}) \tag{6}$$

where g_{DOB} is the DOB low pass filter bandwidth.

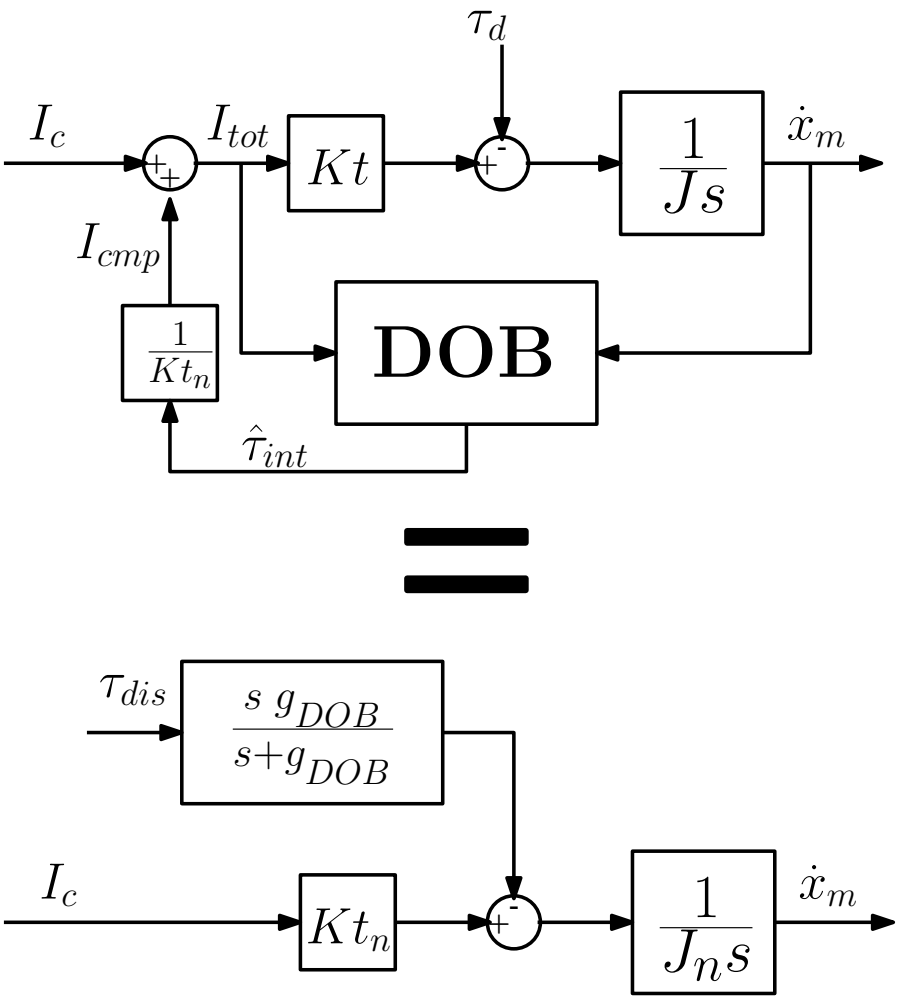

Figure 13: Schematic representation of system's nominalization at low frequencies thanks to DOB.

The inner-loop is closed by using this estimation divided by the nominal torque constant to obtain the compensation current I_{cmp}.

$$I_{cmp} = \frac{1}{Kt}\hat{\tau}_{dis} \tag{7}$$

From an external point of view, the real plant and the related DOB are seen as the nominal plant in the low frequency range specified by the DOB bandwidth. In fact, Fig. 13 shows that only high frequency components of τ_{dis} can not be compensated by DOB.
As already mentioned, the RTOB presents a similar structure to DOB. But, in this case, an identification of the real plant parameters and estimation of friction and load torque are needed. So, the estimated plant parameter values can be written as:

$$\hat{J} = J_n + \Delta\hat{J} \tag{8}$$

$$\hat{Kt} = Kt_n + \Delta\hat{Kt} \tag{9}$$

where $\Delta\hat{J}$ and $\Delta\hat{Kt}$ are the inertia and torque constant uncertainties estimations, respectively.
Consequently, the external interaction torque can be estimated as:

$$\hat{\tau}_{int} = \frac{g_{RFOB}}{s + g_{RFOB}}(\hat{Kt}I_{tot} - \hat{J}\ddot{x}_m - \hat{\tau}_f - \hat{\tau}_l) \tag{10}$$

where g_{RTOB} is bandwidth of the RTOB low pass filter, which is necessary to reduce added noise in the estimations.
After this brief overview of DOB and RTOB/RFOB, it is clear how the following two main aspects should be taken into account to obtain better performances in using such control tools:

- Both DOB and RTOB/RFOB need accurate speed estimations. In fact, a lower added noise in speed signals allows to increase DOB and RTOB/RFOB low pass filters bandwidths and, so doing, better disturbances and external forces estimations can be obtained.
- In order to better estimate external forces/torques, it is fundamental to accurately model and estimate the real plant, in particular, mechanical device parameters such as inertia and viscous and Coulomb friction coefficients.

2.1.3 *Use of acceleration measurements in DOB and RTOB/RFOB*

Final goals of the proposed researches are increasing backdrivability and haptic perception in low-cost RRs, which are typically characterized by high friction and low-resolution position sensors. Unfortunately, such desired features strongly depend on hardware capabilities, such as sensor resolution and actuator technology. In fact, using higher-resolution position sensors, it is possible to obtain more accurate position and speed estimations while, using high quality servo motors or using force sensors allows for more precise force control. All these hardware improvements lead the increasing of overall device performances. However, from a cost-efficiency point of view, these invasive modifications may not be justifiable and, also, may require redesign of the control system.
The use of DOB and RTOB/RFOB control tools, previously described, is a suitable force-sensorless solution to achieve desired goals without deep hardware modifications. In order to increase their performances, the last remarks in Sec. 2.1.2.1 have driven the research described in the following.
Firstly, more accurate speed information of the system are necessary. They are typically obtained bythe discrete time derivative of the encoder signals. Due to quantization process of position measurements, resulting estimations are affected by not negligible noises. Since, the use of more accurate position sensors has not been taken into account, due to their extra costs, the use of estimators, which provide smooth estimates of the actual position, can be a low-cost alternative solution to obtain less noisy speed signals. The use of such approach has been widely used to improve motion control quality. Significant results have been reported in [78, 79]. Among all the possible estimation techniques, those based on Kalman filter (KF) (a brief description can be found in Appx. a) have gained a lot of interest in those application where it is necessary to estimate both position and velocity of the system with low resolution sensors [80, 81]. Recently, a novel KF-based solution has been proposed in [82], which takes inspiration

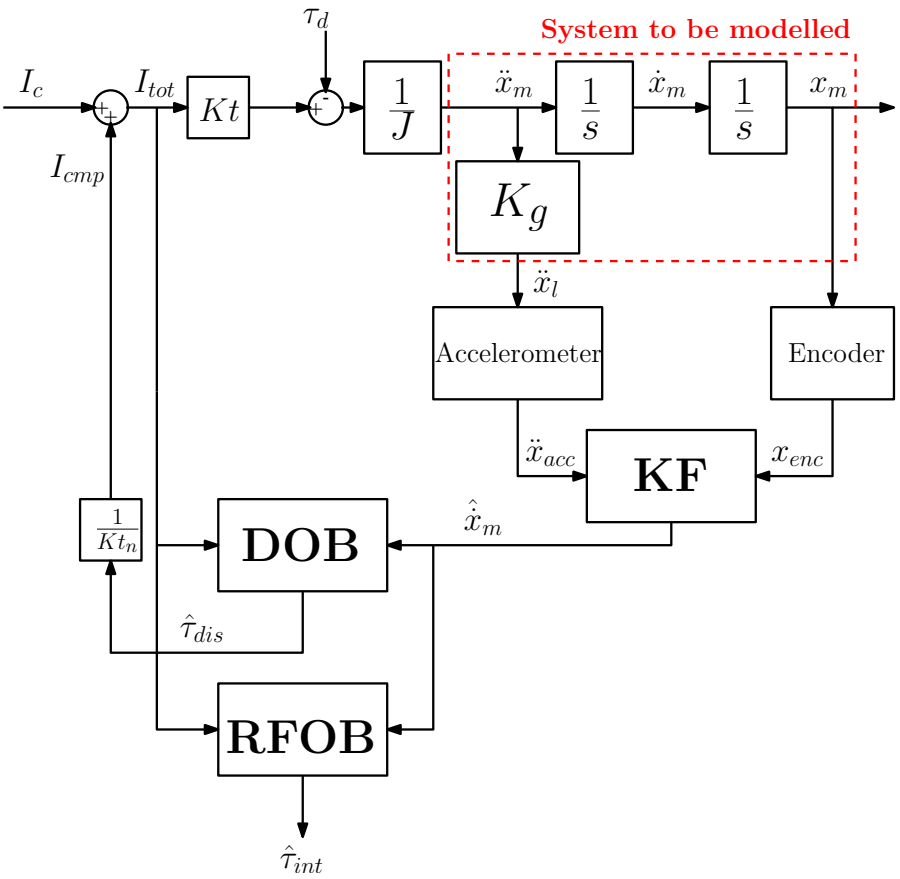

Figure 14: Block diagram showing use of acceleration measurements and related KF in DOB and RTOB/RFOB applications.

from [83]. It consists on a sensor fusion algorithm between position sensors and traditional accelerometer's measurements. On the other hand, direct acceleration measurements can not be used, as they are typically affected by:

- limited bandwidths;
- measurement noise;
- bias and drift;
- linearity errors.

Consequently, their measures can not be simply integrated to obtain speed and position information. For these reasons, proposed KF in [82] makes use of a purely kinematic model that relates motor position x_m and load acceleration $\ddot{x}_l$ (as highlighted in Fig. 14):

$$\frac{d^2 x_m}{dt^2} = K_g \ddot{x}_l \tag{11}$$

where K_g is a possible reduction gear ratio between motor and load. So doing, such sensor fusion algorithm is able to merge these independent position and acceleration measurements, compensating for any accelerometer drift, bias or other undesired effects. So doing, it provides more accurate position, speed and acceleration estimation

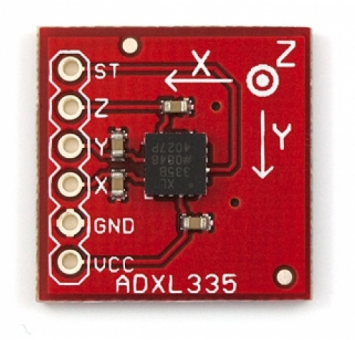

Figure 15: Triple axis low- cost MEMS accelerometer breakout - Analog Devices ADXL335.

of the system. The latter can be used in DOB and RTOB/RFOB in order to increase their performances in terms of wider bandwidths and reduce residual noise (as shown in Fig. 14). As a result, a more accurate force control can be performed and a better haptic perception in a bilateral control system can be achieved.
However, such solution presents some limitations and drawbacks, in particular:

- accelerometers cost. Good results have been achieved in [82, 83] thanks to the use of expensive accelerometers which can provide accurate acceleration measurements. Unfortunately, these acceleration sensors has not an affordable price for low-cost applications;
- bias and drift have not been considered. Their effects may affect robustness of the sensor fusion algorithm, deteriorating estimation's performances and, consequently, control system behavior [84].

2.1.4 *Proposed approach*

In order to address the latter reported issues, an alternative solution has been developed during this research project. It is based on the solution presented in [82] but, instead of using traditional expensive accelerometers, it uses low-cost micro electro-mechanical systems (MEMS) accelerometer's measurements in the sensor fusion algorithm. It also implements an augmented filter model, which takes into account of bias, drift and other undesired effects that typically affect such devices.
There are many positive aspects supporting this option. First, performances of such low-cost accelerometers have been recently improved, in particular from point of view of reduced measurement's noise. On the other hand, their price (about a dollar) and size are both decreasing, thanks to improvements in MEMS fabrication technology (an example of these sensors can be seen in Fig.15). Consequently, it is easy to place and implement them in a robotic device. This leads to a cost-effective way to enhance performances of the existing hardware,

without the need for major system modifications or the use of expensive sensors.
Interesting aspects of the proposed sensor fusion algorithm consist of:

- use of augmented kinematic KF model, which also takes into account of bias, drift and other undesired effects;
- systematic tuning procedure of KF's parameters;
- estimated state reset, taking inspiration from [85].

Focusing on the second aspect described at the end of Sec.2.1.2.1, the proposed researches have been extended by developing a non-linear identification procedure of the main mechanical device parameters:

- inertia;
- Coulomb and viscous friction.

An accurate identification of these parameters is extremely important to obtain precise external force estimations by using RTOB/RFOB, in particular in low-cost robotic devices, where friction phenomenas are usually not negligible. Such identification procedure has been implemented using a RLS algorithm and it can be easily performed during each start-up of the robotic device. So, changes in the mechanical parameters can be identified and properly compensated. This can be useful in low-cost RR, where friction may depend on environment parameters (e.g. temperature), and device inertia may change, in case of different end effectors or handles used.
Particular attention has been made in order to develop algorithms to be as simple as possible from the computational point of view, in order to be easily implemented also in a low-cost micro-controller based systems. So doing, it is possible to design complete and standalone working devices and, at the same time, reduce the number of components and the overall system cost.
The chapter is organized as follow: Sec. 2.2 and Sec. 2.3 describe the proposed sensor fusion algorithm and the recursive identification procedure, respectively. In Sec. 2.4 and Sec.2.5, the experimental set-up and some results are presented, showing benefits of the proposed solutions, when applied in a low-cost robotic prototype for upper-limbs rehabilitation. Finally, some conclusions are reported in Sec. 2.6.

2.2 ACCELEROMETER AIDED KALMAN FILTER ESTIMATOR

2.2.1 *Filter model*

In the proposed solution, the KF implements a sensor fusion algorithm, in order to reduce the effects of the quantization noise affecting the measured position. Measurements are provided, respectively, by position sensor, such as rotative encoders, and low-cost MEMS accelerometers, placed at load side. They are fused by the KF in order to obtain better system position, velocity and acceleration estimations in

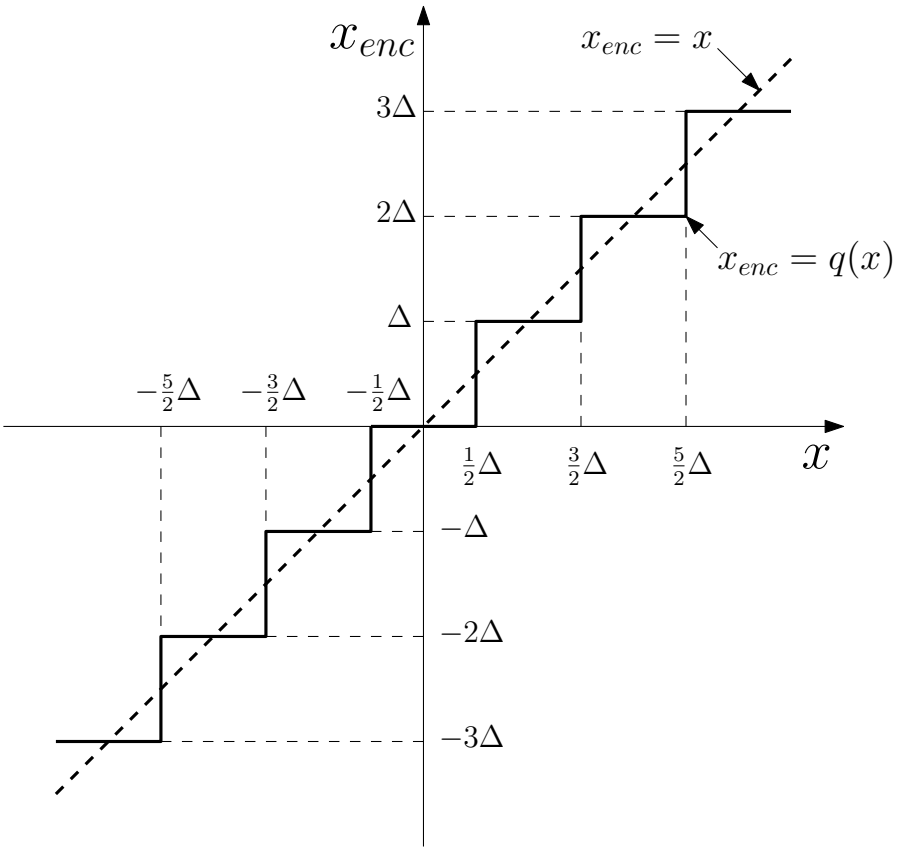

Figure 16: Encoder quantization.

terms of reduced residual noise and large bandwidth estimate. The robustness of the estimate is enhanced by making use of a kinematic model in the KF. With this choice, no mechanical parameters of the system are necessary in the KF implementation, thus ensuring an accurate estimate even in case of large variations of such parameters (e.g. inertia). The KF estimator is also insensitive to the input disturbance and friction forces acting on the plant. On the other hand, traditional estimators, which make use of system command input and position informations, are affected by all those disturbances.
The design of this filter takes inspiration from [82], but some modifications in the filter model are necessary, to overcome measurement's bias, drifts and variation in scaling factors issues, which are not negligible [84].
The filter model has been developed considering kinematic relation between acceleration and position of rigid single-DOF motor-load system (reported in equation (11)) and the added noise in the motor position and load acceleration measurements.
In particular, encoder's measurements can be modelled as:

$$x_{enc} = q(x) = x_m + v_{enc} \tag{12}$$

$$-\frac{\Delta}{2} \leqslant v_{enc} \leqslant \frac{\Delta}{2} \tag{13}$$

where $q(*)$ is the typical quantization function performed by any digital encoders, and described in Fig.16. The position quantization can

also be seen as added noise v_{enc} to the measurements. Such measurement's noise can be modelled as a random process with continuous uniform distribution in the range describe in (13), where Δ is the encoder resolution (quantization step).
Load acceleration's measurements, provided by low-cost MEMS sensors, may affected by bias, drifts and variation in scaling factors, which depend on time and temperature and other stochastic factors [86, 87]. Such additional noise may corrupts the KF optimal condition, related to the gaussianity and zero-mean of the measurement's noise (for additional details see Appx. a). Moreover, the presence of bias is particularly detrimental in all those applications where the acceleration signals is used to obtain the velocity and/or position estimations. This because, integrating such affected measurements, bias may cause drifts in the estimations. Bias issues may be partially or totally solved by implementing an accurate calibration of the sensors (to determine scale factors and bias) and implementing a strict temperature control (or compensation). However, this would require a specific calibration of each sensor, after placement on the robotic device, increasing the implementation cost. Proposed augmented model allows to better represent the real system involved, better estimating and compensate bias and drift drawbacks. A simplified model of the acceleration measurement $\ddot{x}_{acc}$ has been considered:

$$\ddot{x}_{acc} = \ddot{x}_l + a_b + v_{acc} \tag{14}$$

where $\ddot{x}_l$ is the true acceleration value, while a_b and v_{acc} are respectively the bias and noise added to the measurements. As suggested by Fig.17, v_{avv} can be essentially considered as a white Guassian noise process.
As it is possible to see in Fig.18, the bias is modelled as random walk:

$$\dot{a}_b = w_b \tag{15}$$

where w_b is a white random process. Variance of such random process is strongly linked to bias variability. It is worth noticing that the proposed model , far from being complete, is however capable of capturing several important characteristics of MEMS sensors, namely the wide-band noise, the bias and its possible variations, including those due to operating temperature and also changes or uncertainties in scaling factors. A comprehensive model, representing those measurement's disturbances, is reported in [87].
Finally, Fig.18 shows that motor acceleration $\ddot{x}_m$ is also modelled as a random walk, i.e.:

$$\dddot{x}_m = \frac{d\ddot{x}_m}{dt} = w_a \tag{16}$$

where w_a is white random process too.

2.2.1.1 *State space model and tuning procedure*

The KF model presented here is an augmented version of the one presented in [82], which also consider the above model for the biased acceleration measurement into the kinematic model of the system. The

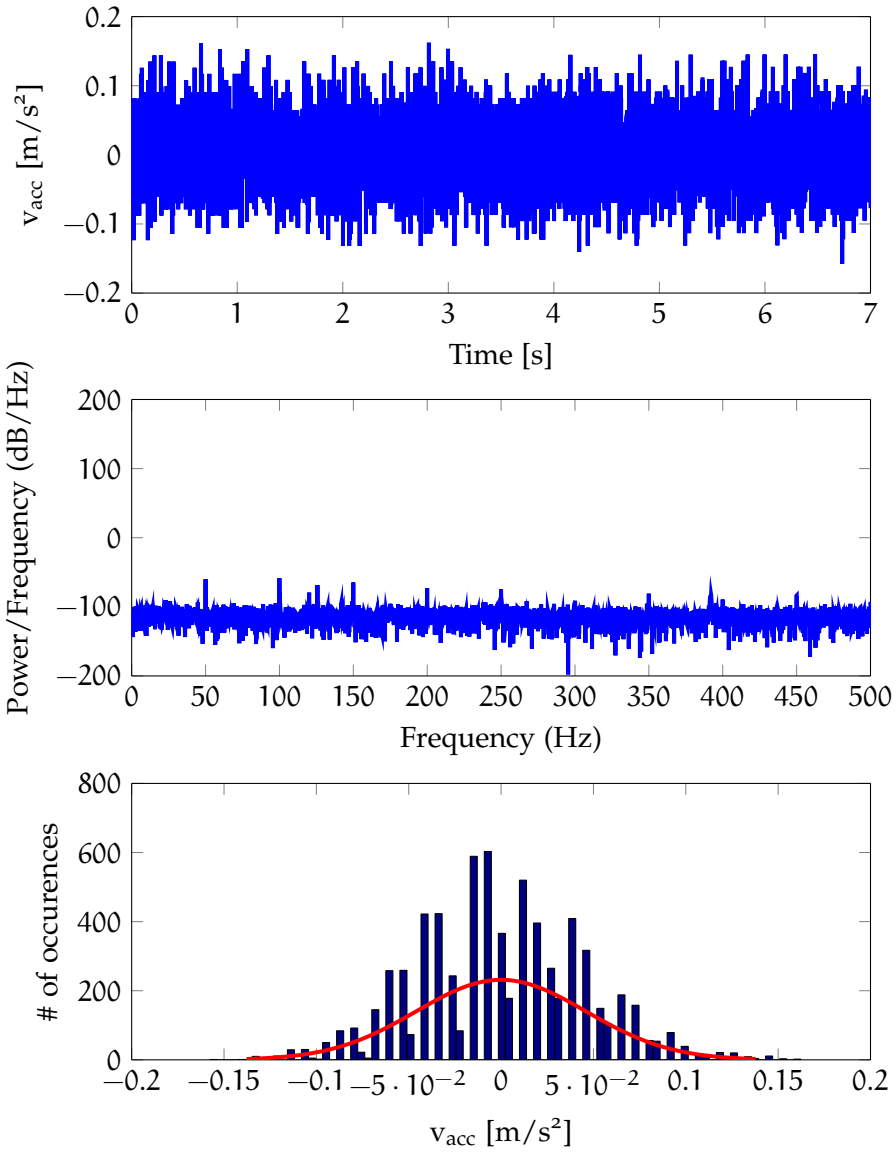

Figure 17: Accelerometer noise after subtracting the bias. First graph shows signal over time, second one shows its power spectral density. The last one plots noise distribution around zero, showing how it can be approximate to a Guassian distribution.

resulting stochastic state-space model describing the relation between acceleration, position and related measurements is:

$$\dot{\mathbf{x}} = \mathbf{A_c}\mathbf{x} + \mathbf{B_c}u + \mathbf{B_{cw}}\mathbf{w} \tag{17}$$

$$\mathbf{y} = \mathbf{C_c}\mathbf{x} + \mathbf{v} \tag{18}$$

where

$$\mathbf{x} = [x_m \ \dot{x}_m \ \ddot{x}_m \ a_b]^T \ , \ u = 0 \ , \ \mathbf{y} = [x_{enc} \ \ddot{x}_{acc}]^T \tag{19}$$

$$\mathbf{v} = [v_{enc} \ v_{acc}]^T \ , \ \mathbf{w} = [w_a \ w_b]^T \tag{20}$$

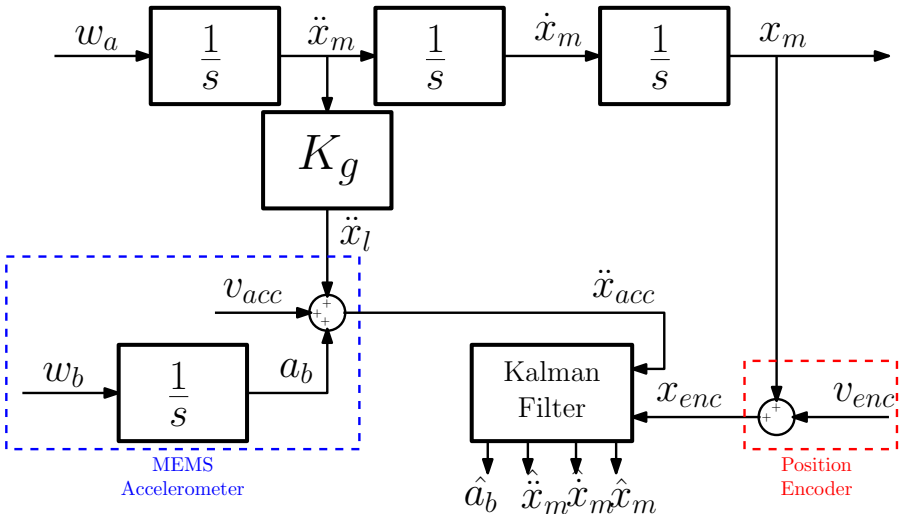

Figure 18: Block diagram of Kalman filter model.

and

$$\mathbf{A_c} = \begin{bmatrix} 0 & 1 & 0 & 0 \\ 0 & 0 & 1 & 0 \\ 0 & 0 & 0 & 0 \\ 0 & 0 & 0 & 0 \end{bmatrix}, \mathbf{B_c} = \begin{bmatrix} 0 \\ 0 \\ 0 \\ 0 \end{bmatrix}, \mathbf{B_{cw}} = \begin{bmatrix} 0 & 0 \\ 0 & 0 \\ 1 & 0 \\ 0 & 1 \end{bmatrix} \tag{21}$$

$$\mathbf{C_c} = \begin{bmatrix} 1 & 0 & 0 & 0 \\ 0 & 0 & \frac{1}{K_g} & 1 \end{bmatrix} \tag{22}$$

Observability matrix can be easily computed from (21) and (22). It has full rank, ensuring the full observability of system state.
No deterministic inputs are present in the model, only stochastic processes, w_a and w_b, which are commonly called process noises, are inputs of the kinematic KF. Outputs of the systems are the measured motor position and load acceleration, affected by v_{acc} and v_{enc} measurement noises. The main difference, compared to [82], model state (19) which has been augmented, by adding the bias variable.
In the KF implementation, both process noises, w_a and w_b, and measurements noises, v_{enc} and v_{acc}, are considered uncorrelated white Gaussian random processes with zero mean and variance σ_a, σ_b, σ_{enc} and σ_{acc}, respectively. As a result, the corresponding process and measurement noise covariance matrices are:

$$\mathbf{Q_c} = \mathbf{E}[\mathbf{w}\mathbf{w}^T] = \begin{bmatrix} \sigma_a & 0 \\ 0 & \sigma_b \end{bmatrix}, \mathbf{R_c} = \mathbf{E}[\mathbf{v}\mathbf{v}^T] = \begin{bmatrix} \sigma_{enc} & 0 \\ 0 & \sigma_{acc} \end{bmatrix} \tag{23}$$

From previous quantization error definition (13), encoder measurement noise variance is defined as $\sigma_{enc} = \Delta^2/12$. Acceleration measurements error variance can be estimate using data provided by the manufacturer or experimentally, measuring the signals variance provided by the accelerometer, when the latter is not moved, and properly cancelling bias that can be considered a constant disturbance, in

a shot time span (see Fig. 17).
Also, process noise variance must experimentally determined. A systematic tuning procedure has been implemented in order to correctly set these filter's parameters. Such procedure is based on a whiteness test (e.g. Bartlett's test [88]) on the process innovation.
Process innovation is essentially the difference between real output measurements and estimated ones, obtained by computing previous available data (further information are reported in Appx.a). Bartlett's test analyzes innovation's power spectral density, also called periodogram, and the related normalized cumulative one. In fact, white processes have flat periodogram and a perfectly straight cumulative one. Resulting white process innovation means that good KF parameters tuning is achieved.
Noticing that measurement noise covariance matrix is experimentally defined, the only tuneable parameter is model noise covariance matrix $\mathbf{R_c}$. In fact, varying its values is possible to change the KF bandwidth. The innovation cumulative periodogram analysis is fundamental to understand how to vary $\mathbf{R_c}$ in order to correctly tune the filter. In particular, if a cumulative periodogram, in the form of left side graph in Fig. 19, is obtained, it means that too many low frequency components are in the innovation signal. Consequently, it is necessary to increase values of matrix $\mathbf{R_c}$ to increase the filter bandwidth. On the other hand, in case of innovation cumulative periodogram in the form of right side graph in Fig. 19, too many high frequency components are in the innovation signals, so it is necessary to decrease $\mathbf{R_c}$ covariance values and, consequently, the filter bandwidth.
Based on previous observations, σ_a and σ_b are varied until difference between the actual and the estimated system outputs, during the actual motion of the device, gets as close as possible to a white noise. Positive results of this test are presented in Fig. 20. Two different innovation signals must be taken into account, as both position and acceleration signals are outputs of the system.
Such tuning procedure of the KF algorithm can be, sometimes, tricky. Anyhow, process noise variances have physical and easy to understand meanings. As a matter of fact, analysing (15) and (16), process noises define respectively motor jerk and bias time derivative, therefore their variance's values are related to speed of change of motor acceleration and bias signals, respectively. So, according to the application and, consequently, the typical motion to be performed, the order of magnitude of σ_a can be estimated. On the other hand, σ_b is commonly set to very small values, compared to σ_a ones, as bias is almost a constant disturbance.

2.2.1.2 *Kalman filter implementation*

In order to be physically implemented in a digital controller or in a computer, the KF algorithm should be designed in a discrete fashion, where Ts is the sampling time. The continuos state-space model, de-

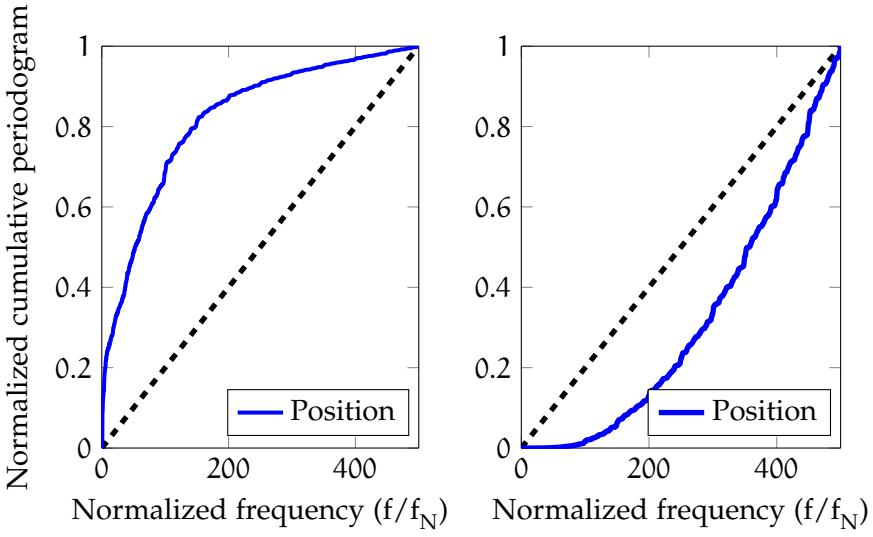

Figure 19: Normalized cumulative periodogram of position innovation signal in case of wrong tuning: too small variance values (left side graph) and to big variance values (right side graph).

scribed in Sec. 2.2.1.1 is discretized using the zero order hold (ZOH) method, as follows:

$$\mathbf{x}_{k+1} = \mathbf{A_d}\mathbf{x}_k + \mathbf{B_d}u_k + \mathbf{B_{dw}}\mathbf{w}_k \tag{24}$$

$$\mathbf{y}_k = \mathbf{C_d}\mathbf{x}_k + \mathbf{v}_k \tag{25}$$

where

$$\mathbf{A_d} = e^{\mathbf{A_c}T_s}\ ,\ \mathbf{B_d} = \int_0^{T_s} e^{\mathbf{A_c}\tau}\mathbf{B_c}d\tau\ ,\ \mathbf{B_{dw}} = \int_0^{T_s} e^{\mathbf{A_c}\tau}\mathbf{B_{cw}}d\tau \tag{26}$$

$$\mathbf{C_d} = \mathbf{C_c} \tag{27}$$

Even model noise covariance is properly discretized, i.e.:

$$\mathbf{Q_d} = \int_0^{T_s} e^{\mathbf{A_c}\tau}\mathbf{Q_c}e^{\mathbf{A_c}^T\tau}d\tau \tag{28}$$

On the other hand, the discretized version of measurement noise covariance $\mathbf{R_d}$ is obtained experimentally.
Considering both process and measurements noises as white Gaussian processes, a time-varying KF is implemented for the state estimator. One of the distinct advantages of such approach, compared to the finite-horizon one, is the time-varying coefficients of the estimator, which allow best transient performances. Implementation details of time-varing KF are reported in a.

2.2.2 *Reset of the state estimation*

Regarding the reset of the estimated state, this is inspired by [85] and driven by observation that, during fast transients, KF algorithm

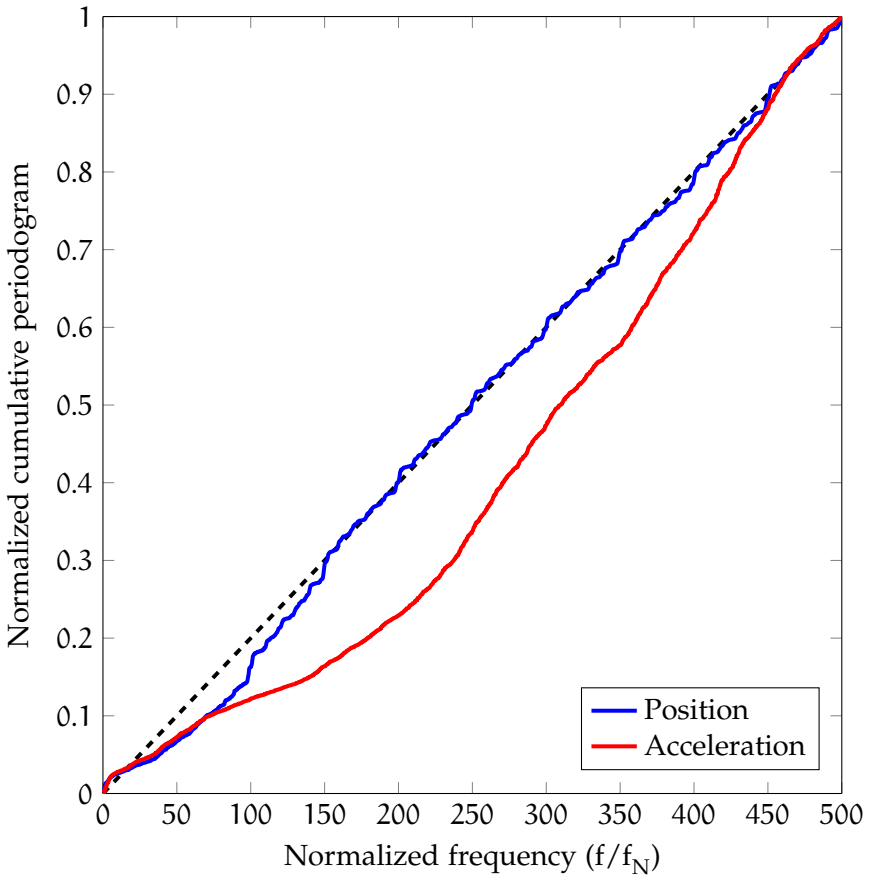

Figure 20: Normalized cumulative periodogram of innovation signals in the proposed KF. Blue and red lines are related to position and acceleration estimation errors, respectively.

may produce inconsistent estimations compared with actual measurements. This is due to errors and uncertainties in model representation.

The basic idea consists in noticing that, at a discrete time k, actual position of the motor is certainly inside predefined range, which can be derived by using (12) and (13), i.e.:

$$x_{enc_k} - \frac{\Delta}{2} \leqslant x_{m_k} \leqslant x_{enc_k} + \frac{\Delta}{2} \tag{29}$$

Furthermore, a similar discussion can be done for motor speed $\dot{x}_{m_k}$. In a digital controller, correct speed estimation can be obtained as:

$$\hat{\dot{x}}_{m_k} = \frac{x_{m_k} - x_{m_{k-1}}}{Ts} \tag{30}$$

where Ts is the sampling time. However, such estimation can not be performed because exact motor positions at sample k and $k-1$, are non available. Despite this, a range of likely speed estimations, using encoder measurements, can be defined using (29) and(30), i.e.:

$$\frac{x_{enc_k} - x_{enc_{k-1}}}{Ts} - \frac{\Delta}{Ts} \leqslant \hat{\dot{x}}_{m_k} \leqslant \frac{x_{enc_k} - x_{enc_{k-1}}}{Ts} + \frac{\Delta}{Ts} \tag{31}$$

Taking into account of (29) and (31), in the state estimation of the KF algorithm, estimated position and speed must comply with these con-

straints. It is worth noticing, both constraints make use of the quantization step Δ in their definitions. Consequently, such boundaries can be very useful to address estimation process. In particular, during fast transients, estimations may be forced to remain inside these predefined boundaries, in oder to provide consistent estimations.
In proposed aaKF, a third step in the algorithm computation has been introduced after the prediction step (see Appx. a). The so called "state estimation reset" step implements a reset procedure of position and speed estimations using variable range saturation functions, based on previous defined boundaries, and described in the following pseudocode:

- State estimation reset:

  if $\hat{x}(1)_{k|k-1} > x_{enc_k} + \frac{\Delta}{2}$ **then**
  $\hat{x}(1)_{k|k-1} = x_{enc_k} + \frac{\Delta}{2}$
  else
  if $\hat{x}(1)_{k|k-1} < x_{enc_k} - \frac{\Delta}{2}$ **then**
  $\hat{x}(1)_{k|k-1} = x_{enc_k} - \frac{\Delta}{2}$
  end if
  end if
  if $\hat{x}(2)_{k|k-1} > \frac{x_{enc_k} - x_{enc_{k-1}}}{Ts} + \frac{\Delta}{T_s}$ **then**
  $\hat{x}(2)_{k|k-1} = \frac{x_{enc_k} - x_{enc_{k-1}}}{Ts} + \frac{\Delta}{T_s}$
  else
  if $\hat{x}(2)_{k|k-1} < \frac{x_{enc_k} - x_{enc_{k-1}}}{Ts} - \frac{\Delta}{T_s}$ **then**
  $\hat{x}(2)_{k|k-1} = \frac{x_{enc_k} - x_{enc_{k-1}}}{Ts} - \frac{\Delta}{T_s}$
  end if
  end if

It is worth noticing, this step makes only use of the encoder measurements, which are available. In particular, the actual and previous time step measurements are necessary.
In order to understand benefits in the introduction of this estimated state reset, a simulation test has been performed. It consists on simulating a mass which is randomly accelerated and require fast KF responses. Position and acceleration measurements, with related noises, are properly simulated. Two aaKF algorithms have been implemented, one without and the other one with the state reset. Consequently, an estimation comparison of speed signals has been performed and it is reported in Fig. 21. Leading expected advantages in using the estimated state reset are:

- more precise estimations;
- reduced overshoots in fast transients.

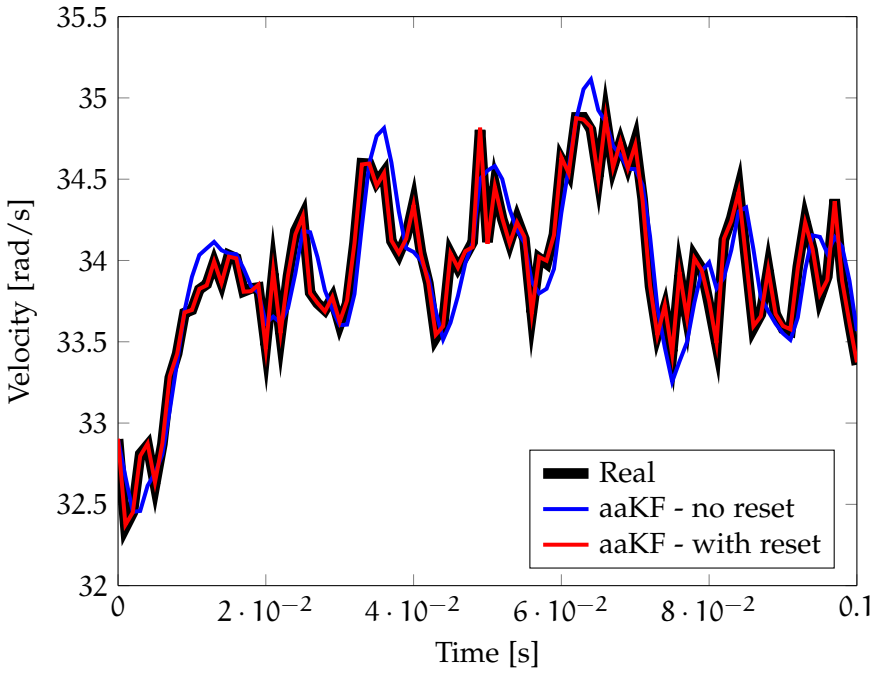

Figure 21: Simulated results comparison between real and estimated speed signals, with and without state reset.

2.3 DEVICE PARAMETERS IDENTIFICATION

2.3.1 *Introduction*

As previously stated, the second part of this research is related to the development of a non-linear identification procedure, in order to estimate the main device parameters:

- Inertia J;
- Viscous friction coefficient b;
- Coulomb friction coefficient f_c.

An accurate estimation of such parameters is essential to increase performances of DOB and RFOB and, consequently, force control and haptics performances, in particular in low-cost robotic devices which typically has not negligible undesired disturbance, such as friction. Furthermore, an additional goal that we want to achieve, is to automate the identification procedure during the device's start-up, by performing a simple and rapid identification test. This because the device parameters may change during usages of the device, due to installation of different handles or changes in the working conditions. Consequently, traditional identification methods, based on the execution of long and particular trajectories by the robot or offline post-processing analysis, have been discarded. Focusing on these aspects, an identification procedure, involving the use of a RLS algorithm, has been developed. This proposed solution can be easily implemented in a digital fashion and, compared to least mean squares (LMS) algorithms, the RLS ones have a faster convergence speed and do not

exhibit the eigenvalue spread problem [89]. Such features allow to perform a fast and online identification of the device parameters.

2.3.2 *RLS identification*

RLS algorithms have wide-spread applications in many areas, such as real-time signal processing, control and communications. In fact, they recursively find the coefficients that minimize a weighted linear least squares cost function and, also, have adaptive abilities. They are particularly used in data analysis tasks where data are not available all at one but arrive sequentially. Moreover, they can be easily implemented in real-time algorithms, aiming at tracking time-varying parameters. This is why, they are a central part of adaptive control or signal processing systems, where the control or filtering action is based on the most recent model, or in fault detection algorithm, allowing to find out whether system significantly changes.
In the proposed application, an RLS algorithm is used to estimate the current vector of parameters $\mathbf{w}_{I_k}$ of a linear system, which can be represented by the following discrete autoregressive moving average (ARMA) model, i.e.:

$$y_{I_k} = \mathbf{w}_{I_k}^T \mathbf{x}_{I_k} \tag{32}$$

where $\mathbf{x}_{I_k}$ is a vector containing delayed input and output signals of the system and y_{I_k} is the related output vector, at time k, respectively. The purpose of the RLS algorithm is to recursively find the best system parameters estimation $\hat{\mathbf{w}}_{I_k}$, given input and output data up to time k, that minimize the following weighted linear least squares cost function:

$$V(\mathbf{w}_{I_k}) = \sum_{i=0}^{k} \lambda^{k-i} {e_{I_k}}_i^2 \tag{33}$$

where

$$e_{I_k} = y_{I_k} - \hat{y}_{I_k} = y_{I_k} - \hat{\mathbf{w}}_{I_k}^T \mathbf{x}_{I_k} \tag{34}$$

and $0 < \lambda \leqslant 1$ is the forgetting factor which gives exponentially less weights to older error samples. $\hat{y}_{I_k} = \hat{\mathbf{w}}_{I_k}^T \mathbf{x}_{I_k}$ is the output prediction, based on observations up to time $k-1$.
It is clear how, minimizing the cost function in (33), the resulting parameters vector gives the best approximation of the system, based on model (32). Making use of exponential weights on data sample, allows to take greater account of newer data in the identification process, while older data are less and less relevant in the next computations.

2.3.3 *System modelling*

Before talking about the RLS algorithm implementation, it is necessary to find a simple but accurate representation of the desired system. It

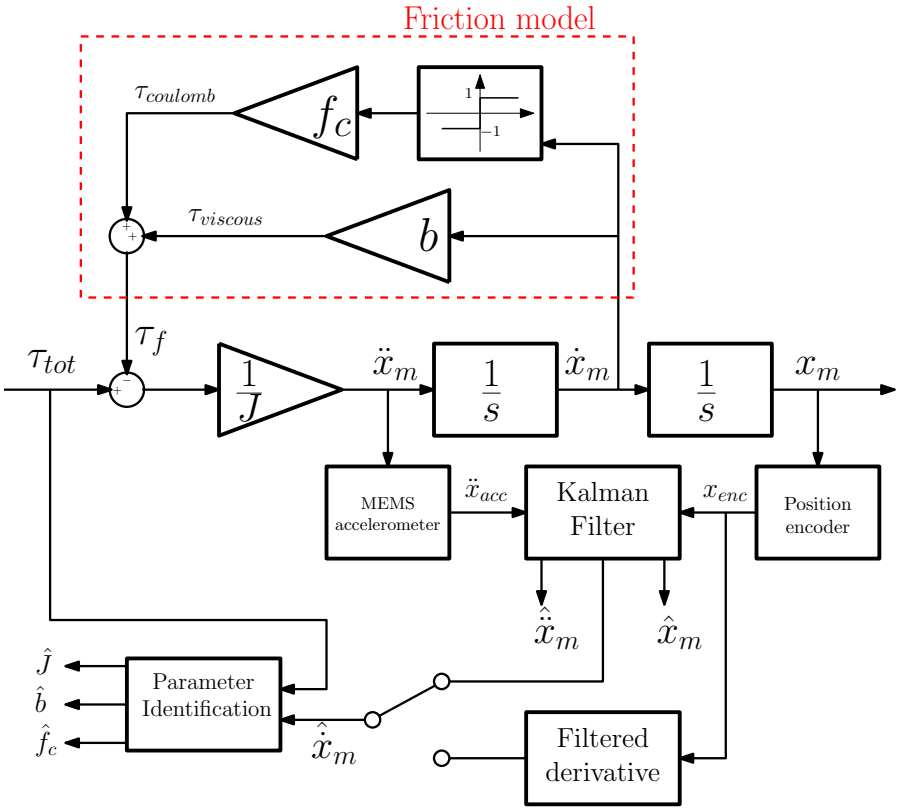

Figure 22: First five leading causes of death in Italy in 2011 [9].

is worth noticing that the suitable system model should be a discrete linear dynamic system, in the form of equation 32.
Unfortunately, the system taken into account, and shown in Fig.22, has a non-linear component, due to the Coulomb friction. Such model can be expressed modifing a linear dynamic model, representing a typical mechanical system with an inertia and viscous friction, i.e.:

$$W_c(s) = \frac{Y(s)}{U(s)} = \frac{1}{Js + b} \tag{35}$$

Equation (35) shows the generic transfer function between torque inputs and inertia speed outputs of the system. However, a modification in the input signal definition is neccessary, in order to take into account of the non-linear term due to the Coulomb friction, i.e.:

$$u(t) = \tau(t)_{tot} + \tau_{coulomb} = \tau(t)_{tot} + f_c sign(\dot{x}_m(t)) \tag{36}$$

Equation (36) shows how the additional non-linear term, depends exclusively on a proportional term f_c, the Coulomb friction coefficient, and on inertia direction of motion and so on its speed sign. System outputs are not modified, i.e.:

$$y(t) = \dot{x}_m(t) \tag{37}$$

As a consequence of the added non-linear term, a straightforward discretization of the system is not possible. First of all, using the ZOH method, the transfer function in (35) is discretized as:

$$W_d(z) = \frac{b_0 z^{-1}}{a_0 - a_1 z^{-1}} \tag{38}$$

where

$$a_0 = 1 \quad , \quad a_1 = e^{-T_s \frac{b}{J}} \quad , \quad b_0 = \frac{1-e^{-T_s \frac{b}{J}}}{b} \tag{39}$$

Such discrete dynamic model can be easily represented in form of equation (32), i.e.:

$$y_k = a_1 y_{k-1} + b_0 u_{k-1} \tag{40}$$

where u_i and y_i are sampled input and output at time step i, respectively.
At this point, as in the continuous case, inputs and outputs are defined, taking into account of the non-linear term, i.e.:

$$u_k = \tau_{tot_k} + f_c sign(\dot{x}_{m_k}) \tag{41}$$

$$y_k = \dot{x}_{m_k} \tag{42}$$

Substituting (41) and (42) in the static discrete model (40) and considering the suitable representation for the identification procedure (see equation (32)), the vector of the model parameters can be defined as:

$$\mathbf{w}_{I_k}^T = [a_1 \ b_0 \ f_c b_0] \tag{43}$$

while, inputs vector and output of the recursive identification algorithm are respectively:

$$\mathbf{x}_{I_k}^T = [\dot{x}_{m_{k-1}} \ \tau_{tot_k} \ sign(\dot{x}_{m_{k-1}})] \tag{44}$$

$$y_{I_k} = \dot{x}_{m_k} \tag{45}$$

2.3.4 *RLS algorithm implementation*

The proposed RLS identification algorithm starts with an initialization step and then two other step are performed at each time step, recursively.
Going into the details, the algorithm is composed by:

- Initialization:
  At the beginning, the state variables of the recursive algorithm are initialized. In particular, if some a priori information about system parameters are available, the initial values of estimated parameters vector $\mathbf{w}_{I_0}$ are computed and set. For example, after the first start-up of the device, such initial values can be set to the final results of the previous performed identification. Otherwise, the typical initialization is:

  $$\hat{\mathbf{w}}_{I_0} = \mathbf{0} \tag{46}$$

  It is worth noticing that its accurate initialization leads to a faster convergence of the algorithm's results.

The second state variable, to be initialized, is the inverse correlation matrix of the input signals, which is commonly set to:

$$P_{I_0} = \delta \mathbf{I} \tag{47}$$

where δ is a regularization factor and I is an square identity matrix of dimension n, which is the length of parameter's vector. It can be proven that such variable is proportional to the covariance matrix of the model parameters vector [90]. Since, in case our knowledge of these parameters at $k = 0$ is very vague, a very high covariance matrix of the parameters is to be expected, and thus high δ values must be assigned. On the contrary, if accurate informations of the system characteristics are known, small δ values must be used. In case of subsequent start-up of the device, the initial uncertainty matrix P_{I_0} can be set to the last P_{I_k} value of the previous identification procedure.

- Filter computation
  At each time step k, the RLS algorithm is computed, as follows:

$$\hat{\mathbf{w}}_{I_k} = \hat{\mathbf{w}}_{I_{k-1}} + e_{I_k} \mathbf{g}_{I_k} \tag{48}$$

where $\hat{\mathbf{w}}_{I_k}$ is the parameter vector estimate at time k and e_{I_k} is the prediction error defined in (34). $\mathbf{g}_{I_k}$ is the gain matrix which determines how much the current prediction error affects the update of the parameter estimate. The corrective term, obtained by using the gain matrix and the prediction error, aims to minimize next prediction errors and so the cost function in (33).
The gain matrix has the following form:

$$\mathbf{g}_{I_k} = P_{I_{k-1}} \mathbf{x}_{I_k} (\lambda + \mathbf{x}_{I_k}^T P_{I_{k-1}} \mathbf{x}_{I_k})^{-1} \tag{49}$$

Also, the uncertainty matrix P_{I_k} is updated, i.e.:

$$P_{I_k} = \lambda^{-1} P_{I_{k-1}} - \mathbf{g}_{I_k} \mathbf{x}_{I_k}^T \lambda^{-1} P_{I_{k-1}} \tag{50}$$

It is worth noticing, the forgetting factor λ is used in the last two equations (49) and (50). This leads to the desired effect of reducing the influence of old data in the parameter estimations.

- Conversion to physical parameters
  Due to sampling, estimated system parameters $\hat{\mathbf{w}}_{I_k}$ have no physical meaning. As a consequence, taking into account of (39) and (43), an inverse step is performed, at each time step, to convert no-physical parameters to physical ones, obtaining the current estimation of viscous and Coulomb friction coefficients and itertia, i.e.:

$$\hat{b}_k = \frac{1 - \hat{\mathbf{w}}_{I_k}[1]}{\hat{\mathbf{w}}_{I_k}[2]} \tag{51}$$

$$\hat{f_{c_k}} = \frac{\hat{\mathbf{w}}_{I_k}[3]}{\hat{\mathbf{w}}_{I_k}[2]} \tag{52}$$

$$\hat{J}_k = -T_s \frac{\hat{b_k}}{\log(\hat{\mathbf{w}}_{I_k}[1])} \tag{53}$$

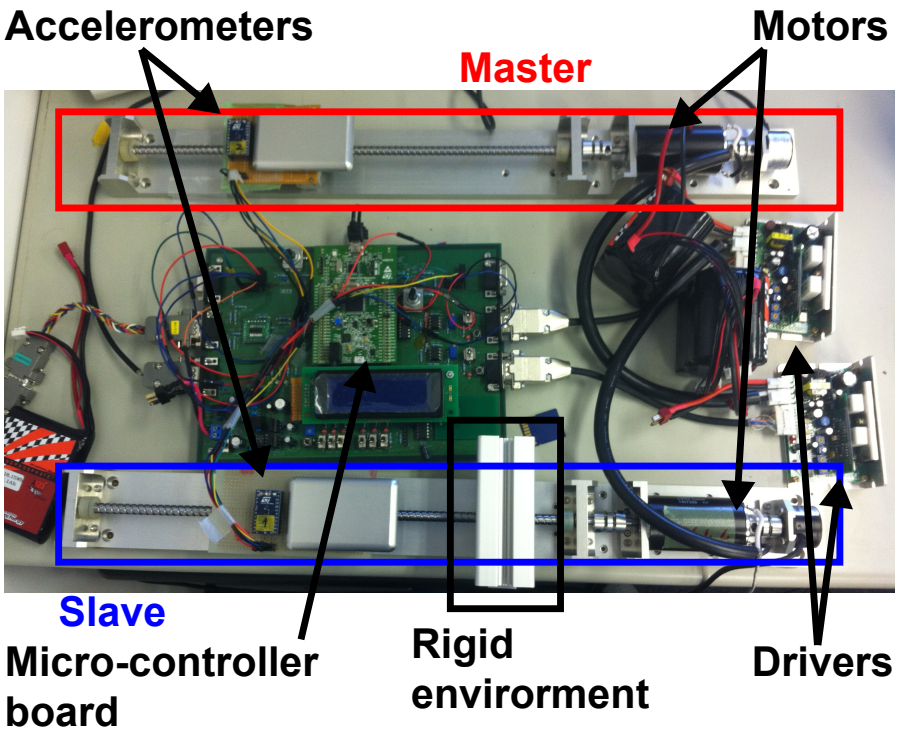

Figure 23: Haptic device prototype, developed by the Ohnishi Laboratory in Keio University.

2.4 EXPERIMENTAL SET-UP

The previously described sensor fusion algorithm and identification procedure have been tested on a low-cost, single-DOF RR prototype for upper-limbs, developed by the Ohnishi Laboratory at the Keio University. This is the newer version of the haptic device, called force transceiver, shown in Fig. 8b. The system is based on a couple of equal subsystems, master and slave side, as its main purpose is to create a bilateral control system for teleoperations. Moreover, the system is very versatile, and it can be used, also, for other robotic rehabilitation therapies, such as stand-alone reaching trainings. Each subsystem is composed by an aluminium mechanical structure, a Maxon DC rotative motor, with related rotative encoder, and a ball screw, which converts the rotative motion in a linear one. Motors are driven by a voltage commanded current driver and they can be interfaced to either a controlling PC, equipped with Matlab-Simulink and a Sensoray 626 data acquisition board or a micro-controller board. The latter system configuration aims at showing the feasibility of the implementation of the proposed solutions as a standalone battery-powered system (see Fig. 23).

Due to the proposed low-cost mechanical solution, the system is affected by a not negligible friction and, also, it presents a high reduction ratio between motor and end-effector side, in order to minimize actuators size and cost. This leads to a poor device backdrivability. The main electrical and mechanical device characteristics are summarised in Tab.1.

As previously stated, the additional acceleration measurements are

Table 1: Mechanical and electrical device characteristics

Motor inertia	J_m	$1.37 \cdot 10^{-5}$	$[kg/m^2]$
Ball screw inertia	J_{bs}	$0.33 \cdot 10^{-5}$	$[kg/m^2]$
Total device inertia	$J = J_m + J_{bs}$	$1.7 \cdot 10^{-5}$	$[kg/m^2]$
Viscous friction coefficient	b	$1.6 \cdot 10^{-5}$	$[Ns]$
Coulomb friction coefficient	f_c	$3 \cdot 10^{-3}$	$[Nm]$
Torque constant	Kt	60.3	$[mNm/A]$
Reduction ratio	K_g	$\frac{0.01}{2\pi}$	$[m/rad]$
Encoder pulses/rotation		21600	
Encoder resolution	Δ	$\frac{2*\pi}{21600}$	$[rad]$
Control sampling time	Ts	1	$[ms]$

Table 2: ADXL335 accelerometer specifications

Measurement range	$\pm$ 3.6	$[g]$
Sensitivity	300	$[mV/g]$
Sensitivity change due to temperature	$\pm$ 0.01	$[\%/°C]$
0g offset vs. temperature	$\pm$ 1	$[mg/°C]$
Noise density	150	$[\mu g/\sqrt{Hz}\ rms]$
Bandwidth	1600	$[Hz]$
Sampling rate	1000	$[Hz]$

obtained placing a low-cost MEMS accelerometer on top of the ball screw nut, where handle is also located (see Fig. 23). Several accelerometers, available in the market, have been tested. Finally, the Analog Devices ADXL335 3-Axis accelerometer has been chosen, since it has a suitable tread-off between sensitivity and noise density features, which are fundamental aspects to obtain good measurements. Characteristics of such accelerometers are reported in Tab.2.

2.5 EXPERIMENTAL RESULTS

The researches, proposed in this chapter, aim to solve backdrivability issues and haptic problems in robotic devices. Several experiments and tests have been performed in order to better show their performance improvements and benefits in real applications. Some preliminary tests, described in Sec. 2.5.1 and Sec. 2.5.2, show estimation performances of aaKF algorithm and identification procedure, respectively. In Sec.2.5.3 and Sec. 2.5.4, benefits, obtained by implementing such tools, in a zero-force control and in a bilateral position-force control system are discussed.

2.5.1 *aaKF estimation*

After properly tuning the KF covariance matrices, a simple test has been performed, in order to understand the quality of the estimations, in typical working conditions. The test consists in freely and randomly moving the device handle, with patient's arm. No control is applied to the device, so the device is simply used as a joystick. This experiment just want to reproduce typical movements, an consequently position, speed and acceleration trajectories, performed in common rehabilitation robotic therapies.
Experimental results are reported in Fig. 24. The figure shows plots of position, speed and acceleration signals, respectively. In particular, encoder signals and its derivatives are compared to related state vector variables of the aaKF algorithm. No particular evidences can be seen in position and velocity graphs, since signals are essentially overlapping. Conversely, acceleration signals show big differences. In fact, acceleration estimations from aaKF are affected by a reduce added noise compared to accelerations, obtained by encoder's information derivatives. As a result, it is understandable, that aaKF speed estimations are, also, smoother and less noisy compared to the encoder's ones, which is the desired positive effect of the sensor fusion implementation.
Moreover, to give a complete overview of the aaKF behaviour, Fig. 25 shows estimation trends of bias affecting acceleration measurements. In a short time, the algorithm accurately estimates the correct bias value.

2.5.2 *Device parameters identification*

In this section, the device parameters identification procedure is reported and the resulting data are shown in Fig. 26.The experimental set-up used in the following tests is the one described in Sec.2.4. However, in this case, only one subsystem is used.
In order to ensure convergence of the estimations and to obtain an accurate identification, system inputs must properly excite the plant. Consequently, the identification procedure proposed in this research consists in providing a band-limited white noise as voltage signal for the motor drivers, corresponding to a random torque excitation to the motor. This is a non invasive procedure, since no particular and wide device movements are necessary. In fact, the robot device merely vibrates in the neighbourhood of a certain position, just for a few seconds. Moreover, the aaKF is implemented, in order to provide more accurate information to the identification procedure. .
The RLS algorithm is implemented in real-time. As a results, at each consecutive time step, the system parameters are estimated, allowing to follow any their changes. Going deeper in the implementation details, the input vector and output of the algorithm (see equation (44) and (45) respectively) need applied torque to the motor, which is available, and motor speed information. As shown in Fig.22, the latter

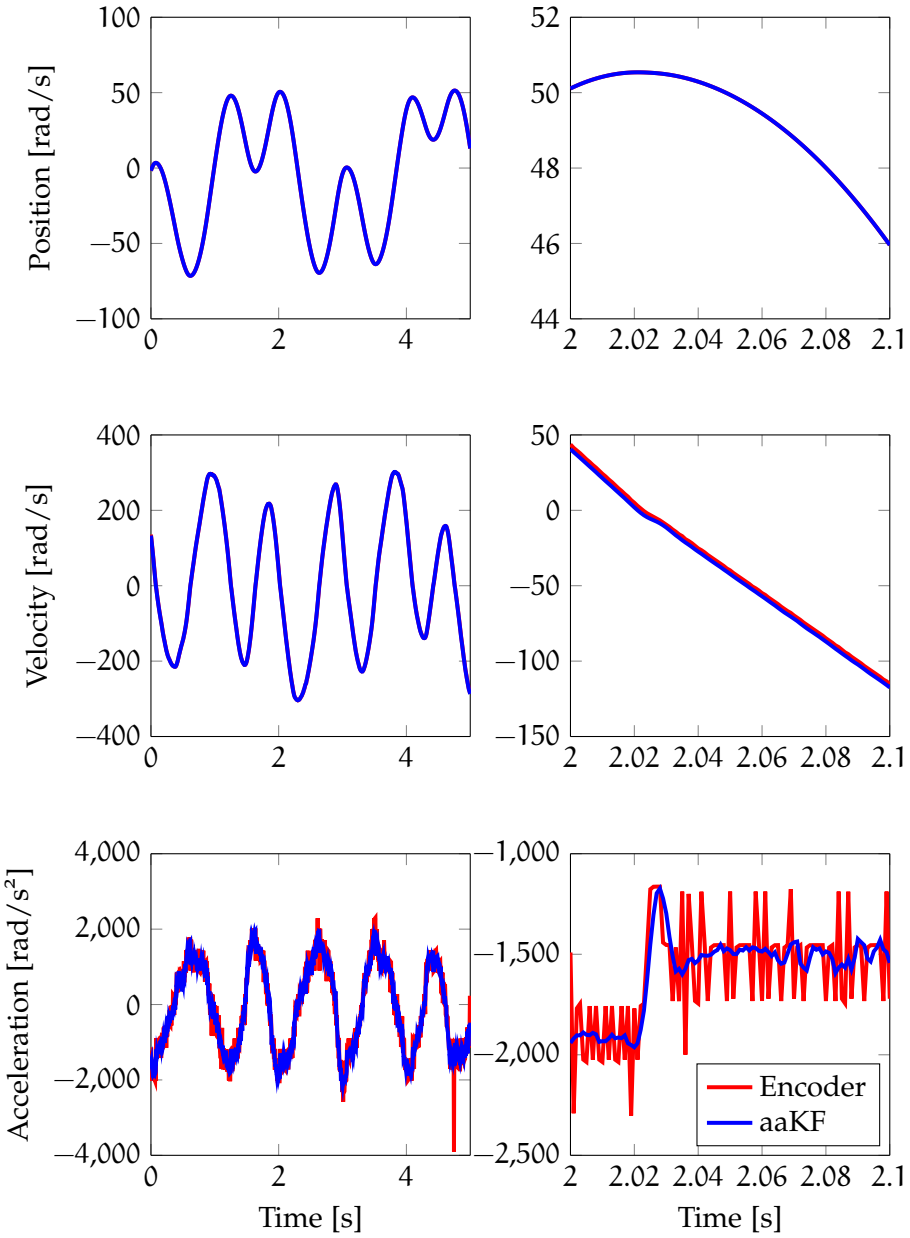

Figure 24: aaKF performance estimations. Position, velocity and acceleration comparisons between informations obtained from encoder signals(red coloured lines) and aaKF estimations (blue coloured lines).

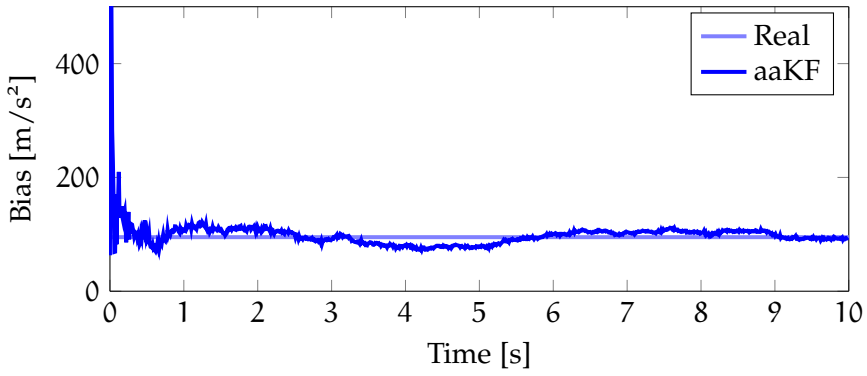

Figure 25: Comparison between KF estimated bias and true one.

can be obtained by the derivative of encoder signals or as output of the sensor fusion algorithm (aaKF). Both approaches have been tested, in order to understand any possible benefits in using the additional acceleration measurements.
Results of both experimental tests are shown in Fig. 26, which plots the estimation results of the desired physical device parameters (inertia and viscous and Coulomb friction coefficients), compared to the real ones, which are estimated from data-sheet's information or from traditional identification procedures. In particular, both identification test lead to the correct estimation of parameters. However, it can be noticed that faster and more accurate estimation can be obtained using speed information from the aaKF. This is an additional advantage, which supports the implementation of such solution. Furthermore, the identification procedure takes around ten seconds to correctly estimate the parameters. This time doesn't affect too much the preparation time for a robotic rehabilitation training, which is typically quite long ($10 - 20$ minutes). Consequently, such identification procedure can be easily performed during the start-up of the device.

2.5.3 *Zero force control*

Previous positive results have been used in the implementation of a zero force control system. The experiments to be performed focus the attention in the force control performances and backdrivability improvements of the robotic system.
The experimental set-up to be used is the same described in Sec. 2.4 with some modifications. In fact, the two subsystems work in different manner. The first one implements a rigid position controller and a sinusoidal trajectory generator, in order to simulate participant's behavior, who performs some simple repetitive movements. This subsystem is connected to the second one using a load cell, so the interaction force between them can be measured. The second subsystem is the real system under test. It implements a zero force control, based on a proportional controller, shown in Fig.28. The controller aim is to keep as close as possible to zero the interaction force signal, used to close the control loop. Consequently, backdrivability issues are counteracted.
The experiments consist in moving the zero-force controlled device by using the first robot which performs repetitive and equal movements. Tests are performed at first with the force control disable, understanding the necessary effort amount to be applied to allow movements. Then the force controller is turned on. Two different control loops are implemented. Firstly, interaction force measurement, from the load cell, is used as control input. Then, this signal is replaced by the interaction force estimation from DOB and RFOB tools. During these experiments the load cell measurements, which are very important informations as they give accurate estimations of the interaction forces, are saved and shown in Fig. 29. Some basic statistical average data are also obtained and reported in Fig.30.

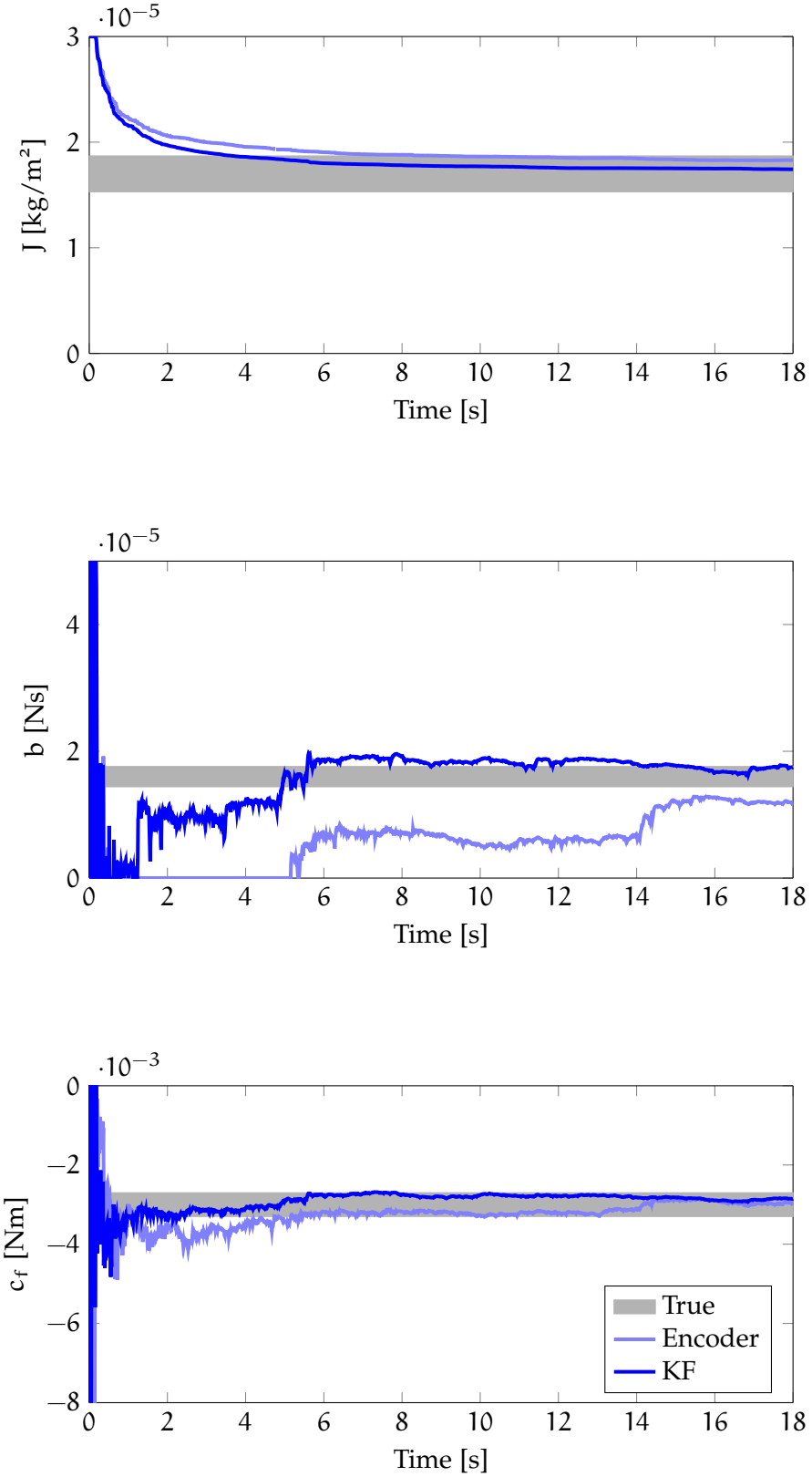

Figure 26: Device parameter identification comparison between, using in the computation, speed information obtained from encoder signal derivatives (light blue coloured line) or from aaKF estimation (blue coloured line) and real values (grey bad, which described a ±10% range value).

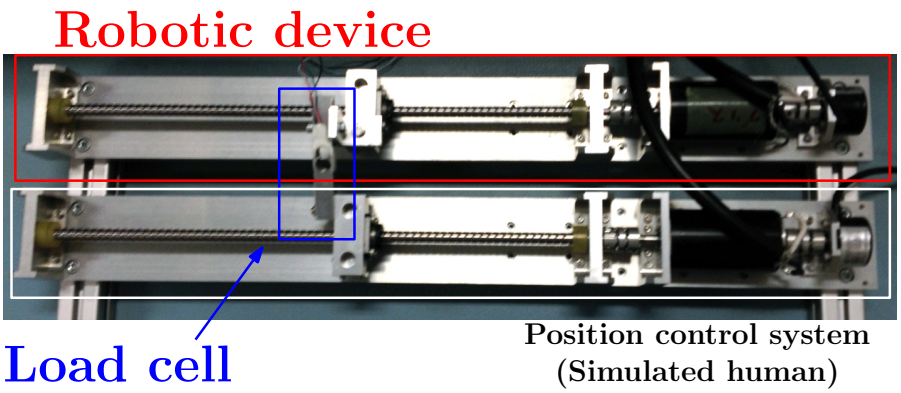

Figure 27: Experimental set-up configuration for the zero force control system test.

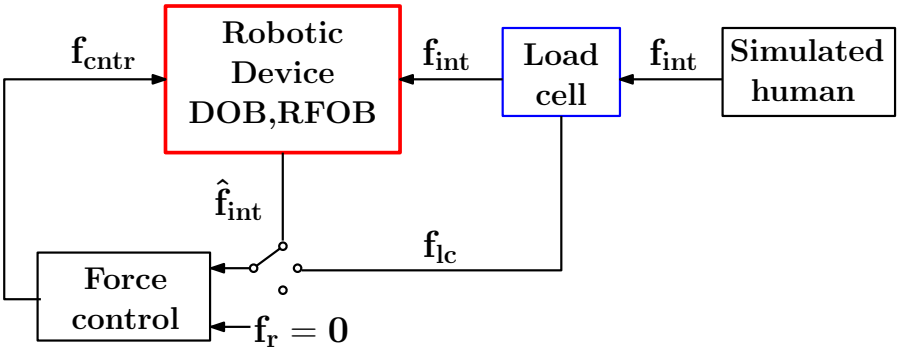

Figure 28: Block diagram of the zero force controller. Where f_r, f_{cntr} are the input reference and control output force,respectively. f_{int}, $\hat{f}_{int}$ are the real and estimated interaction force respectively, and f_{lc} is the interaction force measured by the load cell.

From the experimental results, the robotic device under test shows no good backdrivability capabilities, as high forces must be applied to make it move in an uncontrolled scenario. Such drawback can be solved implementing a zero force controller, previously described. In fact, in the active force control case, applied forces are lower, consequently participants must provide less effort. In fact, friction disturbances are correctly compensated and human effort is used only to beat inertia forces.
Moreover, experimental results show how force sensorless solution, using DOB and RFOB gives similar results compared to the ones obtained by using the load cell measurements. This is a further evidence of the validity of such force sensorless tools. However a fundamental aspect, for the success of this solution, is the accurate estimation of the system parameters and affecting disturbances, otherwise performances will be worse.
Finally, such force controller can be also used as inner loop in more complex control algorithms, in order to ensure the desired robot force is applied to the participants. In this case, the outer control loop output is used as reference input f_r for the inner loop.

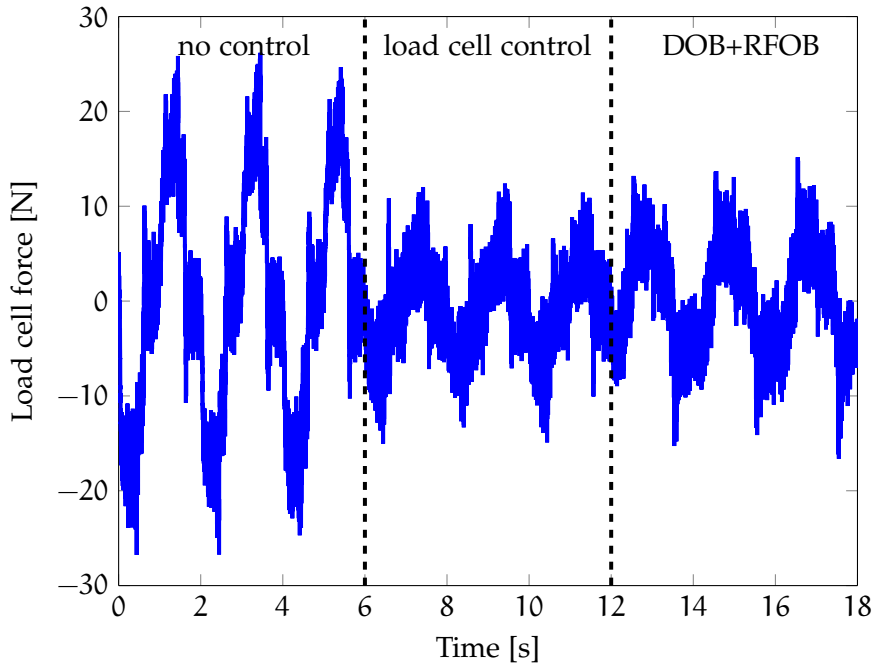

Figure 29: Load cell measurements in three different scenarios: no active control and zero force control using load cell and DOB and RFOB estimation of interaction force.

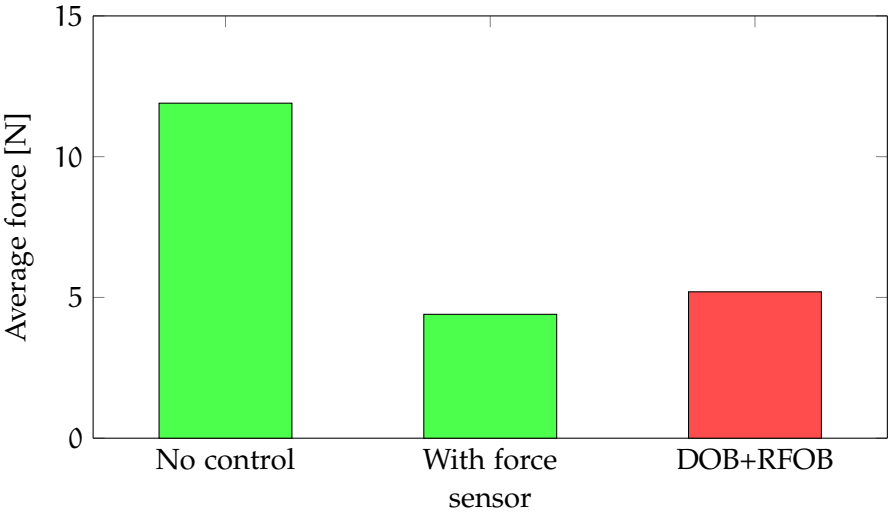

Figure 30: Absolute average force of the load cell signal in Fig. 29.

2.5.4 *Bilateral position-force control*

After showing performances of the proposed sensor fusion and identification tools and accuracy in force control, the last performed test is the implementation of a bilateral position-force control system in which both accurate position/speed and force informations are needed. Such control structure is used to implement teleoperation or haptic system in a wide range of robotic applications and, in particular, in robotic rehabilitation. Such systems are capable of implementing a bidirectional exchange of haptic sensation between one subsystem, usually called master, and an other one called slave (see Fig. 31). In

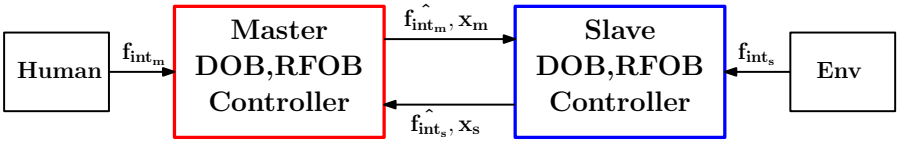

Figure 31: Schematic representation of a bilateral control system, which allows a human to interact with an environment remotely.

robotic rehabilitation, these subsystems are typically driven by patients and therapists, respectively. Such control system aims to reproduce the same movements and interaction forces at both side. From a mathematical point of view and considering a sigle-DOF robotic system, this can be represented as:

$$x_m - x_s = 0 \tag{54}$$

where x_m and x_s are master and slave end-effector position, respectively.

$$f_{int_m} + f_{int_s} = 0 \tag{55}$$

where f_{int_m} and f_{int_s} are master and slave interaction force estimation, respectively. As this is not a crucial aspect of the research, for further details about the controller implementation please refer to the great amount of related works in the literature [74, 91, 92].
Such control system has been implemented in the experimental setup in Fig. 23. No force sensors are used in the control system, so DOB and RTOB/RFOB (related low-pass filter bandwidths are set to $g_{DOB} = g_{RFOB} = 1500 rad/s$) and the previous described identification procedure are also implemented. Moreover, the proposed sensor fusion algorithm is used in the control loop.
The experimental test consist in drive the master side with an human arm, performing free movements and contacts with a rigid environment placed in the slave side. At first, DOB and RTOB/RFOB are using encoder signals in the computation. In the second part of the experiment, encoder signals are replaced by aaKF estimations. In this manner, benefits of the proposed solution can be understood.
Experimental results are shown in Fig. 32. It is worth noticing that, by using the aaKF sensor fusion algorithm, it is possible to increase DOB and RTOB/RFOB bandwidths without introducing additional vibrations, in particular in case of contact with rigid environments. So a better haptic perception can be achieved.

2.6 CONCLUSIONS

In this chapter, some novel researches, aiming to improve backdrivability and haptic performances in robot devices, are presented. These studies are essentially focused on performance improvements of force sensoreless solutions and containing device's costs and complexity. As a result, a sensor fusion algorithm, merging together position encoder measurements and acceleration signals from a low-cost MEMS accelerometer, and a particular identification procedure, based on a

RLS algorithm have been developed.
In particular, the RLS identification procedure allows to properly estimate the main mechanical parameters of the system, such as inertia and Coulomb and viscous friction coefficients, and the aaKF algorithm allows to obtain more accurate, in terms of reduced added noise, position and speed estimation of the device end-effector. Using such more accurate informations, the proposed RLS procedure results in faster and more precise system parameter identification. Such positive results lead to further benefits. In fact, they can improve DOB and RTOB/RFOB performances. Essentially, it is possible to increase DOB and RTOB/RFOB bandwidths and obtain a more accurate force control of the device and better estimation of the human-robot interaction force.
In conclusion, with non invasive and inexpensive hardware modifications (addition of low-cost MEMS accelerometers) and implementation of simple algorithms, it is possible to improve backdrivability and haptics features of robotic devices. This is an important result in order to develop low-cost robotic device with suitable control performances to be used in robotic rehabilitation applications.

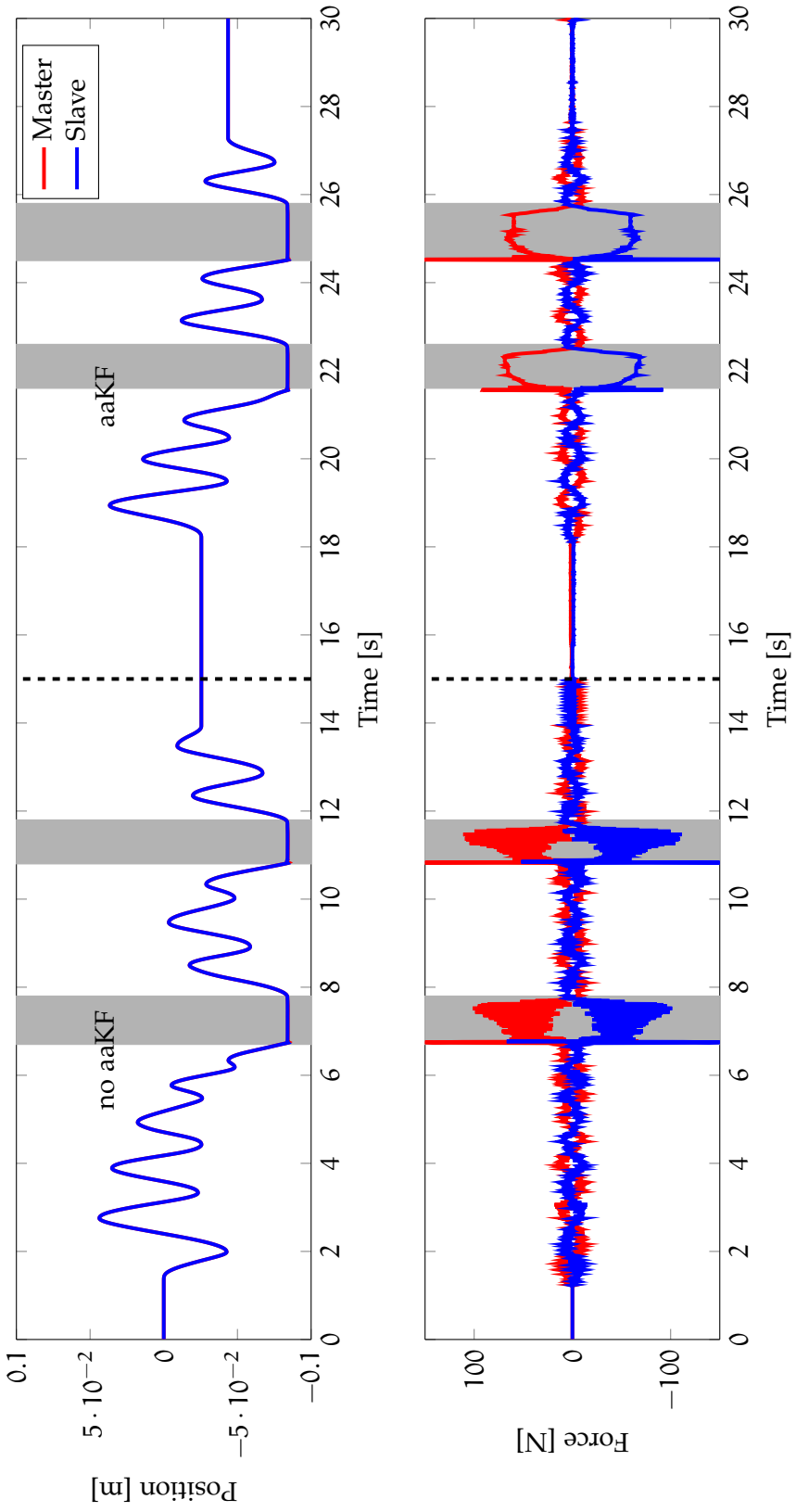

Figure 32: Master (red coloured lines) and slave(blue coloured lines) position and interaction force signals in a bilateral position-force control system during both free movements and contact with a rigid environment (grey areas). First part of the experiment is performed using normal encoder signal and related estimations, while, during the second part, these are replaced by informations from the aaKF.

3

ADAPTIVE COMPLIANCE CONTROL

3.1 INTRODUCTION

Rehabilitation therapies are foundamental in motor recovery process and their benefits are clear and clinically proved. In particular, the amount of recovery is closely linked to the level, intensity and frequency of trainings and practices. Moreover, for stroke patients, it is also very important the timeliness in performing such rehabilitation therapies, after the acute phase of the event. Unfortunately, there are some limitations in making rehabilitation therapies available to all those who need them. Such limitations are mainly related to high costs and limited human resources, concerned with rehabilitation treatments. Rehabilitation robotics is also having an important role in addressing such issues and the related current growth of the demand for rehabilitation therapies. Many research studies have been carried out in order to develop suitable robotic devices, haptic interfaces and related control strategies, to better assist patients during training and to promote the rehabilitation processes.
One of the most promising solutions is the development of stand-alone robotic rehabilitation systems, which allow to perform robotic therapies, without the supervision of specialized personnel. In the following discussion, a typical stand-alone rehabilitation robotic application will be considered, in which the patient interacts with a N-DOF robotic device, which is also interfaced to a VR environment (see Fig.5). In this setting, the patient is asked to track a moving target displayed in the VR environment, by properly moving the robot end-effector. This target repeatedly follows very simple and intuitive trajectories, in order to simulate some functional movements.
The use of such kind of stand-alone robotic devices, combined with virtual reality VR tools, which help to keep the patient involvement high, are becoming a common approach in the rehabilitation robotics. In fact, they can address some of the above mentioned issues, related to rehabilitation treatments, e.g.:

- reduce the problems of high costs and limited human resources related to treatments;
- increase patients' involvement, avoiding their slaking behaviors and tayloring exercises on specific needs;
- provide accurate and objective assessment of the patient's state and information about rehabilitation process to doctors and therapists, who, in this way, can check improvements;
- allow to perform therapies directly at patient's home;

In order to be used as stand-alone devices, without the supervision of specialized personnel, the robotic rehabilitation systems must be

able to adapt their action according to different patients and types and degrees of impairment and, also, to be compliant with the patient's behavior. To obtain this, the the controllers of the robots must be designed in order to provide assistance to the patient only when it is actually needed, promoting his/her active participation.
Not only the system behavior is important in the development of such stand-alone applications. In fact, economical aspects should also be taken into account, in order to keep realization costs within reasonable bounds, so making the device accessible to more people. As a consequence, an other important goal is to maintain the mechanical and electrical structure of the robotic device as simple and inexpensive as possible.

3.1.1 *Assistive controllers*

Active assistance exercise uses an external physical assistance to aid participants in accomplishing desired tasks. Therapists manually implements this in clinical rehabilitation on a regular basis, continuously adapting the amount of assistance, according to patient's needs. Many benefits can be achieved, in particular:

- reduce spasticity and increase limbs range of motion;
- induce brain plasticity;
- promote repetitive and intensive practice.

In order to achieve such desired assistance by using a robotic device, many control techniques and strategies have been developed, which can be grouped in four categories [39]:

- Impedance-based assistance
- Counterbalance-base assistance
- EMG-based assistance
- Performance-based adaptive assistance

3.1.1.1 *Impedance-based assistance*

It is a simple but not really effective fashion to achieve an assistance behavior of the controller. When the participant moves his/her limbs along a desired trajectory, the robot should not provide any assistance. On the other hand, the participant deviates from the right trajectory, the robot provides a restoring force to correct the movements. Such corrective force can be accomplished by implementing a position or an impedance controller, with constant parameters [35, 93, 94]. Such controllers provide a basic form of "assistance-as-needed", since the amount of assistance force increases according to the participant's deviation from the desired trajectory.
A variant of the previous describe controller typology is the trigger assistance, in which the participant is free to attempt movements without any robotic aid, while some form of impedance-based assistance

is initialized after a performance index reaches a threshold. Such triggering event could be participant's interaction force [95, 96], the spatial tracking or speed error [51, 97] or the muscle activity [98, 99]. A problem of using such assistive approach is that the participant may produce only the least force or movements needed to activate the trigger, while the remaining part of the task is performed in a passive way, during the robot-driven movements of the participant's limbs.

3.1.1.2 *Counterbalance-base assistance*

In this case, robot devices are able to partially or totally counterbalance the participant's limbs weights. Such compensation can be achieved by using passive device's components, such as springs or elastic bands[100] or by using the robot's control system [101]. The latter active technique can also compensate for other forces that can restrain participant's free movement, such as those arising from abnormal muscular tone [102]. Such approach may alleviate participant's fatigue, during trainings, allowing longer treatment's duration. Finally, for both passive and active counterbalance techniques, the amount of weight support can be adapted according to participant's impairments and reduced when improvements are detected during trainings.

3.1.1.3 *EMG-based assistance*

Other researches are focused on the development of robotic devices which employ EMG sensors to drive the assistance. Such sensors are capable to measure electrical activity produced by selected skeletal muscles. Post-processed EMG measurements provide informations related to muscle's effort and fatigue, which can be use to trigger assistance. An example of this assistive approach has been proposed with the MIT-MANUS robot [103], where EMG signals are measured from different muscles on the shoulder and elbow, while the assistance is triggered when the properly processed EMG signals exceed specific thresholds.
Other solutions suggest to generate an assisting force proportional to the amplitude of the processed EMG signals both for upper-limbs [104, 105] and lower limbs [28]. With this approach, participants decide the movements to be performed, while the robotic device compensates for weaknesses, providing a force proportional to the EMG signal needed to drive the movement.
Unfortunately, there are some drawbacks and limitations in using such EMG-based assistance. In fact, EMG signals are sensitive to electrode placement, interference from neighbouring muscles and skin properties (e.g. sweat on skin, blood circulation) and, moreover, they depend on the current neurologic condition of the subject. As a result, specialized personnel is responsible for the correct placement of the sensors and subsequent parameter calibration of the signal processing tools. Such procedure must be performed for each training session and it is very difficult to automate. Lastly, other issues are

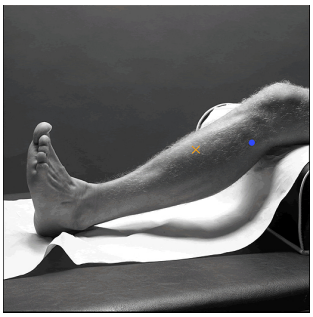

(a)

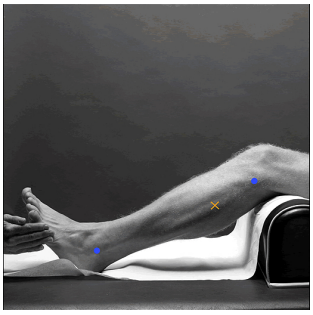

(b)

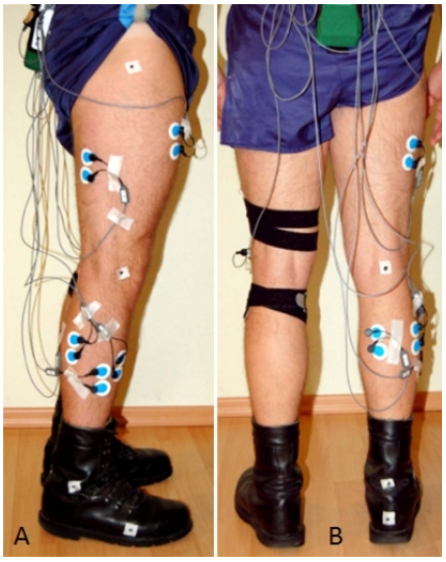

(c)

Figure 33: EMG sensors placement. (a)-(b) Proper movement and posture to correctly identify desired muscle and related sensor position (tibialis anterior and peroneus longus respectively) [106]. (c) Example of EMG electrodes placement on the right leg (involved muscles: tibialis anterior, peroneus longus, biceps femoris, gastrocnemius medialis and lateralis) [107].

related to robot safety. In case participant generates abnormal, uncoordinated muscle activation patterns, the robot could move in an undesired way.
The use of EMG-based robotic assistance seems to be very promising, however, at the moment, it is not suitable to design stand-alone robotic system, since it needs the supervision of qualified personnel during the whole training execution.

3.1.1.4 *Performance-based adaptive assistance*

Previously reviewed assistive control algorithms typically do not perform any online adaptation of their controller's parameters, based on current measurements or information related to participant's performances. On the other hand, such adaptive feature of the controller would bring the advantage of implementing a robotic assistance that can be automatically tuned, according to participant's specific needs, following changing or improvements during the rehabilitation process. So doing, it would be possible to avoid undesired patient's slacking behaviors. Moreover, this is a key feature to implement patient-cooperative robotic trainings, in which the robot adaptively takes into account the patient's intention rather than imposing an inflexible control strategy. Such goals can be achieved by using several approaches, such as:

- optimization algorithms
- iterative learning algorithms

Optimization algorithms

In the patient-cooperative framework, this approach attempts to minimize human-robot interaction forces/torques in real-time, consequently it promotes an higher participation of the subject. This can be achieved by estimating human-robot interaction forces/torques and then attempting to minimize these adapting the parameters of the reference trajectories, as developed by Lokomat in [108].
Within this approach, in order to obtain an "assist-as-needed" behavior of the robot, the device's controller aims to minimize a cost that is the sum of kinematic error (ensuring the task is completed) and robotic assistance (ensuring that the robot provide the minimum assistance necessary to complete desired movements) [109].
Using such optimization algorithms may lead to good robot performances and positive rehabilitation results. Unfortunately, in order to implement these algorithms, the computational effort strongly increase in case of complex tasks to be performed and in case of multi-DOFs robots used.

Iterative learning algorithms

In this approach, robotic system controllers adapt their parameters by computing an update law at each time step. Such update law usually takes into account the previous available information and the current participant's performances. Several adaptive strategies have been proposed, and a typical update law used has the following form:

$$G_{i+1} = fG_i + ge_i \tag{56}$$

where G_i is the adaptable control parameter at time step i (such as robot stiffness, assistance force or movement timing), and e_i is the performance error or measure, which is typically related to participant's ability to initiate movements, reaching or tracking a target. f and g, forgetting and gain factors respectively, are some constant weights of the adaptive law, and properly setting such parameters may change the controller behavior. Such approach has been firstly implemented using MIT-MANUS robot, where the duration of the desired trajectory and controller stiffness are adapted according to participant's impairments [103]. Other researches take advantages of such approach, but adaptation affects different control parameters, such as the maximum and current reaching velocity [110, 111] or controller impedance [112]. All reported controller solutions aim to make tasks simpler when participants can not correctly perform them. On the other hand, when performance errors are low, the update law makes tasks more challenging, such as target to be follows moves faster or decreasing robotic assistance.
Finally, the use of adaptive controllers becomes even more important when the goal is to provide mechanically compliant assistance to the participant, avoiding to perform stiff robot controls, which simply

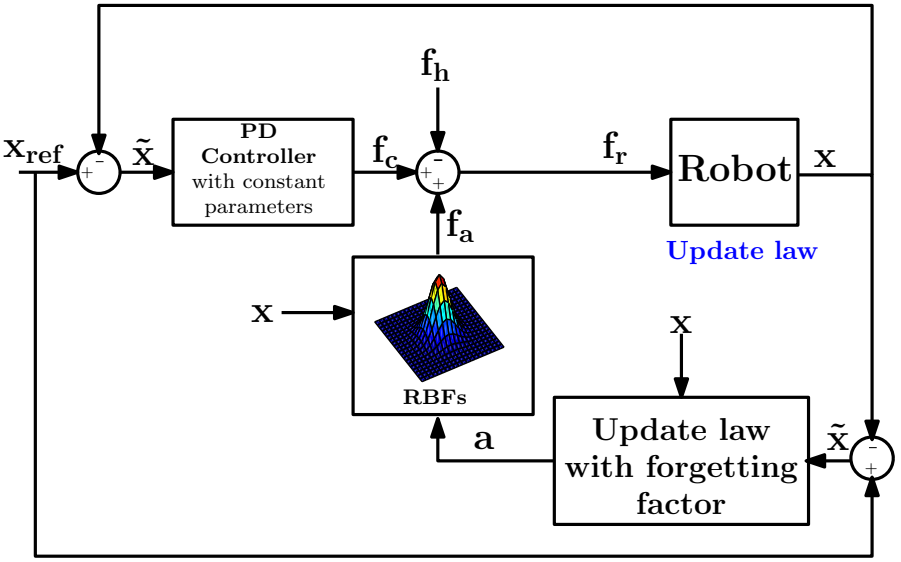

Figure 34: Block diagram of the performance-based adaptive assistance controller proposed in [113].

drives participant's limbs along a desired path. A compliant robot instead must be able to properly calculate the correct amount of force to compensate patient's weaknesses, lack in coordination or other type of impairments. Unfortunately, these undesired effects vary widely among patients. The implementation of adaptive or learning based control algorithm can effectively address such issues.
In one study, such approach as been implemented, providing an adaptive assistive force using only information from position sensors [113]. The main idea is to make use of an adaptive position-force map, which contains the value of the assistive force needed to bring the patient closer to the target position, for each point of the path to be followed. Such position-force map is obtain by using radial-basis function (RBF) model with Gaussian kernel, which allows a efficient approximation of this non-linear function in a digital fashion. The map is, also, updated in real-time, using an adaptive law on the form of (56), based on tracking error during a reaching task. As a result, it provides an assistive force, to compensate participant's impairments in specific locations in which they arise. Including the forgetting term in the adaptive law encourages an active effort from participants, preventing them from relying on the robotic assistance only, and also adapts the assistance to match the level of the participants' impairment, following improvements during the rehabilitation process. Fig. 34 shows a schematic representation of the control algorithm, it is worth noticing that such adaptive assistive force is coupled with a more traditional proportional-derivative (PD) position control with constant parameters. Better understanding and clarifications, about how such controller typology and RBF approximations work, will be provided in the following as the proposed novel control algorithm takes inspiration from this approach.
In conclusion, it is worth noticing that the assistive force is provided in a feedforward fashion, so there are no problems from the point of

view of the control stability. However, this approach presents some limitations and drawbacks:

- feedforward compensation may apply wrong assistive forces, as patients don't always perform errors in the same way. In fact, during the execution of a repetitive task, it may happen that the patient perfectly follows the moving target in a location in which he/she has previously made large errors. In such a case, the feedforward compensation generates a force based on the previous errors and pushes the patient away from the target position;
- it does not always preserve the causal relationship between patient effort and resulting limb movements. Instead, as already reported in the introduction, many research studies have shown how a properly set robot compliance (which implements a clear causal relation between effort and movements), stimulates motor learning process, encouraging patient engagement and effort.

3.1.2 *Proposed approach*

The leading aim of the work described in the following is the development of a suitable control algorithm for stand-alone rehabilitation robotic applications (see Fig. 5) to better assist patients during training and to better promote rehabilitation processes. One of the most promising control strategy to achieve such goals is the so-called "assist-as-needed" controllers, which are conceived to assist patients in completing the desired movements, while providing the minimum force necessary. An other important aspect, taken into in account in the development of the controller, is to maintain the structure of the overall robotic system as simple and inexpensive as possible. As a result, the use of expensive and fragile force/torque sensors or EMG measurements, which are complex to calibrate and to process, have been discarded. Consequently, only control strategies based exclusively on the use of "traditional" position sensors have been taken into account.
Among the previously described assistive control strategies, the solution based on the adaptive assistive force, reported in [113], seems to meet all the desired requirements. As a consequence, the second main activity of this Ph.D project has concerned the development of a novel adaptive assistance control algorithm, which takes inspiration from this iterative learning control but presents fundamental modifications in order to address its previously mentioned issues. As it will be explained later, the essential idea behind the proposed control strategy is based on the observation of the assistive strategy used by the therapists, who usually adapt their compliance to the patients' conditions, helping them to complete the desired movement. The proposed approach makes use of an adaptive PD controller, which allows to vary the mechanical impedance felt by patients while manipulating the robot end-effector. Hence, the supportive action, performed by

the robot, can be adjusted to be more compliant when patients perform a good tracking. On the other hand, when patients perform big errors, the controller becomes harder, in order to better guide patients along the trajectory to be followed. Unlike the solution proposed in [113], the assistive force is generated in a feedback fashion, avoiding the previously described undesired behaviors. On the other hand, the feedback loop leads to a stability issue, which is not straightforward to prove.
The chapter is organised as follows. Sec.3.2 contains an overview of the non-linear adaptive impedance controller algorithm. Then, a complete stability proof of the control algorithm is reported in Sec. 3.3. Sec.3.4 and Sec.3.6 explain the experimental setup and the performed rehabilitation trials, respectively. Some experimental results will be presented in Sec.3.7. At the end, in Sec.3.8 some final remarks will be reported.

3.2 NON-LINEAR ADAPTIVE COMPLIANCE CONTROLLER

As already mentioned, the presented control algorithm has been developed for specific robotic rehabilitation applications (see Fig.5). While other control techniques used in rehabilitation aim at recovering muscle tone and strength, the control strategy proposed in this work mainly focuses on the motor recovery aspects, related to the proper muscle activation, with the final target of a relearn of some simple movements, to be used in everyday life.
Desired controller features, to be achieved in proposed solution, are:

- capability to emulate the therapist behavior during trainings, providing the least assistance needed;
- promote an active participation of patients, driving them to better perform the tasks;
- obtain a tool to estimate and evaluate patient's state, checking for example fatigue states and therapeutic improvements, simply analyzing the current values of the variable control parameters.

A significant aspect taken into account in the design of such control system is its simplicity. In fact, it is based on the tracking error, it does not require any additional sensors, except standard encoders or position sensors, normally integrated in the actuators. Doing so, it is possible to avoid the design of expensive and bulky robotic systems. Moreover, there are no limitations related to the design, mechanical structure and number of DOFs of the robot to be used, as such control algorithm can be easily applied to different types of robot.
Its final target consists in obtaining the best possible performances in terms of promoting patient rehabilitation with a simple and low-cost rehabilitation robot system design. This is one of the biggest challenge concerning the rehabilitation robotics in order to design a robot device which is suitable to perform therapies directly at patient home and, furthermore, to be within everybody's reach.

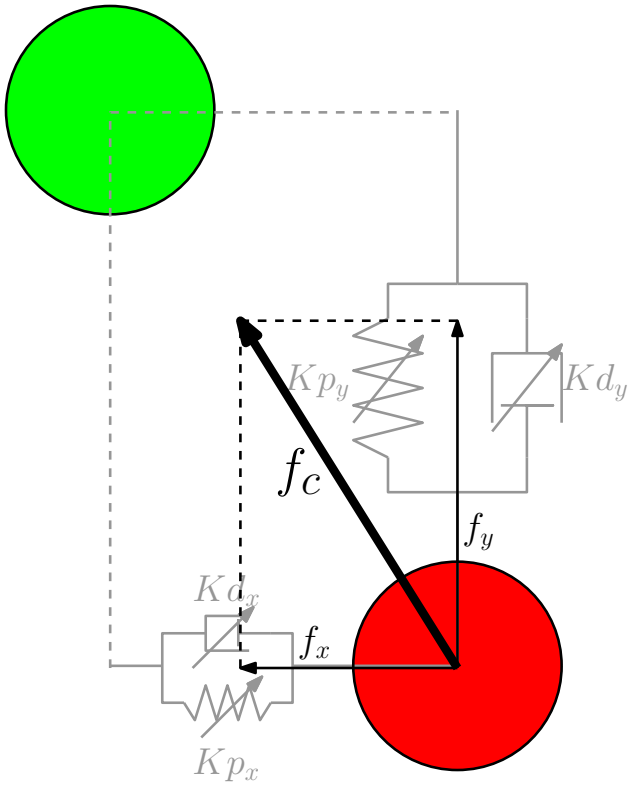

Figure 35: Graphical representation of the adaptive compliance controller for a planar, 2-d.o.f. robot device.

3.2.1 *Control algorithm*

Going deeper into implementation details, the proposed approach is based on merging together an PD control and an adaptive learning control. Both control and adaptation strategies are inspired by the typical assistive action of the therapists, who tend to adapt their compliance to the tracking error of patients. In practice, a stiffer action is exerted on the patients in case they are not able to complete the desired movement, while the support is softer in case they are able to complete the proposed task autonomously. Such behavior better promote rehabilitation, as there is an active participation of the patient, who tries to properly activate his/her muscles.
The proposed controller solution provides an assistive action which approximates such therapist behaviors, simulating N viscoelastic elements, each of them independently acting along one of the workspace coordinates (see Fig.35). The equilibrium point of each virtual spring coincide with the overlap of the red ball (end-effector) with the green ball (target to be followed). Thus, the control generates a variable attractive force $\mathbf{f_c}$ towards the target, as sum of individual forces, one for each DOF (e.g. $\mathbf{f_x}$, $\mathbf{f_y}$ in Fig.35 for planar, 2-d.o.f. robot case).
Moreover, the corresponding physical parameters of such virtual elements, (stiffness $K_{p_1} \dots K_{p_N}$ and viscosity $K_{d_1} \dots K_{d_N}$) are variable, depending on patient weakness, which is determined by evaluating his/her tracking performances. Clearly, due to specific patient's im-

pairments, the tracking error may vary along the target trajectory to be followed and the degree of assistance should change accordingly. Roughly speaking, higher impedance gains are set in workspace locations where patients perform bigger errors. As a result, the proposed controller is implemented as N independent non-linear functions of the N kinematic variables, which relates each point of the workspace to a specific set of controller proportional and derivative gains. Additionally, as will be explained later, such impedances are adapted over time, in order to follow any patient's performance variations.
The strict connection between controller gain values and patient's performances is clear. As a result, such correspondence allows to obtain some synthetic and easy to understand data, to constantly monitor patients during trainings. In fact, the observation of the virtual viscoelastic element values and their trends actually provide information related, for example, to patient's current state, e.g. fatigue or performance improvements.
For the sake of simplicity, let's start the control algorithm explanation by analyzing, at first, the issue of representing a non-linear function of N variables in a computationally efficient way. Among all the possible solutions, the use of radial basis functions RBFs with Gaussian kernel is a common approach, allowing to obtain a simple and efficient representation of non-linear functions. An approximation of a non-linear function spread over the workspace, based on RBFs with Gaussian kernel, can be performed by dividing such workspace into P non-overlapping areas, and placing at the center of each of them a properly weighted Gaussian function. The number of areas P is chosen in order to get the best trade-off between a good approximation and excessive computational complexity. As it can be seen in Fig.36, an approximation of a generic non-linear function, in the workspace, can be obtained by the properly weighted sum of such gaussian functions.
In the presented control algorithm, just the current controller proportional gains k_{p_i} are obtained by computing the N stiffness map, which is approximated by RBFs, in the current end-effector position. At the same time, the controller derivative gains k_{d_i} are defined in order to obtain a constant damping factor of the PD controllers. This is obtained by observing the transfer function between input force u and position in a simple zero reference PD controller, in a single-DOF robot case with unitary mass. This transfer function is equal to a typical second order system with natural undamped frequency w_0 and damping factor ξ, i.e.:

$$\frac{x(s)}{u(s)} = \frac{1}{s^2 + K_d s + K_p} = \frac{1}{w_0 s^2 + 2\xi w_0 s + 1} \tag{57}$$

where x and $\ddot{x}$ are position and acceleration of the system, respectively, and K_p and K_d are the proportional and derivative gains of the controller. Consequently, considering ξ constant, K_d is computed as following:

$$K_d = \frac{\xi}{2}\sqrt{K_p} \tag{58}$$

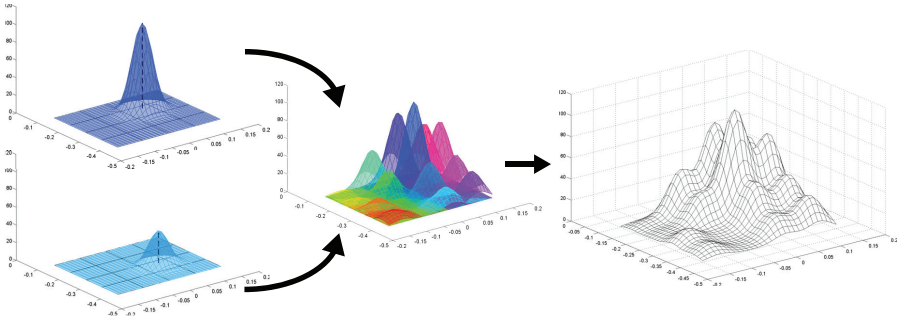

Figure 36: Schematic representation of the approximation process of a non-linear function, through the use of radial basis functions RBFs with Gaussian kernels.

This choice has been made in order to not increase too much the overall computational effort of the control system. As a result, the control parameters computation are obtained as follows:

$$\mathbf{k_p}(\mathbf{x}(t)) = [k_{p_1} \dots k_{p_N}]^T = \widehat{\mathbf{k_p}(\mathbf{x}(t))} = Y(\mathbf{x}(t))\mathbf{a} \tag{59}$$

$$\mathbf{k_d}(\mathbf{x}(t)) = [k_{d_1} \dots k_{d_N}] = [\frac{\xi}{2}\sqrt{k_{p_1}} \dots \frac{\xi}{2}\sqrt{k_{p_N}}] \tag{60}$$

$$\mathbf{a} = [k_{p_{11}} \dots k_{p_{1P}}, k_{p_{21}} \dots k_{p_{2P}}, \dots, k_{p_{N1}} \dots k_{p_{NP}}]^T \tag{61}$$

where $\mathbf{a}$ is a NP vector with the gaussian heights for the stiffness map approximations $\widehat{\mathbf{k_p}(\mathbf{x}(t))}$ and ξ is a constant damping factor of the controller, defined experimentally, while $\mathbf{Y}(\mathbf{x}(t))$ is a $N \times NP$-dimensional Gaussian weight matrix evaluated in the current end-effector location $\mathbf{x}(t)$, defined as follows:

$$Y(\mathbf{x}) = \begin{bmatrix} g_1 \dots g_P & \mathbf{0} & \mathbf{0} \\ \mathbf{0} & \ddots & \mathbf{0} \\ \mathbf{0} & \mathbf{0} & g_1 \dots g_P \end{bmatrix} \tag{62}$$

$$g_i = \frac{c}{2\pi\sqrt{\det \boldsymbol{\Sigma}}} e^{-\frac{1}{2}(\mathbf{x}-\boldsymbol{\mu}_i)^T \boldsymbol{\Sigma}^{-1}(\mathbf{x}-\boldsymbol{\mu}_i)} \tag{63}$$

$$\sum_{i=1}^{P} g_i \leqslant 1 \tag{64}$$

where $\boldsymbol{\mu}_i$ is the center position of the i-th areas of the workspace, $\boldsymbol{\Sigma}$ is the $N \times N$-dimensional covariance matrix of the Gaussian bell and c is a normalizing gain, chosen in order to satisfy condition (64).
The amplitude of the Gaussian function bell depends on the values of the covariance matrix $\boldsymbol{\Sigma}$. It is advisable to set such values depending on the shape and size of the areas in which the workspace has been divided, in order to obtain a properly smooth approximated curve. A similar smooth result can be found in the control parameters variation.
An PD controller, with varying control parameters according to the current end-effector position, has been implemented in the control loop (see Fig.37). As a result, the dynamic equation of a generic robot device is:

$$\mathbf{f_r}(\mathbf{x}(t), \tilde{\mathbf{x}}(t), \dot{\tilde{\mathbf{x}}}(t), t) = \mathbf{f_c}(\tilde{\mathbf{x}}(t), \dot{\tilde{\mathbf{x}}}(t), \mathbf{x}(t)) - \mathbf{f_h}(t) \tag{65}$$

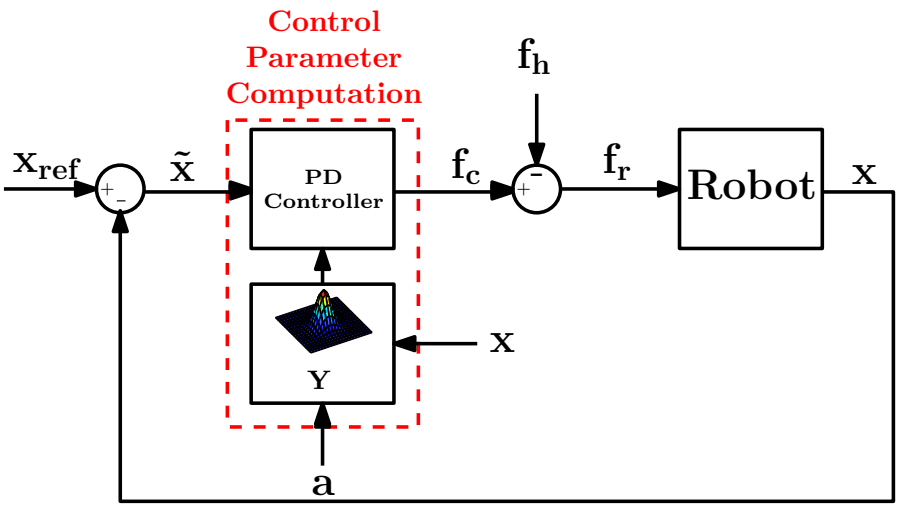

Figure 37: Block diagram of the non-linear compliance control system, showing how its control gains are varying according to the end-effector position and depending on vector $\mathbf{a}$ components.

where $\mathbf{x}$, $\tilde{\mathbf{x}}$ and $\dot{\tilde{\mathbf{x}}}$ are respectively the N-dimensional current end-effector position vector and position and velocity error vectors ($\tilde{\mathbf{x}}(t) = \mathbf{r}(t) - \mathbf{x}(t)$ where $\mathbf{r}(t)$ is the target position), $\mathbf{f_h}$ is the human interaction force and $\mathbf{f_c}$ is the control force that assists the patient in completing the desired movements and defined by:

$$\mathbf{f_c}(\tilde{\mathbf{x}}(t), \dot{\tilde{\mathbf{x}}}(t), \mathbf{x}(t)) = K_p(\mathbf{x}(t))\tilde{\mathbf{x}}(t) + K_d(\mathbf{x}(t))\dot{\tilde{\mathbf{x}}}(\mathbf{t}) \tag{66}$$

$$K_p(\mathbf{x}(t)) = diag(\mathbf{k_p}(\mathbf{x}(t))) \tag{67}$$

$$K_d(\mathbf{x}(t)) = diag(\mathbf{k_d}(\mathbf{x}(t))) \tag{68}$$

3.2.2 *Update law*

In order to follow patients' improvements or changes in their weakness, the control algorithm implements also an adaptation of vector $\mathbf{a}$, which defines the stiffness maps of controllers accordingly.
Indeed, the adaptation of $\mathbf{a}$ is the main aspect of the proposed control solution and, it is proposed to make use of the following update law:

$$\dot{\mathbf{a}}(t) = \overbrace{-\frac{1}{\tau}\mathbf{Y}^T(\mathbf{Y}\mathbf{Y}^T)^{-1}\mathbf{Y}\mathbf{a}(t)}^{\text{forgetting term}} + \overbrace{k\mathbf{Y}^T abs(\tilde{\mathbf{x}}(\mathbf{t}))}^{\text{error term}} \tag{69}$$

$$\mathbf{a}(0) = \alpha_0[1 \dots 1]^T \tag{70}$$

where α_0 is an arbitrary initial positive weight value and, for the sake of readability, position and error dependencies are omitted ($\mathbf{a}(t) = \mathbf{a}(t, \mathbf{x}(t), \tilde{\mathbf{x}}(t))$ and $\mathbf{Y} = \mathbf{Y}(\mathbf{x}(t))$).
The update law (69) consists of two terms:

- *forgetting term*: if no errors are performed, this term leads to an exponential decay of the parameters of $\mathbf{a}$, with a time constant

τ. The decrease of these parameters is weighted more in those areas closer to the current end-effector position, thanks to the matrix $\mathbf{Y}$;

- *error term*: takes into account of errors performed by patients. Large errors cause large increases of the components of $\mathbf{a}$, corresponding to areas which are close to the location where these errors are performed. k is a positive gain and by varying its value it is possible to change the error sensitivity of the update law. It is worth noticing that in (69), the absolute value of error is used in updating $\mathbf{a}$. In this way, we account only for the error amplitude and not for its direction. This because patients do not perform errors always in the same direction. A direct consequence of an augmented $\mathbf{a}$ is the increase of the overall stiffness of the controllers in specific locations, as required.

As a consequence of the updating of $\mathbf{a}$, the control parameters in (59) do not depend on the current end-effector position only, but they may also be updated over time, in order to keep memory of the patient performance history at different working positions. In fact, as long as small errors are performed, the first term of (69) results dominant and determines a decrease of the parameters while, when great errors occur, the dominant term becomes the second, causing an increment of the parameters and, in turn, of the controller stiffness at the position considered. As a result, the latter update law allows to take memory of the history performances of patients, over the workspace.
In order to digitally implement proposed control system, equation (69) has been properly discretised. At each time step k, vector $\mathbf{a}_k = \mathbf{a}(t_k)$ is updated as follows:

$$\mathbf{a}_k = \mathbf{a}_{k-1} + Ts\left(-\frac{1}{\tau}\mathbf{Y}^T(\mathbf{Y}\mathbf{Y}^T)^{-1}\mathbf{Y}\mathbf{a}_{k-1} + k\mathbf{Y}^T abs(\tilde{\mathbf{x}}_k)\right) \tag{71}$$

where $\tilde{\mathbf{x}}_k = \tilde{\mathbf{x}}(t_k)$. Consequently, the control stiffnesses are also computed, i.e.:

$$\mathbf{k_p}(\mathbf{x}_k, k) = \mathbf{Y}(\mathbf{x}_k)\mathbf{a}_k \tag{72}$$

where $\mathbf{x}_k = \mathbf{x}(t_k)$. From (72) and using (60), the current derivative control gains are also updated. Lastly, the assistive force is obtained using the discrete version of (66), i.e.:

$$\mathbf{f_c}(\tilde{\mathbf{x}}_k, \dot{\tilde{\mathbf{x}}}_k, \mathbf{x}_k) = K_p(\mathbf{x}_k)\tilde{\mathbf{x}}_k + K_d(\mathbf{x}_k)\dot{\tilde{\mathbf{x}}}_{\mathbf{k}} \tag{73}$$

where $\dot{\tilde{\mathbf{x}}}_{\mathbf{k}}$ is computed by using the pure time derivative, i.e.:

$$\dot{\tilde{\mathbf{x}}}_{\mathbf{k}} = \frac{1}{Ts}(\tilde{\mathbf{x}}_k - \tilde{\mathbf{x}}_{k-1}) \tag{74}$$

It is worth noticing that, given the adaptation mechanism implemented, the proportional and derivative gains vary according to the current end-effector position and also over time. The overall control system is shown in Fig.38, where it can be clearly seen how the controller works in feedback fashion and how such controller is adapted.

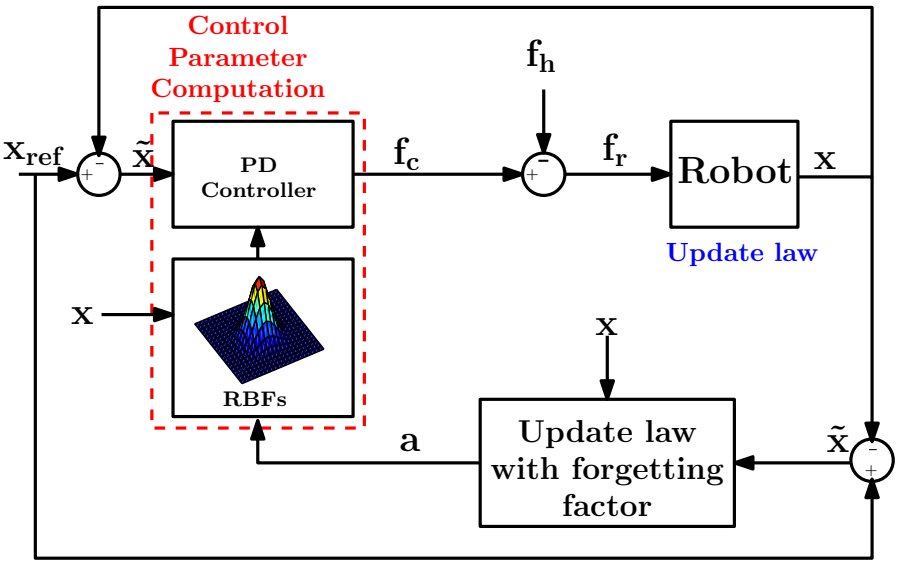

Figure 38: Block diagram of the non-linear compliance control system, really implemented. Compered to block diagram in Fig.37, vector **a** is time-varing.

Different behaviors of the adaptive control can be achieved by properly set values of τ, k and α_0 parameters. The choice of the those parameters is left to the discretion and experience of therapists. Anyway, in oder to understand effects of parameters' changes, a guideline is reported in Tab. 3.

At the end of the control algorithm explanation, it is possible to understand its overall time-varying and non-linear nature. Moreover, k and τ affect the time-varying nature of the controller. Consequently, they can not be arbitrary set. For all the above, a control stability proof is needed and is reported in Sec. 3.3.

3.3 CONTROL STABILITY PROOF

Control stability is a central issues in designing robotic systems, especially the ones that physically interact with humans, as in the case of RR devices. The proposed rehabilitation control strategy, described in chapter 3, presents a no straightforward control stability proof due to:

- time-varying and non-linear nature of the controller;
- update law control parameters tuneable by therapists;
- human-robot force interaction acting in the control loop.

In this section, a complete stability proof of such control system is presented. Particular effort has been made to consider and to model the human-robot force interaction and to derive the necessary control parameter constrains, in order to guarantee the overall control stability.

Table 3: Tuning control parameters guideline

	Small values	Big values
τ	Better tracking of the patient's performances, but noisier values of the controller parameters	Only slow changes in the patient's performance are followed, smooth controller parameters changes
k	Low sensitivity to errors performed by participants	High sensitivity to errors performed by participants
α_0	Weak or absent robotic assistance, at least at the beginning of the trial. Patients are encouraged, at first, to complete the exercise by themselves.	High robotic assistance, at least at the beginning of the trial. Robotic assistance allows to correctly perform the task immediately, so the robot can teach the right movements (useful in case of patients with low cognitive skills).

3.3.1 *Human-robot interaction*

Human-robot interaction force is a fundamental term acting in the control system as it influences the overall system behavior. For better understanding, Fig.39 shows how the participant enters in the control loop. Moreover, such force is a unpredictable input of the system and its contribution may produce control instability. For such reason and in order to simplify the following discussion, it is necessary to find a simple but accurate representation of the human-robot interaction acting on the robot device. To do that, it is important to analyze the common patient's behavior, which tries to properly move the end-effector of the robot, in order to correctly follow the target in the screen. Consequently, the human-robot force interaction can be seen as an attractive force, which aims to overlap end-effector and target position. Such force can be, merely, modelled as impedance $\mathbf{Z_h}$ or second-order linear time invariant (LTI) system. This representation is a standard approach used in the literature [114–117], and it allows to write the following equation for the human force:

$$\mathbf{f_h} = M_h\ddot{\mathbf{x}} + b_h\dot{\mathbf{x}} + K_h\mathbf{x} \tag{75}$$

where M_h, K_h, b_h are, respectively, diagonal and positive-definite human mass matrix and impedance parameter matrices.
However, it is understandable that such human model parameters may varying according to different participants who are performing the trainings. In fact, participants capabilities, in following the moving target, depends on their degree of motor impairments and level of cognitive skills. Moreover such parameters may vary according to their grasping force and end-effector position and so patient's limbs configuration, since their motor impairments are, sometimes, localized in specific area of the workspace.

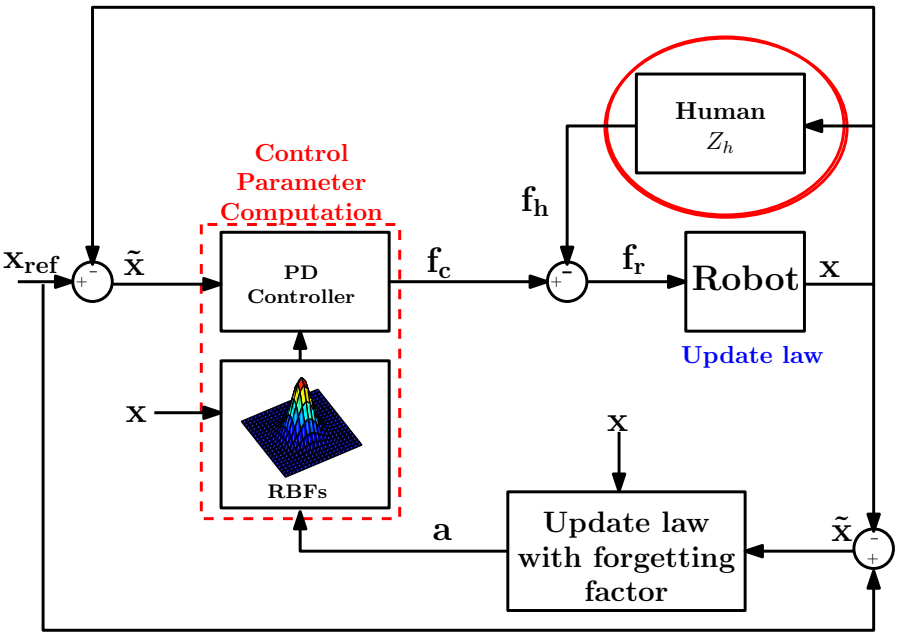

Figure 39: Block diagram of the non-linear compliance control system presented in chapter 3. Human-robot force interaction is highlighted.

3.3.1.1 *Human parameters identification*

Previous rationale has been confirmed performing some human model identification procedures for upper limbs, with healthy subjects. In particular, two different experiment typologies have been performed. The first one aims to show the human parameter variability according to different grasping forces [118]. The experimental set-up is schematically depicted in Fig.40. The experiment consists of shaking the human arm with a band-limited random motion generated with a shaker, while simultaneously sensing both the force and acceleration imparted to the arm. Then, conventional parametric/non-parametric identification procedures can be applied to the force/acceleration acquisitions in order to estimate the parameters of the simplified second order LTI model of the human arm impedance, shown in equation (75). The input bandwidth has been set to 20Hz due to physiological human limits of perception and reaction to stimuli [119].
In order to show how human arm impedance is affected by the way of grasping the sensorized handle, two experimental tests have been conceived, namely the "soft grasp" and the "hard grasp" tests. The two tests differ in the way the handle is grasped during the shaking motion. In the former case, the handle is grasped with only two fingers (Fig. 41a), while in the latter is hold with the whole hand (Fig. 41b).
The model parameters are determined by fitting a second order LTI model on the frequency response data obtained by applying a non parametric identification method, such as the empirical transfer function estimate (ETFE) method [120], to the force and acceleration measures. In the following, only the non-parametric identification results are presented. The tests has been performed on five different subjects and related results are reported in Fig. 42a for the soft grasp experi-

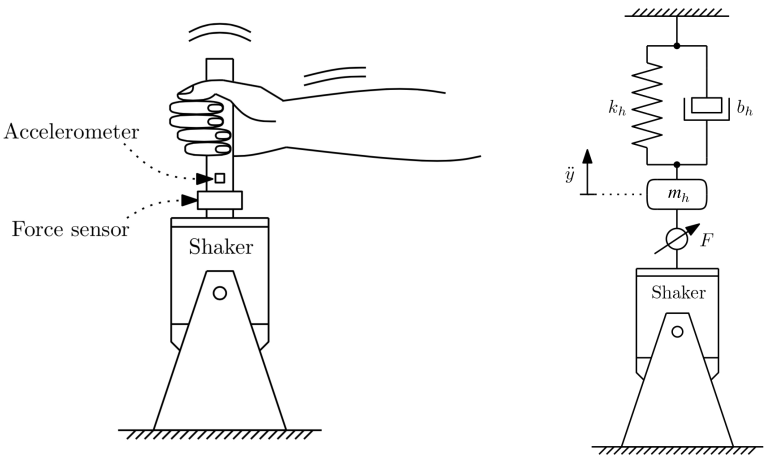

(a) Schematic representation of the experimental set-up (b) Human model

Figure 40: Experimental set-up schematization and related human model rapresetation.

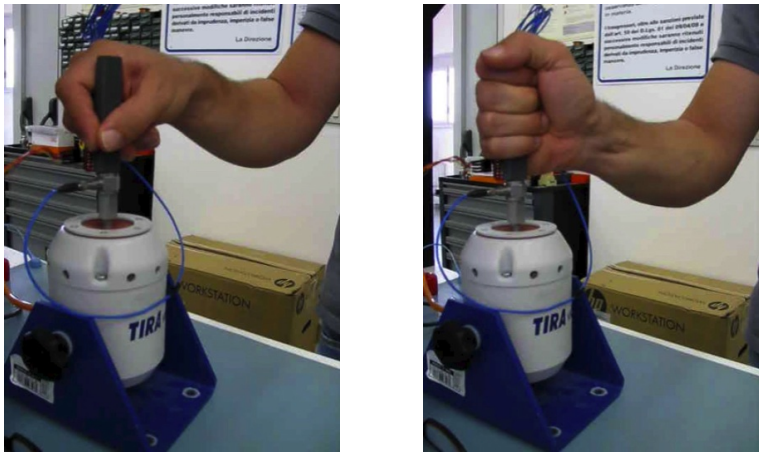

(a) Soft grasp (b) Hard grasp

Figure 41: Experimental tests of the human model parameters identification. Two different hand positions to obtain different grasping forces.

ments and in Fig. 42b for the hard grasp ones.
The second test aims to show variability of human impedance according to different limb configurations and, consequently, different robot end-effector position, in the workspace. An identification procedure, similar to the previous one, has been performed by an healthy subject. In this case, the 2-DOF robot device, described in Sec. 3.4, has been used to perform the tests. The subject has been instructed to, sequentially, maintain the end-effector in four fixed positions (see Fig. 43) for a short period of time, while the robot tries to shake the human arm with a band-limited random motion, in both X and Y directions.

A post-processing analysis, similar to the previous described, has provided the results in Fig 44b and 44a for X and Y axis, respectively.
Finally, experimental results show how the human impedance model can vary from person to person and it is affected by several factors,

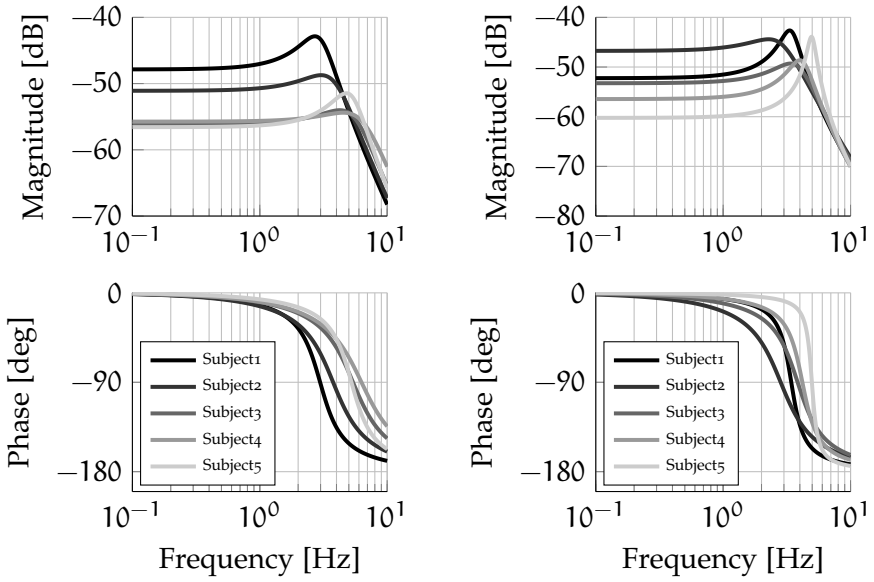

(a) soft (b) hard

Figure 42: Frequency responses of the second order human admittance models depending on different grasping forces of five subjects, identified from the experimental data.

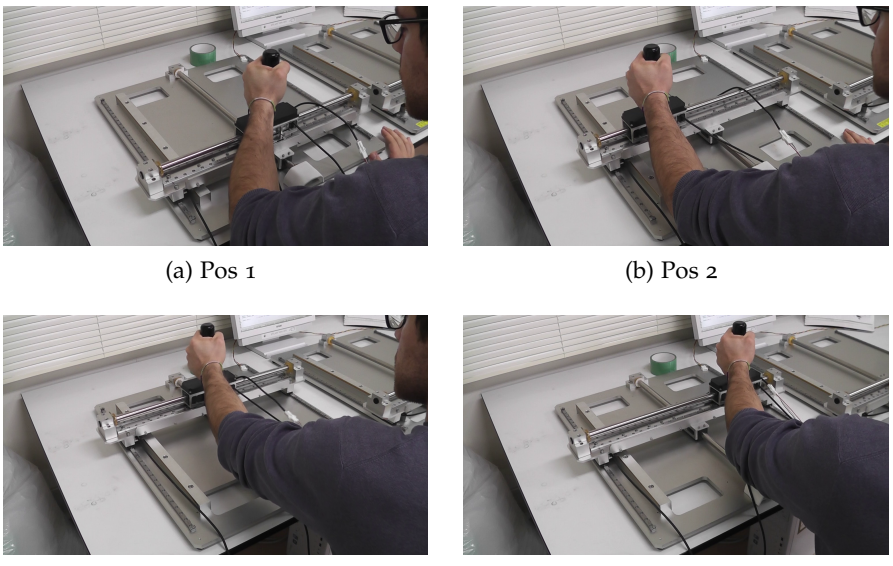

(a) Pos 1 (b) Pos 2

(c) Pos 3 (d) Pos 4

Figure 43: Experimental set-up and tests of the human model parameters identification, according to different limb's configuration and, consequently, robot end-effector position.

such as grasping force and limb configuration. As a result, it is clear how a complete identification of human model parameters and their variations is fundamental to understand which are the more critical values of the model parameters, from the control stability point of view.

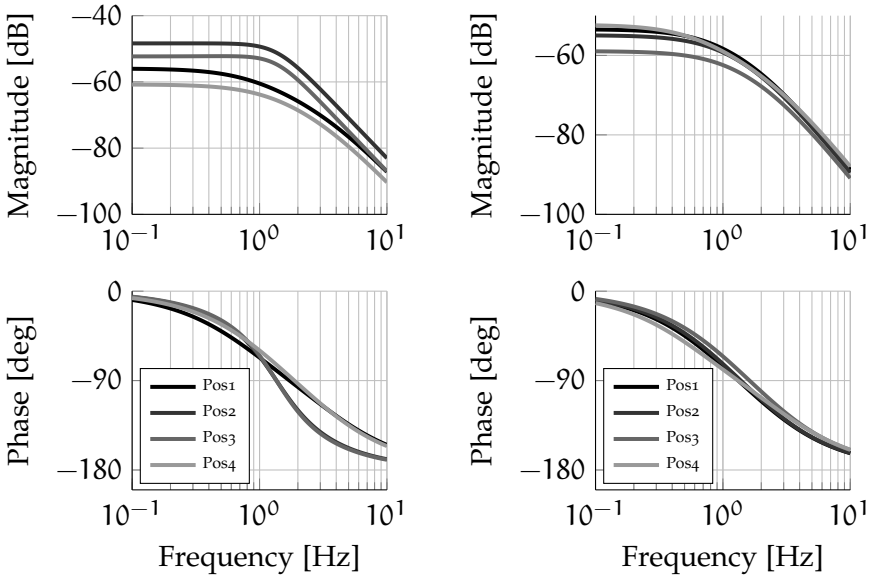

(a) X (b) Y

Figure 44: Frequency responses of the second order human admittance models depending on different upper-limb configurations of a single subject, identified from the experimental data.

3.3.2 *Stability discussion*

Due to the time-varying and non-linear nature of the previously presented compliance controller and presence of a human force acting on the system, its stability proof has been carried out using an energetic approach, taking advantages of the Lyapunov theory [121, 122]. In order to simplify the discussion, some proper constraints and model simplifications are defined:

- limited end-effector and target position and speeds:

$$\|\mathbf{x}(t)\|_\infty \leqslant x_{max} \ , \ \|\mathbf{r}(t)\|_\infty \leqslant r_{max} \tag{76}$$

$$\|\dot{\mathbf{x}}(t)\|_\infty \leqslant \dot{x}_{max} \ , \ \|\dot{\mathbf{r}}(t)\|_\infty \leqslant \dot{r}_{max} \tag{77}$$

- lower bounded stiffness of the N independent PD controllers, in order to prevent system from degenerating into an open loop one:

$$\|\mathbf{a}(t)\|_\infty \geqslant a_{min} > 0 \tag{78}$$

- human interaction force modelled as a second order linear model as previously described in Sec. 3.3.1. Constant values for the human impedance model are set, as their changes, correlated to tracking performance improvements and motion recovery, are slower than the control dynamics. So, their variation effects can be neglected in the stability analysis. Moreover, human interaction force in (75) can be split in two terms, i.e.:

$$\mathbf{f_h} = \mathbf{f_{h1}} + \mathbf{f_{h2}} = \overbrace{M_h\ddot{\mathbf{x}} - K_h\tilde{\mathbf{x}} - b_h\dot{\tilde{\mathbf{x}}}}^{\mathbf{f_{h1}}} + \overbrace{K_h\mathbf{r} + b_h\dot{\mathbf{r}}}^{\mathbf{f_{h2}}} \tag{79}$$

It is worth noticing that $\mathbf{f_{h2}}$ is a feedforward term, consequently it doesn't affect the control stability and it can be omitted in the following discussion, simplifying it.

The stability proof can be carried out in two steps: starting from a single DOF robot case and extending the results to a multi-DOF case.

3.3.2.1 *Single DOF robot device*

Using the 1-DOF version of (65), (66) and $\mathbf{f_{h1}}$ in (79), the dynamic equation of such simple robot system can be written as:

$$m_r\,\ddot{x}(t) = -m_h\ddot{x} + (K_p(t) + K_h)\tilde{x} + (K_d(t) + b_h)\dot{\tilde{x}} \tag{80}$$

where m_r, the manipulator mass, K_p and K_d and the human parameters are positive scalar values. (80) can be rewritten as follows:

$$m_{tot}\ddot{x}(t) = -K_{tot}(t)\tilde{x}(t) - b_{tot}(t)\dot{\tilde{x}}(t) \tag{81}$$

where $m_{tot} = m_r + m_h$, $K_{tot}(t) = K_p(t) + K_h$ and $b_{tot}(t) = K_d(t) + b_h$, which are all positive terms. For better readability, only time dependency is kept in the discussion.
The Lyapunov function, used in the demonstration, takes into account of the total energy stored into the system, as follows:

$$V(t) = \overbrace{\frac{1}{2}m_{tot}(x)\dot{x}(t)^2}^{\text{kinetic energy}} + \overbrace{\frac{1}{2}K_{tot}(t)\tilde{x}(t)^2}^{\text{control energy}} \tag{82}$$

Given that, the Lyapunov asymptotic stability condition is:

$$\dot{V}(t) < 0 \tag{83}$$

The Lyapunov function derivative can be compute as follows:

$$\dot{V}(t) = m_{tot}(x)\;\ddot{x}(t)\dot{x}(t) + K_{tot}(t)(\dot{x}(t) - \dot{r}(t))\tilde{x}(t) + \frac{1}{2}\dot{K_p}(t)\tilde{x}(t)^2 \tag{84}$$

by using the dynamic equation (81):

$$\dot{V}(t) = -K_{tot}(t)\dot{x}(t)^2 - K_{tot}(t)\dot{r}(t)\tilde{x}(t) + \frac{1}{2}\dot{K_p}(t)\tilde{x}(t)^2 \tag{85}$$

therefore Lyapunov stability condition can be rewritten as:

$$-2\,(K_p(t) + K_h)\frac{\dot{r}(t)}{\tilde{x}(t)} + \dot{K_p}(t) < 0 \tag{86}$$

and its expanded representation, using 1-DOF version of (72) and related derivative, is:

$$-2(\,\mathbf{y}(t)\mathbf{a}(t) + K_h)\frac{\dot{r}(t)}{\tilde{x}(t)} + \dot{\mathbf{y}}(t)\mathbf{a}(t) + \mathbf{y}(t)\dot{\mathbf{a}}(t) < 0 \tag{87}$$

Taking into account the control update law computation in (69), previously defined constraints and, also, noticing that Gaussian weights have the following constrains in their maximum values:

$$\|\mathbf{y}(t)\|_\infty < 1 \tag{88}$$

$$\|\dot{\mathbf{y}}(t)\|_\infty = \left\|\dot{x}(t)\frac{\partial \mathbf{y}(x(t))}{\partial x(t)}\right\|_\infty \leqslant \frac{\nu_{max}\, c}{\sigma^2\sqrt{2\pi e}} \tag{89}$$

the stability condition leads to the following boundaries:

$$k < \frac{a_{min}}{x_{max}}\left(\frac{1}{\tau} - \frac{\nu_{max}\, c\, P}{\sigma^2\sqrt{2\pi e}} - 2\frac{\dot{r}_{max}}{x_{max}}\right) - 2K_h\frac{\dot{r}_{max}}{x_{max}^2} \tag{90}$$

$$\tau < \frac{1}{\frac{\nu_{max}\, c\, P}{\sigma^2\sqrt{2\pi e}} + 2\frac{\dot{r}_{max}}{x_{max}} + 2K_h\frac{\dot{r}_{max}}{x_{max}\, a_{min}}} \tag{91}$$

Inequalities in (90) and (91) lead to the definition of two specific boundaries. In particular, the first one, related to parameter k, defines a boundary in maximum error sensitivity of the update law. The second one, related to parameter τ, defines a minimum forgetting rate of the update law.

3.3.2.2 *N DOFs robot device*

In this case, it's better to simplify the proof, firstly consider no human interaction force and no moving target. The dynamic equation of the robot system can be rewritten in the joint space ($\mathbf{q}(t)$, for better readability $\mathbf{q}$, is the joint space coordinate vector):

$$H_r(\mathbf{q})\ddot{\mathbf{q}} + C_r(\mathbf{q},\dot{\mathbf{q}})\dot{\mathbf{q}} = J_a(\mathbf{q})^T\left(-K_p(\mathbf{x}(t))\mathbf{x} - K_d(\mathbf{x}(t))\dot{\mathbf{x}}\right) \tag{92}$$

where J_a is the analytical Jacobian, while $H_r(\mathbf{q})$ is the inertia matrix in the joint space and $C_r(\mathbf{q},\dot{\mathbf{q}})$ is the Coriolis matrix of the manipulator. Also the Lyapunov function can be rewritten, as follows:

$$V = \overbrace{\frac{1}{2}\dot{\mathbf{q}}^T H_r(\mathbf{q})\dot{\mathbf{q}}}^{\text{kinetic energy}} + \overbrace{\frac{1}{2}\mathbf{x}^T K_p(\mathbf{x}(t))\mathbf{x}}^{\text{control energy}} \tag{93}$$

differentiating (93) and using skew-symmetric property of matrix $\dot{H}_r - 2C_r$ the derivative of the Lyapunov function becomes:

$$\dot{V} = -\dot{\mathbf{x}}^T K_d(\mathbf{x}(t))\dot{\mathbf{x}}^T + \frac{1}{2}\mathbf{x}^T K_p(\mathbf{x}(t))\mathbf{x} \tag{94}$$

By noting that the right-hand side of (94) is a quadratic form with diagonal matrices, the stability proof is straightforward. As, it is possible to split it in N independent 1-DOF subproblems, one for each d.o.f.. Consequently, adding the human interaction force and the moving target effects is also straightforward, leading to N independent systems in the form of equation (80). Following the procedure described in Sec. 3.3.2.1, it leads N pair of boundaries, as inequalities (90) and (91). Finally, the more strict k and τ boundaries will be taken into account.

3.4 EXPERIMENTAL SETUP

The presented adaptive control has been implemented in a rehabilitation robot system, designed to realize an haptic bilateral interface

Table 4: Mechanical and electrical X-Y-table system characteristics

Upper axis mass	M_{up}	0.5	[kg]
Lower axis mass	M_{low}	1.0	[kg]
Force constant	Kf	33.0	[N/A]
Encoder resolution	Δ	10	[μm]
Control sampling time	Ts	1	[ms]

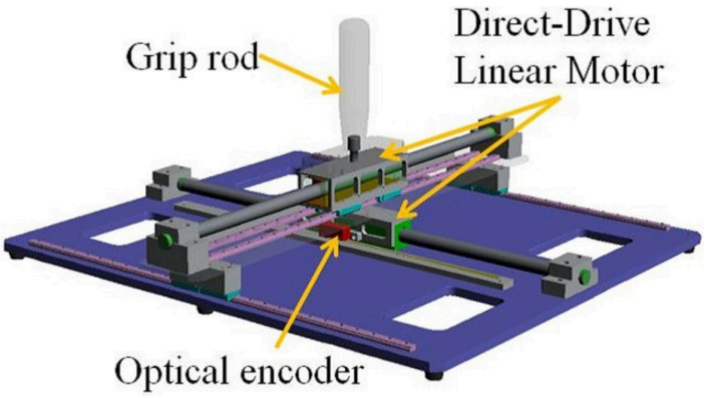

Figure 45: Tridimensional model of the X-Y-table system [123].

[123]. Nevertheless, the proposed application only makes use of one of the two sides of the bilateral system. This consists of a X-Y-table system with two DOFs (see Fig. 46). Each axis is driven by a direct-drive linear motor with a optical encoder as position sensor. Such design is characterized by low friction losses and good back-drivability, allowing to achieve accurate force control. The motion range of X-Y table is approximately 40cm×40cm. A grip rod is installed at the end effector of the robot, in order to facilitate the patient's gripping.A tridimensional representation of the robot is shown in Fig. 45, while main mechanical and electrical characteristics are reported in Tab.4.
The motors are connected to their drivers, which are interfaced to a Linux computer through the use of a DAC board and a counter board for I/O signals. A user-friendly virtual reality (VR) environment has been implemented in the Linux system. A simple reaching task, that will be explained in Sec.3.6, has been programmed. The use of VR allows to keep patient involvement high, providing a visual feedback, during the training. For further details about the overall system please refer to the related paper [123].
As seen in Fig.48, the workspace area has been divided in a 6×6 matrix of equal squares. So, the number P of non-overlapping areas has been set to 36. Such choice has been made in order to limit the computation time, avoiding it exceeds the control sampling time, set to 1ms.

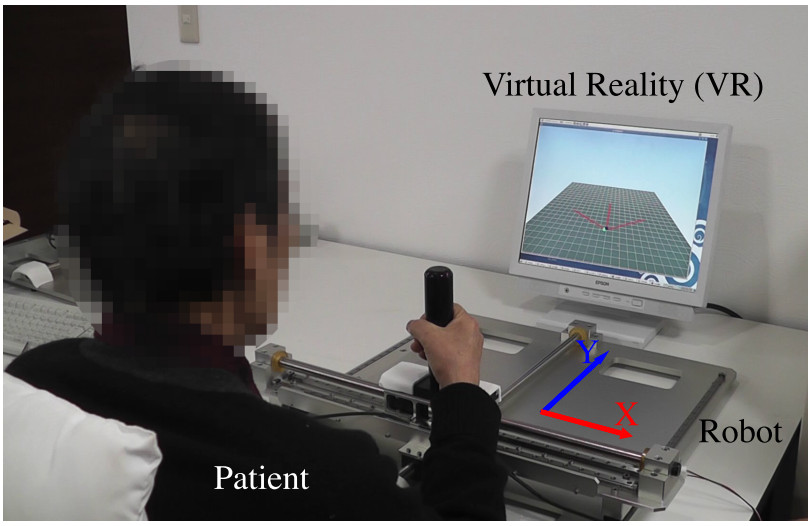

Figure 46: Overview of the experimental setup and a typical rehabilitation trial.

3.5 PRELIMINARY TESTS

For the sake of better understanding how the control algorithm works, a preliminary test has been performed on an healthy subject. Before the execution of the test, the controller parameters must be set. To do that, it is necessary to accomplish the following simple procedure:

- identification of the human parameters in several position in the workspace area and with different grasping forces, by following the identification tests described in Sec. 3.3.1;
- investigation of more critical human parameters from the stability point of view and, consequently, definition of the boundaries for parameters k and τ;
- setting k and τ values, according previously defined boundaries, and definition of the initial value α_0.

In proposed experiment, control parameters have been set as following:

- $k = 1000 N/m^2$
- $\tau = 5s$
- $\alpha_0 = 10 N/m$

Such control parameters meet the defined boundaries and are selected in order to obtain a faster and clear response of the adaptive controller.
Specifically, this preliminary test consists in asking the participant to follow a moving target on a circular trajectory. At first, the participant simulated a bad tracking, performing errors along a single axis or both axes, at the same time, and always in the same specific location of the trajectory to be followed. Then, accurate tracking has been performed.

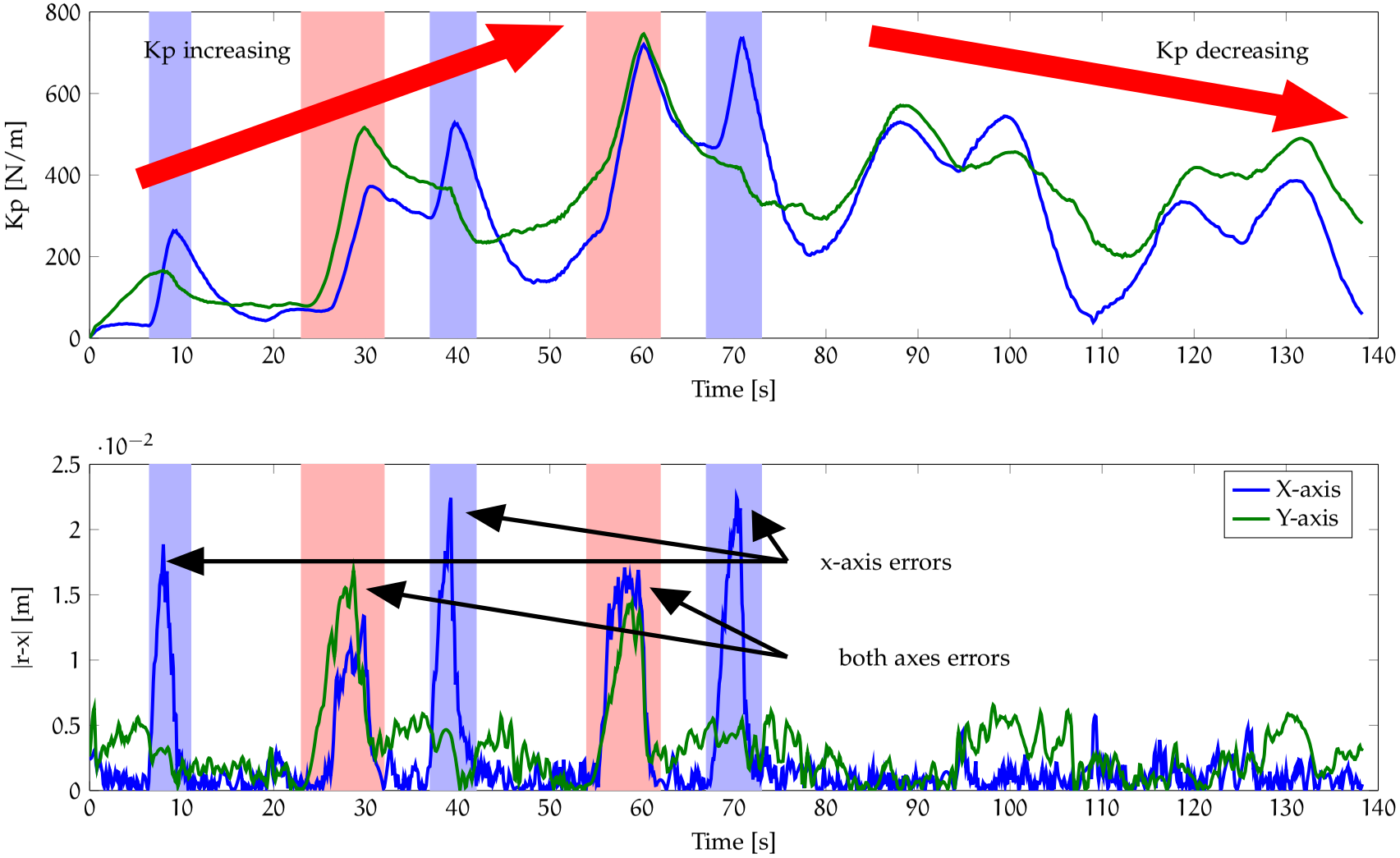

Figure 47: Comparison between current proportional control gains and absolute position error, during a demo training with an healthy subject. Simulated tracking errors are performed during the first half of the trial, then accurate tracking is performed.

Clearly, such experimental test wants to show the adaptive behavior of the controller. In fact, the so-called "assist-as-needed" behavior is shown in Fig.47. As explained in Sec.3.2, the control stiffness is adapted according patient's weaknesses. When a poor tracking of the target is performed, the controller tends to become harder. On the contrary, when a good tracking is achieved, the controller becomes softer, decreasing the total assistive force. Graphs in Fig.47 are time-varying, but, since the target is moving, stiffness variations are located only in neighbourhood of current end-effector position and also taking into account of the performance history in such specific workspace area. This is obtained thanks to the update law definition and the gaussian weights in the computation.

3.6 REHABILITATION TRIALS

In order to show the effectiveness of the proposed control system, some preliminary rehabilitation trials with patients have been performed.
Type of trials and schedule have been decided together with specialists and physiotherapists. The first rehabilitation task chosen for the tests was an easy reaching one. During trainings, subjects were encouraged to properly moving the robot end-effector, following a target which is repeatedly moving back and forth in three different directions (see Fig. 48). The resulting movement somehow emulates a common and useful daily-life activity of reaching some objects, placed in front of a person.
All tunable control parameters have been set by relying on the experience of the. In particular, in order to obtain a smooth adaptation of the controller, the update parameter τ and k have been set to 20s and $500N/m^2$, respectively. At the same time, the controller has been initialized with $\alpha_0 = 10N/m$, corresponding to a very low stiffness of the controller. In such a way, at the beginning of the training, the robot assistance was minimized, encouraging patients to perform movements by themselves.
Four aged adults attended the trials. Two of them were chronic stroke patients while the other two were effected by middle-dementia and Parkinsonism, respectively (see Tab.5). It's worth noting that the last two patients had no impairments in their limbs motions, while they were affected by low cognitive skills. This affected their ability in maintaining their attention focused on the task, during training.
Trials have been performed by the first two patients by using their stroke affected arm, while, the others have been using their dominant arm.
Each subject attended four rehabilitation sessions, once a week. Five trainings have been performed in each session. During each training, patients were asked to follow the moving target along the previously described reaching trajectory, repeating such movements for three times. Such task was completed in about 150s (target speed has been set to $1.8cm/s$).

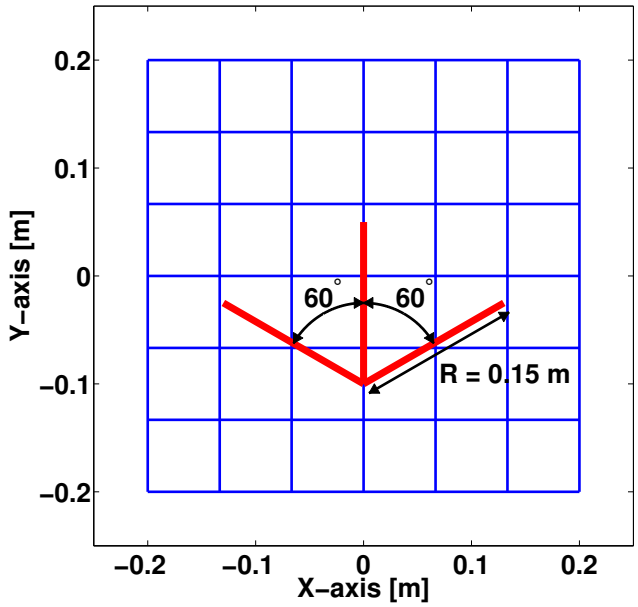

Figure 48: Schematic representation of the workspace partition and the path to be followed in the rehabilitation task. Length, directions and speed of the target have been decided by therapists.

In order to better understand the benefits of the treatment, the five trainings were not all the same. In fact, the first and the last ones have been performed with disabled motors drives, as it can be seen in Tab.6. In such cases, no force feedback has been sent to patients, allowing free movements. Nevertheless, the adaptive control algorithm was active, allowing the computation of the stiffness map over the workspace. So, some pre- and post- treatment performance information have been made available.

Table 5: Subjects involved in the trials

Subject #	1	2	3	4
Gender	Male	Male	Female	Female
Age	72	73	83	76
Disorder	Stroke	Stroke	Dementia	Parkinsonism
Affected side	Left	Right	-	-

3.7 EXPERIMENTAL RESULTS

During trials, current end-effector and reference positions, current control parameters and values of the NP gaussian heights for the N stiffness maps have been saved. So, a huge amount of data was obtained for each patient. However, to show the proposed solution advantages, the attention is mainly focused on data from two reha-

Table 6: Training schedule for a weekly session

Trial #	1	2	3	4	5
Controller computation	ON	ON	ON	ON	ON
Motor driver	OFF	ON	ON	ON	OFF

Table 7: Subject-1 (stroke patient): mean absolute (MAE) and standard deviation (SDE) error results

	X-axis		Y-axis	
trial #	MAE [mm]	SDE [mm]	MAE [mm]	SDE [mm]
1	5.45	5.66	5.19	4.73
2	3.96	4.41	2.93	3.64
3	3.34	4.01	3.38	2.92
4	4.16	4.46	3.75	3.89
5	4.57	5.50	3.94	4.74

bilitation sessions, performed by one stroke (Subject-1) and one no-stroke (Subject-3) patient.
First of all, looking at free movement columns in Fig.49, it is possible to understand how the proposed approach provides a tool to easily evaluate patient's degrees of impairment and locations where they are more significant. The colored graphs have been obtained by computing the controller stiffness map, from the last values of vector **a**, for each trial. Last values have been chosen, since they better summarized patient behavior during training, as the controller has time to correctly adapted its parameters. Red colored areas show low patient tracking performances, as stiffness is higher. Meanwhile, blue areas suggest good tracking performances, as the controller is soft. This relationship is also clear by observing averages and standard deviations of position errors in the Tab.7. In fact, graphs characterized by bigger red areas show also higher absolute error average and standard deviation values. Compared to simple statistical data in Tab.7, the graphs in Fig.49 provide additional information about tracking performance distribution over the workspace. Such information can be very useful to therapists, in order to better understand and promote rehabilitation process. In fact, comparing first and last graphs in Fig.49, therapists can check some patients improvements, as the red colored areas are smaller and less visible. Such evaluation can be executed in the active control training too. Here, therapists can obtain additional details, for example related to patient wearying (see active control graphs in Fig.49, patient performances get worse in the fourth

Table 8: Subject-3 (no-stroke patient): mean absolute (MAE) and standard deviation (SDE) error results

	X-axis		Y-axis	
trial #	MAE [mm]	SDE [mm]	MAE [mm]	SDE [mm]
1	28.94	29.71	28.39	25.20
2	7.28	8.86	5.57	6.71
3	6.41	7.64	4.50	6.28
4	6.56	9.26	5.83	5.96
5	25.59	19.36	26.29	19.71

trial compared to previous ones).
Another key benefit, achieved by using the proposed control solution, is to promote the active participation of patient and keep his/her involvement high. This is an important issue in patients with low cognitive capabilities. Although some of such patients doesn't have physical impairments, they only need trainings to preserve muscle tone of their limbs. So, the assistive force is merely helpful to better teach tasks to these patients and correctly complete their movements. Fig.50 shows some results performed by a patient affected by middle-dementia. The clear discrepancy in the performance results between the inactive and active control trainings is proving the previous mentioned control benefits. Such result is also confirmed by numerical data in Tab.8.

During active-control trails, just a small assistive force was needed to correctly perform tasks, while in free movement trials tracking performances got strongly worse, showing how the visual feedback itself wasn't enough to achieve good performances.
Lastly, some general data, from all performed training sessions, are reported in Fig. 51. Here, total MAE data of assessment's trials, performed at the beginning and at the end of each training session, are reported. In particular, focusing in single sessions, pre- and post- assessments shows slight tracking capability's improvements, in almost all cases (in Fig. 51, red squares are typically below blue dots). Otherwise, deterioration of subject's capabilities is due to justifiable physical weariness during trainings, as already noticed. Finally, from a general point of view, it can be notice an overall improving trend of subjects performances during proposed training sessions, as errors average typically decreased, showing how proposed solution have positive effects not only in short terms but also in long terms.

3.8 CONCLUSIONS

A novel adaptive compliance controller for rehabilitation purposes has been presented in this chapter. Its simple and effective structure

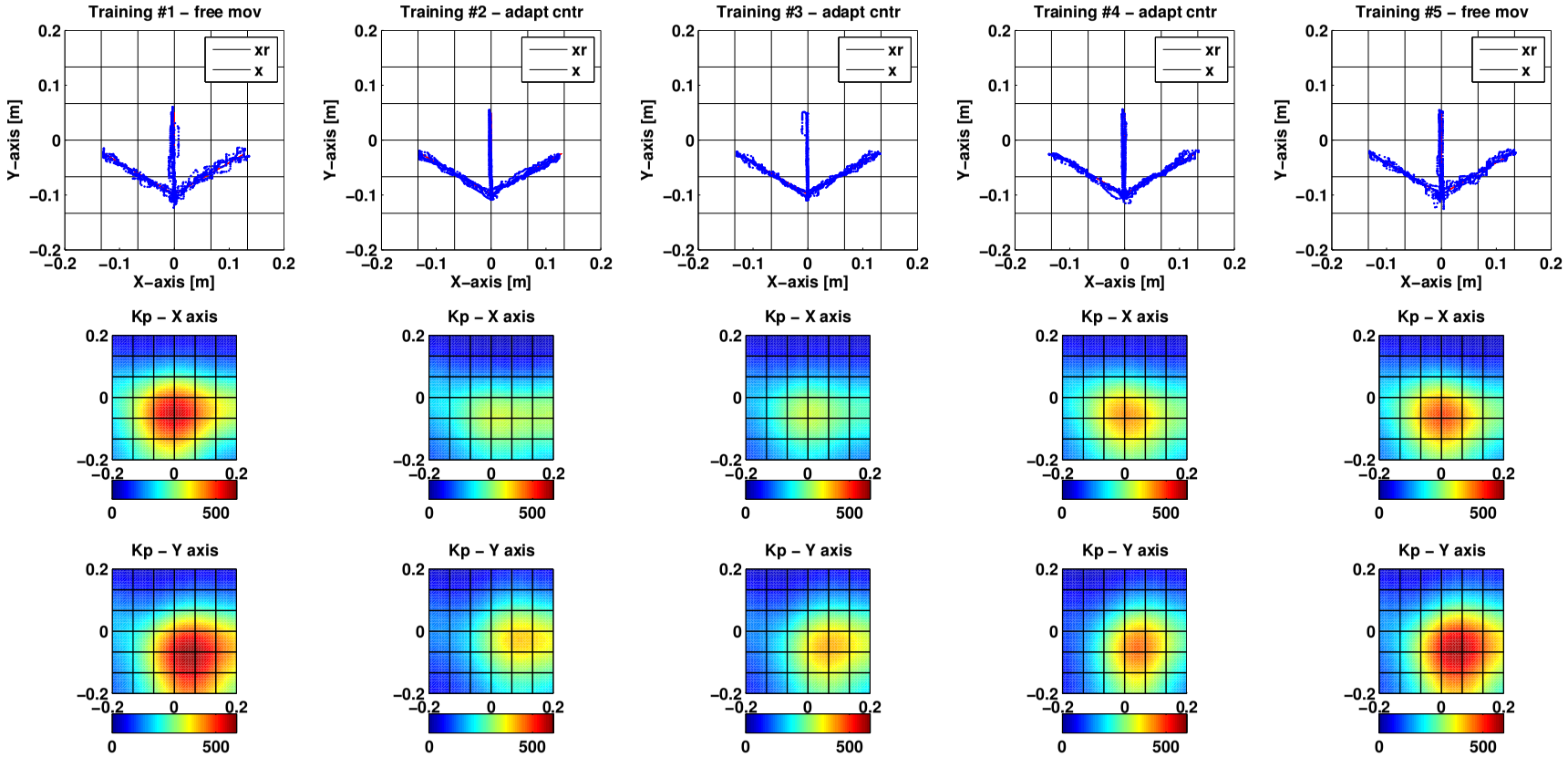

Figure 49: Subject-1 (stroke patient): the figure shows three different graphs for each training in a session. First row compares reference position and end-effector position, sampled during trainings. Second and third row show the final stiffness impedance map for X and Y axes, respectively.

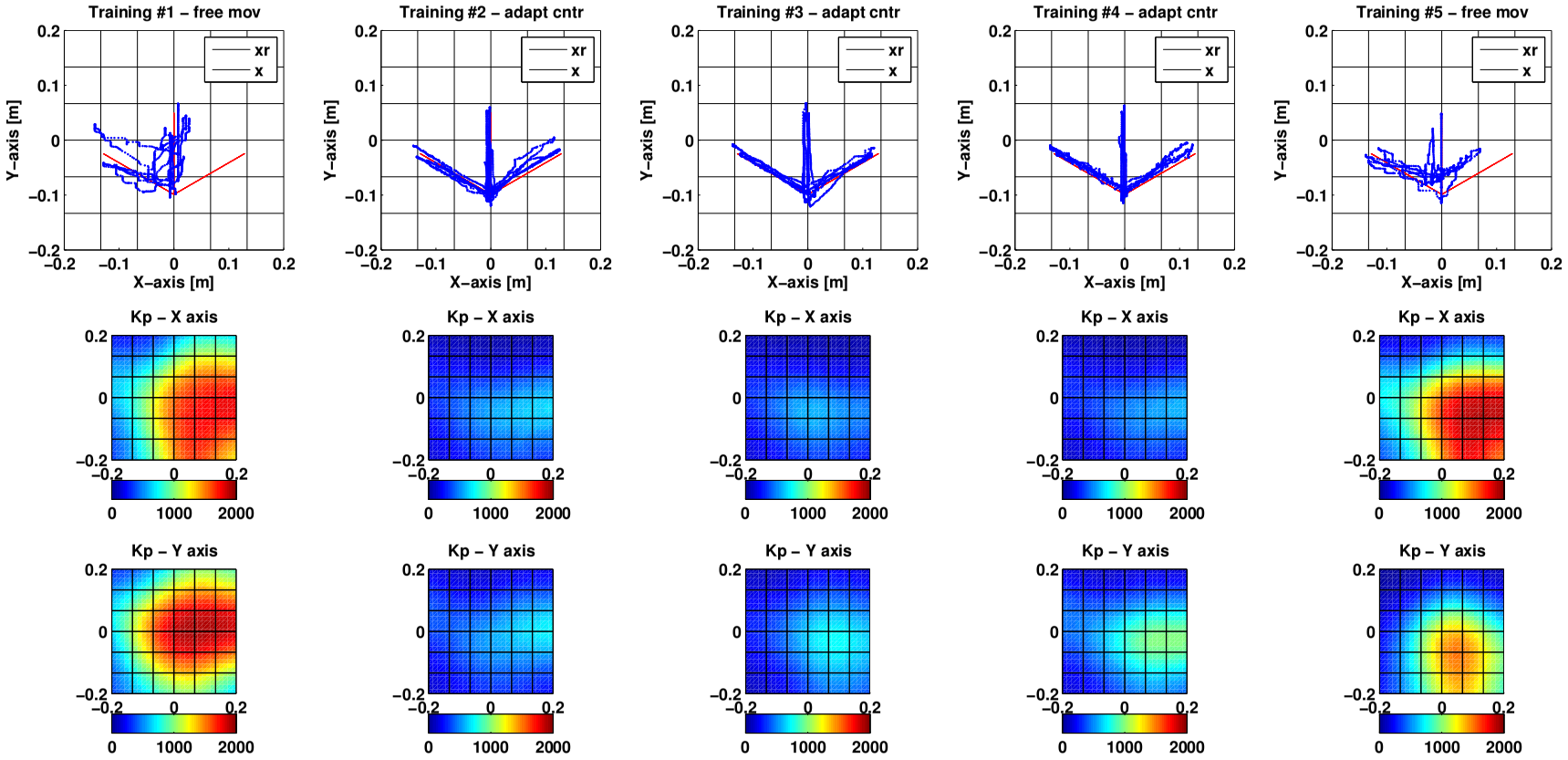

Figure 50: Subject-3 (no-stroke patient): the figure shows three different graphs for each training in a session. First row compares reference position and end-effector position, sampled during trainings. Second and third row show the final stiffness impedance map for X and Y axes, respectively.

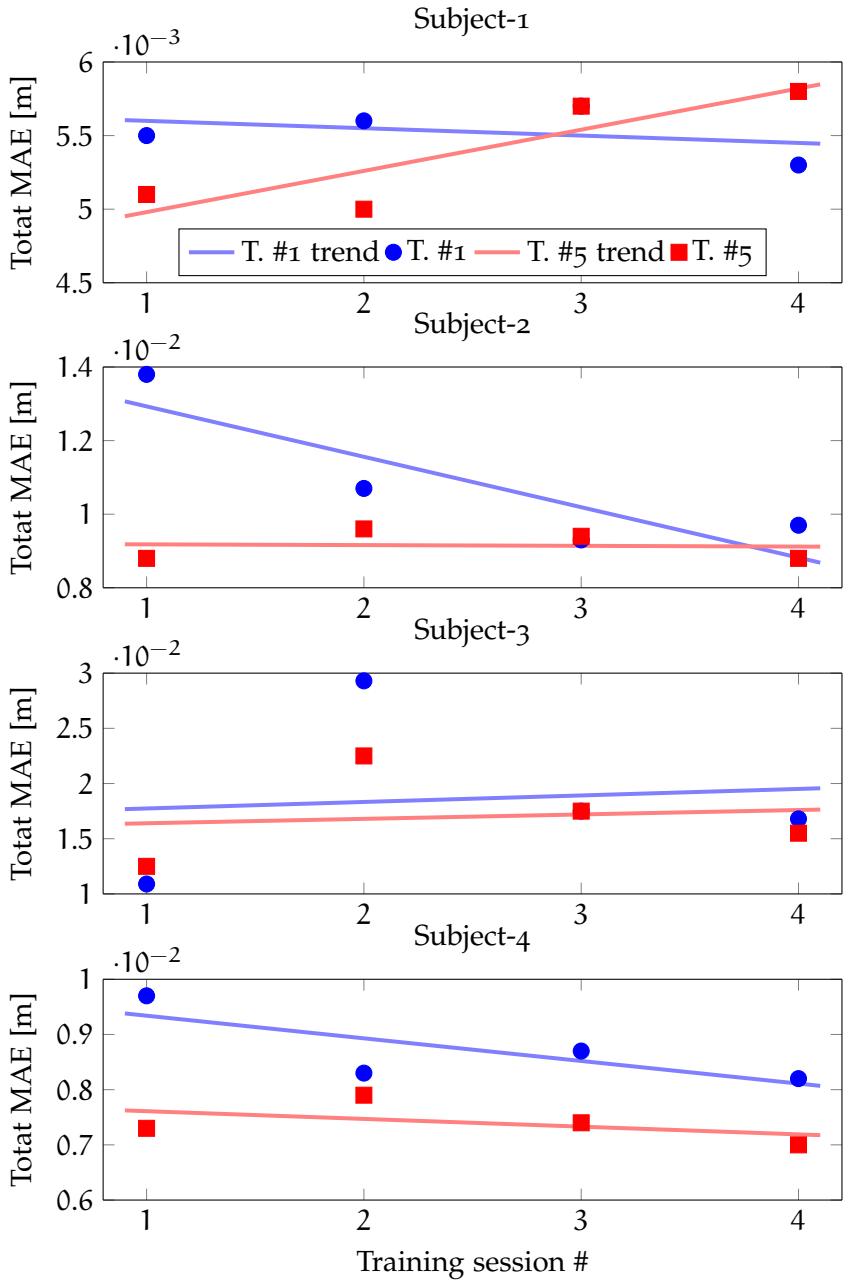

Figure 51: Total MAE values and related trends of pre- and post-treatment assessments, first and last trial respectively. Reported data concern each subject and each training session.

allows to be easily implemented in several typologies of robot device. As a result, it is possible to develop useful stand-alone rehabilitation robot systems capable to adapt their assistance according to specific participant's needs.
In order to guarantee stability of the system in all working conditions, a complete stability proof of the proposed control strategy has been reported. Some boundaries in the maximum error sensitivity and minimum forgetting rate of the update law have been defined. Important aspect, in the proper definition of such boundaries, is a complete identification of human model parameters, describing the interaction force with the device.

Some preliminary clinical tests have been performed with real patients, in order to evaluate benefits of such control approach. In particular, the experimental results have shown its effective "assist-as-needed" behavior, which encourages the active participation of patient in the execution of tasks. Moreover, by properly analyzing the control parameters, it possible to obtain an useful patient's performance evaluation tool. In fact, it gives information about degree and location of patients' weaknesses.

4

CONCLUSIONS

Some novel control system solutions and tools have been successfully developed and implemented in order to support the use of stand-alone and low-cost rehabilitation robot devices, improving their features and performances.
A sensor fusion algorithm, merging together position encoder measurements and acceleration signals from a low-cost MEMS accelerometer, and a particular identification procedure, based on a RLS algorithm have been developed. Regarding the aaKF algorithm, it makes use of an augmented Kalman filter model to compensate effect of bias affecting measurements of low-cost MEMS accelerometers. So doing, it allows to obtain more accurate, in terms of reduced added noise, position and speed estimation of the device end-effector. Using such more accurate informations in the RLS identification procedure, it is possible to obtain faster and more precise estimation of the main mechanical system's parameters, such as inertia and Coulomb and viscous friction coefficients. Such better information are useful to improve performances of well known force-sensorless control tools, DOB and RTOB/RFOB, which are capable to nominalize the system and to estimate interaction forces cancelling inertia and friction effects, respectively. In particular, it is possible to increase DOB and RTOB/RFOB bandwidths and obtain a more accurate force control of the device and better estimation of the human-robot interaction force.
Consequently, with an inexpensive and not invasive system modification (addition of small and low-cost MEMS accelerometers) and use of suitable software tools, it is possible to improve backdrivability and haptics features of robotic devices, even in low-cost ones. Moreover, due to their simplicity and adaptability, such control tools may be extended and implemented in other robotic applications, such as servo positioning control systems.
A novel adaptive assistance controller for rehabilitation purposes has been, also, presented in this work. Its simple and effective structure allows to be easily implemented in several typologies of robot device. As a result, it provides a useful control tool in order to design low-cost stand-alone rehabilitation robot systems capable to automatically adapt thier assistance according to specific participant's needs. Such control algorithm is based on an adaptive non-linear compliance controller, in which the adaptation of PD control parameters is driven by the patient's ability to tracking a moving target displayed in a screen. A proper update law guarantees a soft compliance control in case of good tracking performances, while, in case of bad tracking performances, an hard control is performed and higher robotic forces correctly drive participant's movements. Furthermore, the use of a forgetting term inside the update law is capable to take memory of previous participant's performances and to follow improvements

during treatments.

In order to guarantee stability of the system in all working conditions, a complete stability proof of the proposed control strategy has been reported. Finally, some preliminary clinical tests have been performed with real patients, in order to evaluate benefits of proposed control algorithm approach. In particular, the experimental results have shown its effective "assist-as-needed" behavior, which encourages the active participation of patient in the execution of tasks, better promoting rehabilitation. Moreover, by properly analyzing the control parameters, it possible to obtain an useful patient's performance evaluation tool. In fact, distribution of soft/hard compliance controller's parameters in the workspace gives information about degree and location of patients' weaknesses. Finally, comparing control parameter distribution obtained in different training sessions, it is possible to evaluate any improvements and benefits of the robotic assistance.

In conclusion, due to their simple implementation, low computational effort and not invasive hardware modifications, results of described researches can be easily implemented in a wide variety of robotic devices, even very simple ones. In particular, they have provided useful tools to improve devices features and performances and to develop suitable rehabilitation robotic therapies.

Part III

APPENDIX

a

KALMAN FILTER

Kalman filtering, also known as linear quadratic estimation (LQE), is an algorithm typically used in state estimation or sensor fusion applications. The filter name is due to Rudolf E. Kalman, whom is one of the first developers of this theory [124].
KF has been subject of extensive researches and applications, particularly in the engineering area of signal processing, guidance, navigation and control of vehicles, automation and robotics (e.g. motion planning, trajectory optimization and control). Moreover, it has been applied in other research field, such as economics and finance.
The algorithm inputs are typically series of measurements observed over time, that may contain statistical noise and other inaccuracies. The algorithm produces estimation of unknown state variables, merging together the inputs according to the implemented system model. Such novel informations tend to be more precise compared to those can be obtain by using a single measurement alone.
The algorithm works in a two-step process. In the prediction step, the KF produces estimates of the current state variables. Such estimation is obtain updating the state of the previous time step by using the state model describing the system. Such estimations may be corrupted by errors due to model uncertainties. Once the outcome of the next measurement (necessarily corrupted with some amount of measurement error, e.g. random noise) is observed, the correction step can be performed. The estimates are updated and corrected using a weighted average. More weight is given to measurements with higher certainty and lower added noise. The algorithm is recursive and it can be easily implemented in a digital fashion and run in real time. In fact, it uses only the present input measurements and the previously calculated state and some other additional information related to model and measurement noise variance matrices. No additional past informations are required.
The KF does not require any assumption that the model or measurement errors are Gaussian. However, the filter yields the exact conditional probability estimate in the special case that all errors are zero-mean and Gaussian-distributed. In such case, it is called LQE. Rarely such optimal condition actually exists, but the filter apparently works well for many applications in spite of this situation.

A.1 TIME-VARING KF ALGORITHM

Aim of KF is to estimate current state $\mathbf{x_k}$ at time step k of a system, affected by noise, given current inputs u_k and outputs $\mathbf{y}_k$ signals.

Discrete system model can be represented in a state space fashion, i.e.:

$$\mathbf{x}_{k+1} = \mathbf{A_d}\mathbf{x}_k + \mathbf{B_d}u_k + \mathbf{B_{dw}}\mathbf{w}_k \tag{95}$$

$$\mathbf{y}_k = \mathbf{C_d}\mathbf{x}_k + \mathbf{v}_k \tag{96}$$

where $\mathbf{w}_k$ and $\mathbf{v}_k$ are stochastic process called respectively process noise and measurement noise. Their related variance matrices can be defined as:

$$\mathbf{Q_d} = \mathbf{E}[\mathbf{w}_k\mathbf{w}_k^T] = , \ \mathbf{R_d} = \mathbf{E}[\mathbf{v}_k\mathbf{v}_k^T] \tag{97}$$

The algorithm is divided in two main steps, as previously stated. In the following discussion, notation $*_{n|m}$ represents the estimate of $*$ at time step n, given observations from up to and including time $m \leqslant n$. The state of the filter is represented by two variables:

- $\hat{\mathbf{x}}_{k|k}$, the a posteriori model state estimate at time k given observations up to and including at time k. The initial value is typically $\hat{\mathbf{x}}_{0|0} = \mathbf{0}$.
- $\hat{\mathbf{P}}_{k|k}$, the a posteriori state estimation error covariance matrix, which give information according to accuracy in the estimation. Its initial value $\hat{\mathbf{P}}_{0|0}$ is set in relation to the initial accuracy wherewith the initial model state is known.

The algorithm is composed as follows:

- Prediction:
  Firstly, at a generic time instant k, the actual state vector $\hat{\mathbf{x}}_{k|k-1}$ is predicted from state $\hat{\mathbf{x}}_{k-1|k-1}$, computed at the previous time step $k-1$, by using system model (95), i.e.:

  $$\hat{\mathbf{x}}_{k|k-1} = \mathbf{A_d}\hat{\mathbf{x}}_{k-1|k-1} + \mathbf{B_d}u_k \tag{98}$$

  Moreover, the estimation error covariance matrix is predicted:

  $$\mathbf{P}_{k|k-1} = \mathbf{A_d}\mathbf{P}_{k-1|k-1}\mathbf{A_d}^T + \mathbf{B_{dw}}\mathbf{Q_d}\mathbf{B_{dw}}^T \tag{99}$$

- Update:
  At time k, new output system signals are available. These current observations are used to update and to refine prediction values. An estimator gain matrix $\mathbf{K}_k$ is calculate by the optimal design technique of the KF:

  $$\mathbf{K}_k = \mathbf{P}_{k|k-1}\mathbf{C_d}^T(\mathbf{C_d}\mathbf{P}_{k|k-1}\mathbf{C_d}^T + \mathbf{R_d})^{-1} \tag{100}$$

  The innovation or measurement residual is, also, competed:

  $$\mathbf{e}_k = \mathbf{y}_k - \mathbf{C_d}\hat{\mathbf{x}}_{k|k-1} \tag{101}$$

  which is essentially the difference between the real and predicted outputs.

Using the estimator gains and innovation signals, the current a posteriori estimate of model state and related covariance matrix are update, as follows:

$$\hat{\mathbf{x}}_{k|k} = \hat{\mathbf{x}}_{k|k-1} + \mathbf{K}_k \mathbf{e}_k \tag{102}$$

$$\mathbf{P}_{k|k} = (\mathbf{I} - \mathbf{K}_k \mathbf{C}_\mathbf{d}) \mathbf{P}_{k|k-1} \tag{103}$$

Such procedure is constantly repeated at each time step.

BIBLIOGRAPHY

[1] United Nations department of Economic and Social Affairs population division. "World Population Prospects: The 2015 Revision, custom data acquired via website." In: (2015).

[2] European Registers of Stroke (EROS) Investigators et al. "Incidence of stroke in Europe at the beginning of the 21st century." In: *Stroke* 40.5 (2009), pp. 1557–1563.

[3] Randolph J Nudo. "Mechanisms for recovery of motor function following cortical damage." In: *Current opinion in neurobiology* 16.6 (2006), pp. 638–644.

[4] Gert Kwakkel. "Impact of intensity of practice after stroke: issues for consideration." In: *Disability and rehabilitation* 28.13-14 (2006), pp. 823–830.

[5] Gert Kwakkel, Boudewijn Kollen, and Jos Twisk. "Impact of time on improvement of outcome after stroke." In: *Stroke* 37.9 (2006), pp. 2348–2353.

[6] Hilde Feys, Willy De Weerdt, Geert Verbeke, Gail Cox Steck, Chris Capiau, Carlotte Kiekens, Eddy Dejaeger, Gustaaf Van Hoydonck, Guido Vermeersch, and Patrick Cras. "Early and repetitive stimulation of the arm can substantially improve the long-term outcome after stroke: a 5-year follow-up study of a randomized trial." In: *Stroke* 35.4 (2004), pp. 924–929.

[7] GBD MORTALITY. "Global, regional, and national age-sex specific all-cause and cause-specific mortality for 240 causes of death, 1990-2013: a systematic analysis for the Global Burden of Disease Study 2013." In: *Lancet* 385 (2015), pp. 117–171.

[8] Valery L Feigin, Mohammad H Forouzanfar, Rita Krishnamurthi, George A Mensah, Myles Connor, Derrick A Bennett, Andrew E Moran, Ralph L Sacco, Laurie Anderson, Thomas Truelsen, et al. "Global and regional burden of stroke during 1990–2010: findings from the Global Burden of Disease Study 2010." In: *The Lancet* 383.9913 (2014), pp. 245–255.

[9] Istituto Superiore di Sanitá. URL: http://w3.iss.it/site/mortalita/.

[10] Hilde M Feys, Willy J De Weerdt, Beat E Selz, Gail A Cox Steck, Ruth Spichiger, Luc E Vereeck, Koen D Putman, and Gustaaf A Van Hoydonck. "Effect of a therapeutic intervention for the hemiplegic upper limb in the acute phase after stroke a single-blind, randomized, controlled multicenter trial." In: *Stroke* 29.4 (1998), pp. 785–792.

[11] WR Staines, WE McIlroy, SJ Graham, and SE Black. "Bilateral movement enhances ipsilesional cortical activity in acute stroke: a pilot functional MRI study." In: *Neurology* 56.3 (2001), pp. 401–404.

[12] Steven L Wolf, Sarah Blanton, Heather Baer, Jenifer Breshears, and Andrew J Butler. "Repetitive task practice: a critical review of constraint-induced movement therapy in stroke." In: *The neurologist* 8.6 (2002), p. 325.

[13] Gert Kwakkel, Robert C Wagenaar, Jos WR Twisk, Gustaaf J Lankhorst, and Johan C Koetsier. "Intensity of leg and arm training after primary middle-cerebral-artery stroke: a randomised trial." In: *The Lancet* 354.9174 (1999), pp. 191–196.

[14] Edward Taub, Gitendra Uswatte, Rama Pidikiti, et al. "Constraint-induced movement therapy: a new family of techniques with broad application to physical rehabilitation-a clinical review." In: *Journal of rehabilitation research and development* 36.3 (1999), pp. 237–251.

[15] Dr. Anthony Komaroff. *What is stroke rehabilitation?* 2012. URL: http://www.askdoctork.com/what-is-stroke-rehabilitation-201207132220.

[16] Windsor Healthcare Communities. *Post Acute Stroke Rehab*. URL: http://www.windsorhealthcare.org/post-acute-stroke-rehab.

[17] Robert Riener, Martin Frey, Michael Bernhardt, Tobias Nef, and Gery Colombo. "Human–centered rehabilitation robotics." In: *Rehabilitation Robotics, 2005. ICORR 2005. 9th International Conference on*. IEEE. 2005, pp. 319–322.

[18] Nadina B Lincoln, D Willis, SA Philips, LC Juby, and P Berman. "Comparison of rehabilitation practice on hospital wards for stroke patients." In: *Stroke* 27.1 (1996), pp. 18–23.

[19] Robert Allen Keith and Katherine Sharp Cowell. "Time use of stroke patients in three rehabilitation hospitals." In: *Social science & medicine* 24.6 (1987), pp. 529–533.

[20] G Colombo, M Wirz, V Dietz, et al. "Driven gait orthosis for improvement of locomotor training in paraplegic patients." In: *Spinal cord* 39.5 (2001), pp. 252–255.

[21] Sašo Jezernik, Gery Colombo, and Manfred Morari. "Automatic gait-pattern adaptation algorithms for rehabilitation with a 4-DOF robotic orthosis." In: *Robotics and Automation, IEEE Transactions on* 20.3 (2004), pp. 574–582.

[22] Lars Lünenburger, Gery Colombo, and Robert Riener. "Biofeedback for robotic gait rehabilitation." In: *Journal of NeuroEngineering and Rehabilitation* 4.1 (2007), p. 1.

[23] Stanley Fisher, Leah Lucas, and T Adam Thrasher. "Robot-assisted gait training for patients with hemiparesis due to stroke." In: *Topics in stroke rehabilitation* 18.3 (2011), pp. 269–276.

[24] R Gary West. *Powered gait orthosis and method of utilizing same*. US Patent 6,689,075. 2004.

[25] Motorika. *ReoAmbulator*. URL: http://www.motorika.com/?categoryId=90004.

[26] Keith E Gordon, Gregory S Sawicki, and Daniel P Ferris. "Mechanical performance of artificial pneumatic muscles to power an ankle–foot orthosis." In: *Journal of biomechanics* 39.10 (2006), pp. 1832–1841.

[27] Yong-Lae Park, Bor-rong Chen, Diana Young, Leia Stirling, Robert J Wood, Eugene Goldfield, and Radhika Nagpal. "Bio-inspired active soft orthotic device for ankle foot pathologies." In: *Intelligent Robots and Systems (IROS), 2011 IEEE/RSJ International Conference on*. IEEE. 2011, pp. 4488–4495.

[28] Daniel P Ferris, Joseph M Czerniecki, Blake Hannaford, University of Washington, and VA Puget Sound Healthcare System. "An ankle-foot orthosis powered by artificial pneumatic muscles." In: *Journal of Applied Biomechanics* 21.2 (2005), p. 189.

[29] Daniel P Ferris, Keith E Gordon, Gregory S Sawicki, and Ammanath Peethambaran. "An improved powered ankle–foot orthosis using proportional myoelectric control." In: *Gait & posture* 23.4 (2006), pp. 425–428.

[30] Julien Bogousslavsky, Louis R Caplan, Helen M Dewey, Karin Diserens, Geoffrey A Donnan, Marco Tulio Medina, Gerhard Rothacher, Luis César Rodríguez Salinas, Jonathan Sturm, and Amanda G Thrift. *Stroke: selected topics*. Demos Medical Pub., 2006.

[31] David J Reinkensmeyer, Leonard E Kahn, Michele Averbuch, Alicia McKenna-Cole, Brian D Schmit, and W Zev Rymer. "Understanding and treating arm movement impairment after chronic brain injury: progress with the ARM guide." In: *Journal of rehabilitation research and development* 37.6 (2000), pp. 653–662.

[32] Peter S Lum, Charles G Burgar, Peggy C Shor, Matra Majmundar, and Machiel Van der Loos. "Robot-assisted movement training compared with conventional therapy techniques for the rehabilitation of upper-limb motor function after stroke." In: *Archives of physical medicine and rehabilitation* 83.7 (2002), pp. 952–959.

[33] RJ Sanchez Jr, E Wolbrecht, R Smith, J Liu, S Rao, S Cramer, T Rahman, JE Bobrow, and DJ Reinkensmeyer. "A pneumatic robot for re-training arm movement after stroke: Rationale and mechanical design." In: *Rehabilitation Robotics, 2005. ICORR 2005. 9th International Conference on*. IEEE. 2005, pp. 500–504.

[34] David J Reinkensmeyer, Clifton T Pang, Jeff Nessler, Christopher C Painter, et al. "Web-based telerehabilitation for the upper extremity after stroke." In: *Neural Systems and Rehabilitation Engineering, IEEE Transactions on* 10.2 (2002), pp. 102–108.

[35] Hermano Igo Krebs, Neville Hogan, Mindy L Aisen, and Bruce T Volpe. "Robot-aided neurorehabilitation." In: *Rehabilitation Engineering, IEEE Transactions on* 6.1 (1998), pp. 75–87.

[36] Jaka Ziherl, Domen Novak, Andrej Olensek, Matjaz Mihelj, and Marko Munih. "Evaluation of upper extremity robot-assistances in subacute and chronic stroke subjects." In: *Journal of neuroengineering and rehabilitation* 7.1 (2010).

[37] Kathryn Hayward, Ruth Barker, and Sandra Brauer. "Interventions to promote upper limb recovery in stroke survivors with severe paresis: a systematic review." In: *Disability and rehabilitation* 32.24 (2010), pp. 1973–1986.

[38] Gwyn N Lewis and Eric J Perreault. "An assessment of robot-assisted bimanual movements on upper limb motor coordination following stroke." In: *Neural Systems and Rehabilitation Engineering, IEEE Transactions on* 17.6 (2009), pp. 595–604.

[39] Laura Marchal-Crespo and David J Reinkensmeyer. "Review of control strategies for robotic movement training after neurologic injury." In: *Journal of neuroengineering and rehabilitation* 6.1 (2009), p. 20.

[40] Martin Lotze, Christoph Braun, Niels Birbaumer, Silke Anders, and Leonardo G Cohen. "Motor learning elicited by voluntary drive." In: *Brain* 126.4 (2003), pp. 866–872.

[41] Laura Marchal Crespo and David J Reinkensmeyer. "Effect of robotic guidance on motor learning of a timing task." In: *Biomedical Robotics and Biomechatronics, 2008. BioRob 2008. 2nd IEEE RAS & EMBS International Conference on*. IEEE. 2008, pp. 199–204.

[42] Laura Marchal Crespo and David J Reinkensmeyer. "Haptic guidance can enhance motor learning of a steering task." In: *Journal of motor behavior* 40.6 (2008), pp. 545–557.

[43] Richard A Schmidt and Robert A Bjork. "New conceptualizations of practice: Common principles in three paradigms suggest new concepts for training." In: *Psychological science* 3.4 (1992), pp. 207–217.

[44] Angela Weiss, Toshimi Suzuki, Jonathan Bean, and Roger A Fielding. "High intensity strength training improves strength and functional performance after stroke." In: *American journal of physical medicine & rehabilitation* 79.4 (2000), pp. 369–376.

[45] Michelle M Ouellette, Nathan K LeBrasseur, Jonathan F Bean, Edward Phillips, Joel Stein, Walter R Frontera, and Roger A Fielding. "High-intensity resistance training improves muscle strength, self-reported function, and disability in long-term stroke survivors." In: *Stroke* 35.6 (2004), pp. 1404–1409.

[46] Susan L Morris, Karen J Dodd, and Meg E Morris. "Outcomes of progressive resistance strength training following stroke: a systematic review." In: *Clinical Rehabilitation* 18.1 (2004), pp. 27–39.

[47] Amo HA Stienen, Edsko EG Hekman, Frans CT Der Helm, Gerdienke B Prange, Michiel JA Jannink, Arthur MM Aalsma, and Herman Van der Kooij. "Dampace: dynamic force-coordination trainer for the upper extremities." In: *Rehabilitation Robotics, 2007. ICORR 2007. IEEE 10th International Conference on*. IEEE. 2007, pp. 820–826.

[48] Jungwon Yoon, Jeha Ryu, and Kil-Byung Lim. "Reconfigurable ankle rehabilitation robot for various exercises." In: *Journal of Robotic Systems* 22.S1 (2006), S15–S33.

[49] Sheng Bi, Linhong Ji, and Zixi Wang. "Robot-aided sensorimotor arm training methods based on neurological rehabilitation principles in stroke and brain injury patients." In: *Engineering in Medicine and Biology Society, 2005. IEEE-EMBS 2005. 27th Annual International Conference of the*. IEEE. 2006, pp. 5025–5027.

[50] Tania Lam, Markus Wirz, Lars Lünenburger, and Volker Dietz. "Swing phase resistance enhances flexor muscle activity during treadmill locomotion in incomplete spinal cord injury." In: *Neurorehabilitation and Neural Repair* 22.5 (2008), pp. 438–446.

[51] Sai K Banala, Suni K Agrawal, and John P Scholz. "Active Leg Exoskeleton (ALEX) for gait rehabilitation of motor-impaired patients." In: *Rehabilitation Robotics, 2007. ICORR 2007. IEEE 10th International Conference on*. IEEE. 2007, pp. 401–407.

[52] Michael D Ellis, Theresa Sukal, Tobey DeMott, and Julius PA Dewald. "Augmenting clinical evaluation of hemiparetic arm movement with a laboratory-based quantitative measurement of kinematics as a function of limb loading." In: *Neurorehabilitation and neural repair* (2008).

[53] James L Patton, Mary Ellen Stoykov, Mark Kovic, and Ferdinando A Mussa-Ivaldi. "Evaluation of robotic training forces that either enhance or reduce error in chronic hemiparetic stroke survivors." In: *Experimental brain research* 168.3 (2006), pp. 368–383.

[54] James L Patton, Mark Kovic, and Ferdinando A Mussa-Ivaldi. "Custom-designed haptic training for restoring reaching ability to individuals with poststroke hemiparesis." In: *Journal of rehabilitation research and development* 43.5 (2006), p. 643.

[55] Darcy S Reisman, Robert Wityk, Kenneth Silver, and Amy J Bastian. "Locomotor adaptation on a split-belt treadmill can improve walking symmetry post-stroke." In: *Brain* 130.7 (2007), pp. 1861–1872.

[56] Yejun Wei, Preeti Bajaj, Robert Scheidt, and James Patton. "Visual error augmentation for enhancing motor learning and rehabilitative relearning." In: *Rehabilitation Robotics, 2005. ICORR 2005. 9th International Conference on*. IEEE. 2005, pp. 505–510.

[57] Bambi Roberts Brewer, Roberta Klatzky, and Yoky Matsuoka. "Visual feedback distortion in a robotic environment for hand rehabilitation." In: *Brain research bulletin* 75.6 (2008), pp. 804–813.

[58] Tobias Nef, Matjaz Mihelj, and Robert Riener. "ARMin: a robot for patient-cooperative arm therapy." In: *Medical & biological engineering & computing* 45.9 (2007), pp. 887–900.

[59] Alberto Montagner, Antonio Frisoli, Luigi Borelli, Caterina Procopio, Massimo Bergamasco, Maria C Carboncini, and Bruno Rossi. "A pilot clinical study on robotic assisted rehabilitation in VR with an arm exoskeleton device." In: *Virtual Rehabilitation, 2007*. IEEE. 2007, pp. 57–64.

[60] Olivier Lambercy, Ludovic Dovat, Roger Gassert, Etienne Burdet, Chee Leong Teo, and Theodore Milner. "A haptic knob for rehabilitation of hand function." In: *Neural Systems and Rehabilitation Engineering, IEEE Transactions on* 15.3 (2007), pp. 356–366.

[61] JL Patton, G Dawe, C Scharver, FA Mussa-Ivaldi, and R Kenyon. "Robotics and virtual reality: the development of a life-sized 3-D system for the rehabilitation of motor function." In: *Engineering in Medicine and Biology Society, 2004. IEMBS'04. 26th Annual International Conference of the IEEE*. Vol. 2. IEEE. 2004, pp. 4840–4843.

[62] SV Adamovich, AS Merians, R Boian, M Tremaine, GS Burdea, M Recce, and H Poizner. "A virtual reality based exercise system for hand rehabilitation post-stroke: transfer to function." In: *Engineering in Medicine and Biology Society, 2004. IEMBS'04. 26th Annual International Conference of the IEEE*. Vol. 2. IEEE. 2004, pp. 4936–4939.

[63] Margaret McLaughlin, Albert Rizzo, Younbo Jung, Wei Peng, S Yeh, and Weirong Zhu. "Haptics-enhanced virtual environments for stroke rehabilitation." In: *Proc. IPSI* (2005).

[64] J Fung, F Malouin, BJ McFadyen, F Comeau, A Lamontagne, S Chapdelaine, C Beaudoin, D Laurendeau, L Hughey, and CL Richards. "Locomotor rehabilitation in a complex virtual environment." In: *Engineering in Medicine and Biology Society, 2004. IEMBS'04. 26th Annual International Conference of the IEEE*. Vol. 2. IEEE. 2004, pp. 4859–4861.

[65] Rares F Boian, Judith E Deutsch, Chan Su Lee, Grigore C Burdea, and Jeffrey Lewis. "Haptic effects for virtual reality-based post-stroke rehabilitation." In: *Haptic Interfaces for Virtual Environment and Teleoperator Systems, 2003. HAPTICS 2003. Proceedings. 11th Symposium on*. IEEE. 2003, pp. 247–253.

[66] The Japan times. *Wi-Fi device relays force in real time*. 2013. URL: http://www.japantimes.co.jp/news/2013/12/23/national/wi-fi-device-relays-force-in-real-time/#.VkM5voSXdOE.

[67] MJ Matari, J Eriksson, DJ Feil-Seifer, and CJ Winstein. "Socially assistive robotics for post-stroke rehabilitation." In: *J Neuroeng Rehabil* 4.5 (2007).

[68] Byron Reeves and Clifford Nass. *How people treat computers, television, and new media like real people and places*. CSLI Publications and Cambridge university press, 1996.

[69] Jon Eriksson, Maja J Mataric, and C Winstein. "Hands-off assistive robotics for post-stroke arm rehabilitation." In: *Proc. IEEE International Conference on Rehabilitation Robotics (ICORR'05)*. 2005, pp. 21–24.

[70] Yasutaka Fujimoto, Tsutomu Kominami, and Hiroshi Hamada. "Development and analysis of a high thrust force direct-drive linear actuator." In: *Industrial Electronics, IEEE Transactions on* 56.5 (2009), pp. 1383–1392.

[71] Robotiq. *Robotics force torque sensor*. URL: http://www.http://robotiq.com/.

[72] K Ohishi. "Torque-speed regulation of DC motor based on load torque estimation." In: *Proceedings of the IEEJ international Power Electronics Conference, IPEC-TOKYO, March 1983*. Vol. 2. 1983, pp. 1209–1216.

[73] Toshiyuki Murakami, Fangming Yu, and Kouhei Ohnishi. "Torque sensorless control in multidegree-of-freedom manipulator." In: *Industrial Electronics, IEEE Transactions on* 40.2 (1993), pp. 259–265.

[74] Wataru Iida and Kouhei Ohnishi. "Reproducibility and operationality in bilateral teleoperation." In: *Advanced Motion Control, 2004. AMC'04. The 8th IEEE International Workshop on*. IEEE. 2004, pp. 217–222.

[75] Seiichiro Katsura, Yuichi Matsumoto, and Kouhei Ohnishi. "Modeling of force sensing and validation of disturbance observer for force control." In: *Industrial Electronics, IEEE Transactions on* 54.1 (2007), pp. 530–538.

[76] Tobias Nef and Peter Lum. "Improving backdrivability in geared rehabilitation robots." In: *Medical & biological engineering & computing* 47.4 (2009), pp. 441–447.

[77] Kouhei Ohnishi, Masaaki Shibata, and Toshiyuki Murakami. "Motion control for advanced mechatronics." In: *Mechatronics, IEEE/ASME Transactions on* 1.1 (1996), pp. 56–67.

[78] K Ohishi, Y Ogawa, and H Dohmeki. "Speed Control Method for PM Motor using Speed Observer and Low Resolution Encoder." In: *TRANSACTIONS-INSTITUTE OF ELECTRICAL ENGINEERS OF JAPAN D* 122.3 (2002), pp. 209–216.

[79] Manuel Nandayapa, Chowarit Mitsantisuk, and Kiyoshi Ohishi. "High performance velocity estimation for controllers with short processing time by FPGA." In: *IEEJ Journal of Industry applications* 1.1 (2012), pp. 55–61.

[80] Heui-Wook Kim and Seung-Ki Sul. "A new motor speed estimator using Kalman filter in low-speed range." In: *Industrial Electronics, IEEE Transactions on* 43.4 (1996), pp. 498–504.

[81] Se-Han Lee, Ty Lasky, Steven Velinsky, et al. "Improved velocity estimation for low-speed and transient regimes using low-resolution encoders." In: *Mechatronics, IEEE/ASME Transactions on* 9.3 (2004), pp. 553–560.

[82] Chowarit Mitsantisuk, Kiyoshi Ohishi, and Seiichiro Katsura. "Estimation of action/reaction forces for the bilateral control using Kalman filter." In: *Industrial Electronics, IEEE Transactions on* 59.11 (2012), pp. 4383–4393.

[83] Soo Jeon and Masayoshi Tomizuka. "Benefits of acceleration measurement in velocity estimation and motion control." In: *Control Engineering Practice* 15.3 (2007), pp. 325–332.

[84] Riccardo Antonello, Kazuaki Ito, and Roberto Oboe. "Acceleration Measurement Drift Rejection in Motion Control Systems by Augmented–State Kinematic Kalman Filter." In: ().

[85] Jinchuan Zheng and Minyue Fu. "A reset state estimator using an accelerometer for enhanced motion control with sensor quantization." In: *Control Systems Technology, IEEE Transactions on* 18.1 (2010), pp. 79–90.

[86] Minha Park and Yang Gao. "Error and performance analysis of MEMS-based inertial sensors with a low-cost GPS receiver." In: *Sensors* 8.4 (2008), pp. 2240–2261.

[87] Farid Gulmammadov. "Analysis, modeling and compensation of bias drift in MEMS inertial sensors." In: *Recent Advances in Space Technologies, 2009. RAST'09. 4th International Conference on*. IEEE. 2009, pp. 591–596.

[88] George W Snedecor and Witiiam G Cochran. "Statistical methods 8. ed." In: *Iowa State Univ* (1989).

[89] Simon S Haykin. *Adaptive filter theory*. Pearson Education India, 2008.

[90] G Picci. "Metodi statistici per l'identificazione di sistemi lineari." In: *Dispense, Padova* (2007).

[91] Asif Sabanovic and Kouhei Ohnishi. *Motion control systems*. John Wiley & Sons, 2011.

[92] Robert J Anderson and Mark W Spong. "Bilateral control of teleoperators with time delay." In: *Automatic Control, IEEE Transactions on* 34.5 (1989), pp. 494–501.

[93] Mindy Lipson Aisen, H Igo Krebs, Neville Hogan, Fletcher McDowell, and Bruce T Volpe. "The effect of robot-assisted therapy and rehabilitative training on motor recovery following stroke." In: *Archives of neurology* 54.4 (1997), pp. 443–446.

[94] Lance L Cai, Andy J Fong, Chad K Otoshi, Yongqiang Liang, Joel W Burdick, Roland R Roy, and V Reggie Edgerton. "Implications of assist-as-needed robotic step training after a complete spinal cord injury on intrinsic strategies of motor learning." In: *The Journal of neuroscience* 26.41 (2006), pp. 10564–10568.

[95] Rui CV Loureiro and William S Harwin. "Reach & grasp therapy: design and control of a 9-DOF robotic neuro-rehabilitation system." In: *Rehabilitation Robotics, 2007. ICORR 2007. IEEE 10th International Conference on*. IEEE. 2007, pp. 757–763.

[96] Jyh-Jong Chang, Wen-Lin Tung, Wen-Lan Wu, Mao-Hsiung Huang, and Fong-Chin Su. "Effects of robot-aided bilateral force-induced isokinetic arm training combined with conventional rehabilitation on arm motor function in patients with chronic stroke." In: *Archives of physical medicine and rehabilitation* 88.10 (2007), pp. 1332–1338.

[97] L Khan, M Zygman, W Rymer, and D Reinkensmeyer. "Robot-assisted reaching exercise promotes arm movement recovery in chronic hemiparetic stroke: A randomised controlled pilot study 6." In: *Journal of NeuroEngineering & Rehabil* 3.2 (2006), pp. 1–13.

[98] Joel C Perry, Jacob Rosen, and Stephen Burns. "Upper-limb powered exoskeleton design." In: *Mechatronics, IEEE/ASME Transactions on* 12.4 (2007), pp. 408–417.

[99] Laura Dipietro, Mark Ferraro, Jerome Joseph Palazzolo, Hermano Igo Krebs, Bruce T Volpe, and Neville Hogan. "Customized interactive robotic treatment for stroke: EMG-triggered therapy." In: *Neural Systems and Rehabilitation Engineering, IEEE Transactions on* 13.3 (2005), pp. 325–334.

[100] Robert J Sanchez, Jiayin Liu, Sandhya Rao, Punit Shah, Robert Smith, Tariq Rahman, Steven C Cramer, James E Bobrow, and David J Reinkensmeyer. "Automating arm movement training following severe stroke: functional exercises with quantitative feedback in a gravity-reduced environment." In: *Neural Systems and Rehabilitation Engineering, IEEE Transactions on* 14.3 (2006), pp. 378–389.

[101] Matjaž Mihelj, Tobias Nef, and Robert Riener. "A novel paradigm for patient-cooperative control of upper-limb rehabilitation robots." In: *Advanced Robotics* 21.8 (2007), pp. 843–867.

[102] David J Reinkensmeyer, Craig D Takahashi, Wojciech K Timoszyk, Andrea N Reinkensmeyer, and Leonard E Kahn. "Design of robot assistance for arm movement therapy following stroke." In: *Advanced robotics* 14.7 (2001), pp. 625–637.

[103] Hermano Igo Krebs, Jerome Joseph Palazzolo, Laura Dipietro, Mark Ferraro, Jennifer Krol, Keren Rannekleiv, Bruce T Volpe, and Neville Hogan. "Rehabilitation robotics: Performance-based

progressive robot-assisted therapy." In: *Autonomous Robots* 15.1 (2003), pp. 7–20.

[104] Joel Stein, Kailas Narendran, John McBean, Kathryn Krebs, and Richard Hughes. "Electromyography-controlled exoskeletal upper-limb–powered orthosis for exercise training after stroke." In: *American journal of physical medicine & rehabilitation* 86.4 (2007), pp. 255–261.

[105] Rong Song, Kai-yu Tong, Xiaoling Hu, and Le Li. "Assistive control system using continuous myoelectric signal in robot-aided arm training for patients after stroke." In: *Neural Systems and Rehabilitation Engineering, IEEE Transactions on* 16.4 (2008), pp. 371–379.

[106] SENIAM project. 2015. URL: http://www.seniam.org/.

[107] Open Access Biomedical Image Search Engine. 2015. URL: https://openi.nlm.nih.gov/detailedresult.php?img=3162209_TOORTHJ-5-302_F2&req=4.

[108] Robert Riener, Lars Lünenburger, Sašo Jezernik, Martin Anderschitz, Gery Colombo, and Volker Dietz. "Patient-cooperative strategies for robot-aided treadmill training: first experimental results." In: *Neural Systems and Rehabilitation Engineering, IEEE Transactions on* 13.3 (2005), pp. 380–394.

[109] Jeremy L Emken, James E Bobrow, and David J Reinkensmeyer. "Robotic movement training as an optimization problem: designing a controller that assists only as needed." In: *Rehabilitation Robotics, 2005. ICORR 2005. 9th International Conference on*. IEEE. 2005, pp. 307–312.

[110] LE Kahn, WZ Rymer, and DJ Reinkensmeyer. "Adaptive assistance for guided force training in chronic stroke." In: *Engineering in Medicine and Biology Society, 2004. IEMBS'04. 26th Annual International Conference of the IEEE*. Vol. 1. IEEE. 2004, pp. 2722–2725.

[111] Duygun Erol and Nilanjan Sarkar. "Intelligent control for robotic rehabilitation after stroke." In: *Journal of Intelligent and Robotic Systems* 50.4 (2007), pp. 341–360.

[112] Jeremy L Emken, Susan J Harkema, Janell Beres-Jones, Christie K Ferreira, David J Reinkensmeyer, et al. "Feasibility of manual teach-and-replay and continuous impedance shaping for robotic locomotor training following spinal cord injury." In: *Biomedical Engineering, IEEE Transactions on* 55.1 (2008), pp. 322–334.

[113] Eric T Wolbrecht, Vicky Chan, David J Reinkensmeyer, and James E Bobrow. "Optimizing compliant, model-based robotic assistance to promote neurorehabilitation." In: *Neural Systems and Rehabilitation Engineering, IEEE Transactions on* 16.3 (2008), pp. 286–297.

[114] Eric J Perreault, Robert F Kirsch, and Ana Maria Acosta. "Multiple-input, multiple-output system identification for characterization of limb stiffness dynamics." In: *Biological cybernetics* 80.5 (1999), pp. 327–337.

[115] Toshio Tsuji, Pietro G Morasso, Kazuhiro Goto, and Koji Ito. "Human hand impedance characteristics during maintained posture." In: *Biological cybernetics* 72.6 (1995), pp. 475–485.

[116] Keng Peng Tee, Etienne Burdet, Chee-Meng Chew, and Theodore E Milner. "A model of force and impedance in human arm movements." In: *Biological cybernetics* 90.5 (2004), pp. 368–375.

[117] Jerome J Palazzolo, Mark Ferraro, Hermano Igo Krebs, Daniel Lynch, Bruce T Volpe, and Neville Hogan. "Stochastic estimation of arm mechanical impedance during robotic stroke rehabilitation." In: *Neural Systems and Rehabilitation Engineering, IEEE Transactions on* 15.1 (2007), pp. 94–103.

[118] Riccardo Antonello and Roberto Oboe. "Force controller tuning for a master-slave system with proximity based haptic feedback." In: *Industrial Electronics Society, IECON 2014-40th Annual Conference of the IEEE*. IEEE. 2014, pp. 2774–2779.

[119] Michael J Fu and M Cenk Çavuşoğlu. "Three-dimensional human arm and hand dynamics and variability model for a stylus-based haptic interface." In: *Robotics and Automation (ICRA), 2010 IEEE International Conference on*. IEEE. 2010, pp. 1339–1346.

[120] Lennart Ljung. "System Identification: Theory for the user." In: *PTR Prentice Hall Information and System Sciences Series* 198 (1987).

[121] Aleksandr Mikhailovich Lyapunov. "The general problem of the stability of motion." In: *International Journal of Control* 55.3 (1992), pp. 531–534.

[122] Jean-Jacques E Slotine, Weiping Li, et al. *Applied nonlinear control*. Vol. 199. 1. Prentice-hall Englewood Cliffs, NJ, 1991.

[123] Chikara Morito, Tomoyuki Shimono, Naoki Motoi, Yasutaka Fujimoto, Takao Tsuji, Yohei Hasegawa, Kiyohiko Abe, Yasushi Sakurai, and Shin Ishii. "Development of a haptic bilateral interface for arm self-rehabilitation." In: *Advanced Intelligent Mechatronics (AIM), 2013 IEEE/ASME International Conference on*. IEEE. 2013, pp. 804–809.

[124] Rudolph Emil Kalman. "A new approach to linear filtering and prediction problems." In: *Journal of Fluids Engineering* 82.1 (1960), pp. 35–45.